الجمهورية الجزائرية الديمقراطية الشعبية

People's Democratic Republic of Algeria

Ministry of Higher Education and Scientific Research

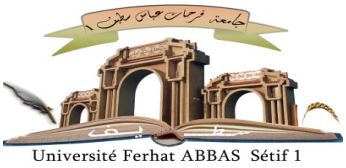

FERHAT ABBAS UNIVERSITY – SETIF 1

FACULTY OF TECHNOLOGY

THESIS

Presented to the Department of Electronics

For the attainment of the degree of

DOCTORATE

Field: Science and Technology

Spécialisation: Electronics **Option: Telecommunication networks and systems**

By

Ms. DJOUADA Djahida

THEME

Dielectric Characterization of Heterogeneous Materials Using Two Hyper-Frequency Measurement Techniques

Defended on19/12/ 2024 In front of the jury:

AMARDJIA Nourredine	**Professor**	**Univ. Ferhat Abbas Sétif 1**	**President**
BOUZIT Nacerdine	**Professor**	**Univ. Ferhat Abbas Sétif 1**	**Thesis supervisor**
BOUROUBA Nacerdine	**Professor**	**Univ. Ferhat Abbas Sétif 1**	**Examiner**
BENTOUMI Miloud	**M.C.A**	**Univ. M'sila**	**External Examiner**
BAKHTI Haddi	**M.C.A**	**Univ. M'sila**	**External Examiner**
KHOUNI Habib	**M.C.A**	**Univ. Ferhat Abbas Sétif 1**	**Invited**

Academic Year

2023-2024

"Laboratory of Scientific Instrumentation "LIS

Acknowledgments

I would like to express my heartfelt gratitude to my thesis advisor, **Professor BOUZIT Nacerdine,** from the Department of Electronics at Ferhat Abbas University of Sétif-1. I am deeply thankful for his constant support, trust, invaluable availability, pertinent advice, and encouragement. His numerous ideas have been a precious support and contributed significantly to this work.

I also extend my sincere thanks to **JUAN PABLO Martinez Jimenez**, Professor and Director of the Electromagnetic Characterization Laboratory at the University of Zaragoza in Spain. My thanks also go to **Professor BOUROUBA Nacerdine**.

I respectfully thank **Professor AMARDJIA Nourredine** from the Department of Electronics at Ferhat Abbas University of Sétif-1 for presiding over my thesis jury. I am very grateful for his thorough reading of my manuscript and his interest in my work. I also thank the jury members for endorsing this work.

I extend my gratitude to the examiners:

- **Dr. BAKHTI El Haddi**, Senior Lecturer at Mohamed Boudiaf University of M'sila, for honoring me by accepting to be an examiner of this work.

- **Dr. BENTOUMI Miloud**, Senior Lecturer at Mohamed Boudiaf University of M'sila, and **Dr KHOUNI Habib**, Senior Lecturer Class A in the Department of Electronics at Ferhat Abbas University of Sétif-1, for being jury members of this thesis.

My sincere thanks also go to the members of the (LIS) laboratory at Ferhat Abbas University of Sétif-1 for their unconditional help and availability during the sample preparation phase.

Furthermore, I would like to thank the members of my family, starting with my **dear Mother** and **Father**, may God protect them, my **Brothers** and **Sisters**, my **Husband Harek Tarek**, my **Daughter Chebaila**, and **my son Laith**, as well as all my friends who have contributed, directly or indirectly, to the realization of this work.

I extend my gratitude to **Mrs. BARROUCHE Rima**, Laboratory Engineer in the Department of Electronics at Ferhat Abbas University of Sétif-1, for her invaluable assistance and continuous availability in the laboratory.

I would like to thank all the doctoral researchers at the Scientific Instrumentation Laboratory (LIS) in the Department of Electronics at Ferhat Abbas University of Sétif-1 (**Dr.**

Delfouf Rabah., **Mrs Chioukh Labiba**., **Mr Abid S**., **Bouchama Mohamed**., **Dr. Arab Tarek**., ***Dr. Brahimi,*** **Mrs Agaba Chahinaz.,** and others).

Dedication

To my dear parents,

To my husband, Tarek,

To my son, Laith,

To my daughter, Chebailla,

To my sisters and brothers,

To the whole family,

To all my friends

Who have given me affection and support during the completion of this work

DJOUADA Djahida

List of Figures

CHAPTER I :Guided Electromagnetic Propagation

CHAPTER II:Measurement Technique (Wideband and X-Band).

List of Figures

CHAPTER III:Dielectric Materials and Mixing Laws

CHAPTER IV: Modeling of Dielectric Composite

List of Figures

List of Tables

List of Abbreviations

RE: Epoxy Resin

TB, $BaTiO_3$: Barium Titanate

P_e: Electronic Polarization

P_a: Atomic Polarization (Ionic)

P_d: Dipole Polarization (Orientation)

Pi: Interfacial Polarization

P_{TO}: Total Polarization

EM: Electromagnetic

TDS: Time Domain Spectroscopy

TDR: Time Domain Reflectometry

WEM: EM Wave (Electromagnetic Wave)

MLL: Modified Lichtenecker law

LIS : Laboratory of Scientific Instrumentation

MTB: Microwave test bench

ρ: Charge density (measured in $C.m^{-3}$)

E: The electric field (measured in $V.m^{-1}$)

D: Electric induction (measured in $C.m^{-2}$)

B: Magnetic induction (measured in T)

H: The magnetic field (measured in $A.m^{-1}$)

J: In metals, the current density (measured in $A.m^{-2}$)

DUT: Device Under Test, which is placed inside a section of a rectangular waveguide called The measurement cell

sommaire

CHAPTER II :Measurement Technique (Wideband and X-Band).

CHAPTER III: Dielectric Materials and Mixing Laws

CHAPTER IV: Modeling of Dielectric Composite

General Introduction

General Introduction

Over the past forty years, electronics has significantly expanded across various industries, mainly driven by the telecommunications boom. This growth has led to enhanced integration and frequency in electronic systems, requiring cost-effective adaptations and stricter criteria for electronic functions such as filtering. Composite materials, studied for over a century, are a promising research area due to their tailored properties. These materials, like concrete, reinforced plastics, and metals, combine constituents to meet criteria like lightness, rigidity, and resistance. Reinforcements often include silica glass or graphite, while matrices are typically plastics, metals, or ceramics. Dielectric materials, crucial in microwave communication, have advanced with modern insulators like ceramics and polymers. The miniaturization of electronic components, especially capacitors using BT due to its high permittivity, highlights the importance of composite materials. Analytical and theoretical formulas for predicting composite properties have evolved, yet still face challenges. Recent numerical methods improve the accuracy of these predictions, aiding efficient material modeling and saving time and cost.

The development of composite and heterogeneous materials for dielectric properties in microwave frequencies began from the need for high technical quality in the field of microwave electronics, with high dielectric constants and negligible losses. A composite material results from the combination of two different materials, differing in shape as well as mechanical or chemical properties, to enhance their performance. The two constituents of the composite are the matrix and the reinforcement, which together form a heterogeneous, often anisotropic material, meaning its properties vary depending on the direction. The materials chosen for the composite are typically selected based on the intended application. To conduct an effective study, we have implemented two measurement techniques.

This thesis addresses two parts; The first part: investigates the dielectric properties of a BT and epoxy resin composite using two microwave techniques (TDR and MTB), comparing empirical mixture laws and experimental results to understand the effects of BT volume fraction on dielectric behavior.[1]

This work includes dielectric characterization of heterogeneous materials using two microwave measurement techniques, In the second part, we discuss my topic, which I presented at a conference: characterization of dielectric materials in heterogeneous multilayers at microwave frequencies. This work involves studying heterogeneous multilayer dielectric materials at microwave frequencies. We employ a fixed frequency measurement characterization technique. The multilayer dielectric materials (CT), resulting from stacking heterogeneous layers, create a new medium with unique properties that differ from standard constants. Composite materials demonstrate superior performance compared to homogeneous materials, making them very promising for applications. The permittivity of heterogeneous mixtures has been studied by several researchers, and numerous theories and empirical formulas have been proposed and developed to model the dielectric behavior of composites.

General Introduction

This thesis is structured as follows:

The first chapter serves as a bibliographic review, offering a comprehensive overview of the scientific context. It begins with generalities, including essential definitions and historical background, setting the stage for deeper understanding. Key concepts in guided electromagnetic propagation are explored, focusing on both coaxial and rectangular waveguides. The chapter aims to establish a foundational knowledge base, crucial for grasping advanced topics discussed later. Definitions are clarified, historical developments are traced, and fundamental principles are outlined. This structured approach ensures readers are well-prepared for subsequent chapters. By addressing basic concepts, it bridges the gap between introductory material and specialized content. The inclusion of both coaxial and rectangular propagation provides a balanced perspective. This review not only contextualizes the subject matter but also highlights its evolution and core principles.

The second chapter provides an extensive overview of microwave measurement techniques, crucial for both theoretical and practical applications in the field. It delves into Time Domain Spectroscopy (TDS), elucidating its principles, equipment, and typical applications. The chapter also covers the X-Band Microwave Test Bench (MTB), detailing the setup, calibration, and measurement procedures essential for accurate results. A significant portion is dedicated to measurement methodology and protocols, emphasizing the importance of precision and reproducibility in experimental processes. Additionally, Broadband Waveguide Characterization is explored using a network analyzer, highlighting its capabilities in analyzing Waveguide properties across a wide frequency range. The integration of these techniques provides a comprehensive framework for advanced microwave research and development.

The third chapter delves into the introduction of dielectric materials, focusing on their properties and behavior. It begins by explaining the fundamental characteristics of dielectric materials, highlighting their significance in various applications. Theoretical and empirical mixing laws are discussed in detail, providing a framework for understanding how different materials interact when combined. These mixing laws are then applied to composite materials, illustrating practical applications and enhancing comprehension. The chapter aims to build a solid foundation in dielectric material science, ensuring readers grasp both theoretical and practical aspects. By exploring the properties and behavior of dielectrics, it sets the stage for advanced topics. The integration of mixing laws offers insights into material optimization and innovation. Through clear explanations and examples, the chapter bridges the gap between theory and real-world applications. Overall, it equips readers with essential knowledge of dielectric materials and their composite applications.

In the final section, the modeling of composite materials, specifically Resin-Titanate composites, is comprehensively examined. This part begins with the preparation methods for creating these resin-titanate composites, focusing on the precise techniques required for consistent results.

General Introduction

The study then shifts to exploring the dielectric properties of the composites, with particular attention given to the influence of varying barium titanate concentrations. Utilizing advanced mixing models, the section predicts the dielectric properties of these composites with high accuracy. The results and discussion are meticulously detailed, providing insights into the simulations and modeling processes. These findings highlight the critical relationship between barium titanate concentration and the resulting dielectric properties, offering valuable data for future applications and research.

The section concludes with an in-depth analysis of the implications of these results, solidifying the understanding of resin-titanate composite behavior.

Reference:

[1] D. Djouada, et al. "Dielectric characterization of heterogeneous composites using time-domain spectroscopy and microwave test benches in microwave frequency." ECS Journal of Solid State Science and Technology 12.6 (2023)

Guided Electromagnetic Propagation

Chapter 1 Guided Electromagnetic Propagation .

I. Recalls of Electromagnetism

I.1 History

The birth of electromagnetism began with the famous experiment conducted by Hans Christian Oersted in 1820 on the effect of an electric current on a magnetic needle [1]. He discovered the relationship between electricity and magnetism, paving the way for electromagnetism, which would become one of the cornerstones of 19th-century physics.

In 1864, James Clerk Maxwell successfully formalized the concepts of the electric field and the magnetic field based on the works of Ampère and Faraday. He established the fundamental laws or equations of electromagnetism (twenty equations) that characterize the "electromagnetic state" at any point in space. This theory allowed for the calculation of the speed of propagation of electrical and magnetic phenomena, but experimental verification was lacking.

Heinrich Hertz, in 1888, experimentally demonstrated these fundamental laws. Using electrical discharges, he generated waves of long wavelengths (called Hertzian waves) and measured their propagation speed, confirming their identity with the speed of light. This experiment also revealed the phenomena of wave reflection and refraction. Using four relatively simple equations, Heaviside successfully unified electricity, magnetism, and optics, completing Maxwell's theory.

Since then, electromagnetism has experienced renewed momentum with continuous technological development in the fields of electronics and telecommunications. However, this development is accompanied by the emergence of electromagnetic interference (EMI). EMI has significantly increased with the invention of high-density electronic components, such as the bipolar transistor in the 1950s, the integrated circuit in the 1960s, and microprocessor chips in the 1970s. As a result, the frequency spectrum used has become much broader to meet the growing technological needs [2].

I.2 Electromagnetic Waves

An electromagnetic wave consists of both an electric field and a magnetic field oscillating at the same frequency. These two fields, perpendicular to each other, propagate through a medium in an orthogonal direction (see Figure I.1). The propagation of these waves occurs at a speed that depends on the medium involved. In a vacuum, the speed of propagation of electromagnetic waves is equal to the speed of light, which is 3.10^8 m/s.

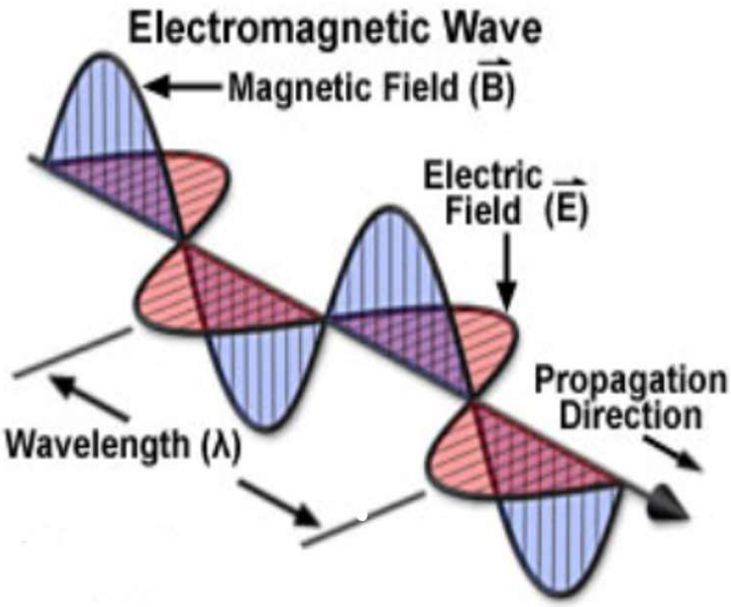

Figure I.1. Electromagnetic wave

I.2.1 Electric Field

The electric field is a force field associated with an electric charge. It usually originates from the movement of charged particles, such as negatively charged electrons or positively charged protons.

I.2.2 Magnetic Field

The magnetic field is generated by the movement of electric charges inside an atom. It can result from the rotation of electrons on themselves (called electron spin) or from the movement of electrons in the conduction bands of the atom.[3-7]

I.2.3. Electromagnetic Spectrum

The electromagnetic spectrum illustrates the arrangement of electromagnetic waves according to their wavelength, frequency, or energy (see Figure I.2).

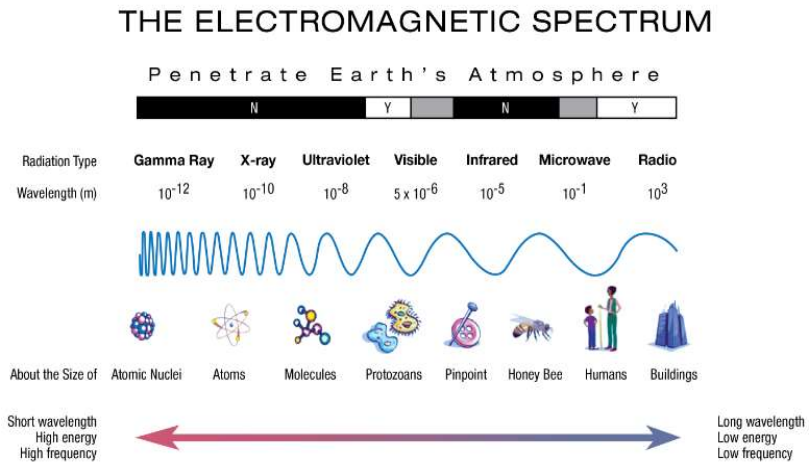

Figure I.2 Electromagnetic spectrum

– **Gamma Rays (γ):**They are due to radiation emitted by radioactive elements. Highly energetic, they easily penetrate matter and are very dangerous to living cells. Their wavelengths range from 10^{-14} m to 10^{-12} m.

–**X-rays:**highly energetic radiation that can more or less easily penetrate material bodies and are slightly less harmful than gamma rays. They are used notably in medicine for radiography, in industry (such as baggage inspection in air transport), and in research for studying matter. X-rays have wavelengths ranging from 10^{-11} meters to 10^{-8} meters.

– **Ultraviolet rays:**radiation that remains quite energetic and is harmful to the skin. Fortunately for us, a large portion of ultraviolet rays is blocked by atmospheric ozone, which serves as a protective shield for cells. Their wavelengths range from 10^{-8} meters to 4.10^{-7} meters.

– **Visible Light:**This corresponds to the very narrow part of the electromagnetic spectrum that is perceptible by our eyes. It is within the visible light spectrum that solar radiation reaches its peak (0.5 μm), and it is also within this portion of the spectrum that we can distinguish all the colors of the rainbow, from blue to red. It extends from 4.10^{-7} meters (blue light) to 8.10^{-7} meters (red light).

– **Infrared:** Radiation emitted by all bodies with temperatures above absolute zero (-273°C). In remote sensing, certain spectral bands of infrared are used to measure the temperature of land and ocean surfaces, as well as clouds. The infrared range covers wavelengths from 8.10^{-7} meters to 10^{-3} meters.

–**Radar or Microwave Frequencies:**This region of the spectrum is used to measure the radiation emitted by the Earth's surface and is similar in this case to thermal infrared remote sensing, but also by active sensors like radar systems. A radar sensor emits its electromagnetic radiation, and by analyzing the backscattered signal, it allows for locating and identifying objects, and calculating their speed if they are in motion. This can be done regardless of cloud cover, day or night. The microwave frequency domain extends from wavelengths on the order of centimeters to meters.

– **Radio Waves:**This domain of wavelengths is the broadest in the electromagnetic spectrum and encompasses waves with the lowest frequencies. It extends from wavelengths of a few centimeters to several kilometers. Relatively easy to emit and receive, radio waves are used for information transmission (radio, television, and telephone). The FM band of radio stations corresponds to wavelengths on the order of meters, while those used for cell phones are around 10 centimeters.**[3-8]**

I.3 Maxwell's Equations

I.1 Definition

The Maxwell equations mathematically model the interactions between electric charges, electric currents, electric fields, and magnetic fields. Put simply, they describe electrical, magnetic, and optical phenomena.

These equations are highly significant in physics and derive their elegance from their simplicity: just four equations to describe the vast realm of electromagnetism.

I.2 Description of Maxwell's Equations

$$\overrightarrow{\nabla \wedge \vec{H}} = \vec{J} + \frac{\partial \vec{D}}{\partial t} \quad \text{(I.1)}$$

With

$$\overrightarrow{\nabla \wedge \vec{H}} = \left(\frac{\partial H_z}{\partial y} - \frac{\partial H_y}{\partial z}\right).\vec{x} + \left(\frac{\partial \mathrm{H}}{\partial z} - \frac{\partial \mathrm{H}}{\partial x}\right).\vec{y} + \left(\frac{\partial \mathrm{H}}{\partial x} - \frac{\partial H_x}{\partial y}\right).\vec{z} \quad \text{(I.2)}$$

$$\overrightarrow{\nabla \wedge \vec{E}} = -\frac{\partial \vec{B}}{\partial t} \quad \text{(I.3)}$$

$$\nabla.\vec{D} = \rho \quad \text{(I.4)}$$

$$\nabla.\ \vec{B} = 0 \quad \text{(I.5)}$$

$$\nabla.\left(\vec{J} + \frac{\partial \vec{D}}{\partial t}\right) = 0 \quad \text{(I.6)}$$

A global current emerges. $J + (\partial D/\partial t)$ where the first term is the classical conduction current, and the second is a current, known as displacement current, which does not exist in steady-state conditions and can potentially propagate without a material medium; it refers to the current carried by the wave.

The equations above mathematically express a physical reality, the electromagnetic wave, which consists of an associated electric field and magnetic field propagating through space and varying with time.

I.4. Boundary Conditions

When a wave propagates through media of different natures, it undergoes modification as it passes from one medium to another according to laws called boundary conditions.

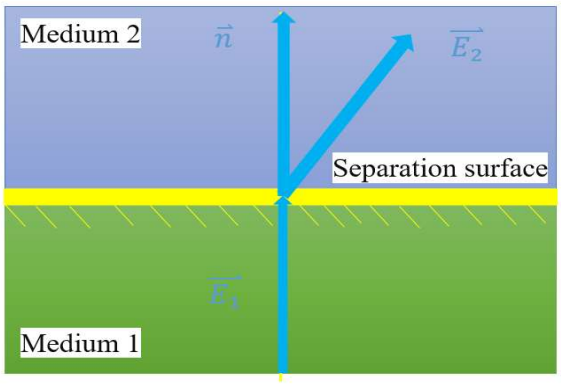

Figure I.3. Diffraction of an electromagnetic wave

($\vec{n}$ is the unit vector directed from medium 1 to medium 2 perpendicular to the surface. Figure I-3)

$$\left(\overrightarrow{B_2} - \overrightarrow{B_1}\right).\vec{n} = 0 \quad \text{(I.7)}$$

$$\left(\overrightarrow{D_2} - \overrightarrow{D_1}\right).\vec{n} = \quad \text{(I.8)}$$

$$\left(\overrightarrow{E_2} - \overrightarrow{E_1}\right) \wedge \vec{n} = 0 \quad \text{(I.9)}$$

$$\left(\overrightarrow{H_2} - \overrightarrow{H_1}\right) \wedge \vec{n} = -\overrightarrow{J_s} \quad \text{(I.10)}$$

With ρ_s and $\overrightarrow{J_s}$ are the surface charge density and current density in C.m^2 and A.m^{-2} respectively[9, 10].

I.5. Guided Propagation

I.5.1. Waveguides

Direct currents or low-frequency currents propagate along simple conductive wires. However, in high frequencies, the conductive wire becomes an antenna. If one wishes to channel the radiation, hollow cylindrical conductors of any section, but usually rectangular, circular, elliptical, or coaxial, must be used, with dimensions related to the wavelength. Propagation on a transmission line or waveguide is determined by studying the distribution of electromagnetic fields in the general structure shown in Figure (I.4):

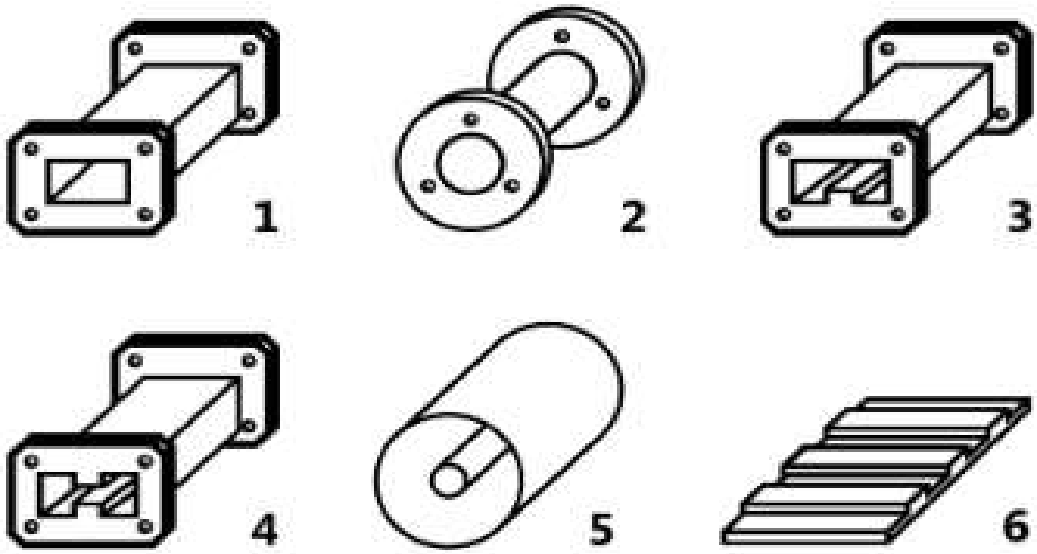

Figure I.4. Structure of a waveguide

If the section of the guide is bounded by a metallic enclosure, the electromagnetic energy propagates inside this enclosure without being able to escape. It is then said that the guide is 'closed'. In all other cases, the guide is said to be open, and the energy can escape through radiation **[11-14, 7,16-18].**

The characterization of a guide consists of determining how the energy propagates within it. At each point in the cross-sectional plane of the guide, this energy can be characterized based on the transverse components of the electric field $\vec{E}$ and magnetic field $\vec{H}$.

These fields are related by the Maxwell's equations [11-15], which are expressed as follows:

$$\overrightarrow{\nabla \wedge \vec{E}} = -\frac{\partial \vec{B}}{\partial t} = j\omega\vec{B} = -j\omega\mu\vec{H} \quad \text{(I.11)}$$

$$\overrightarrow{\nabla \wedge \vec{H}} = \vec{J} + \frac{\partial \vec{D}}{\partial t} = (\rho + j\omega)\vec{D} = (\sigma - j\omega\varepsilon)\vec{E} \quad \text{(I.12)}$$

$$\nabla.\vec{D} = \rho \quad \text{(I.13)}$$

$$\nabla.\vec{H} = 0 \quad \text{(I.14)}$$

Where $\vec{H}$: Magnetic induction.

$\vec{D}$: Electric displacement.

$\overrightarrow{\rho}$: Local charge density.

$\vec{J}$: Conduction current density.

$\varepsilon = \varepsilon' - j\varepsilon''$: Complex permittivity of the medium.

$\mu = \mu' - j\mu''$: Complex permeability of the medium.

Due to the translation invariance of the waveguide, the fields$\vec{E}$and $\vec{H}$, as well as all associated quantities have a variation in$e^{-\gamma}$ γ, is a constant known as the propagation constant $(\gamma = \alpha - j\beta)$.

Where

α is called the attenuation constant. t represents the decrease of the wave in the direction of propagation. Its inverse $\delta = (1/\alpha)$s the skin depth, the distance over which the signal decreases by a factor of $1/e$.

The imaginary part β is the phase constant, indicating the phase variation of the wave in the direction of propagation. The wavelength along the line or guide, denoted by λ_g, is inversely proportional to β:

$$\lambda_g = \frac{2\pi}{\beta} \quad \text{(I.15)}$$

The issue at hand is to define, based on frequency, this propagation constant and the spatial arrangement of the fields. It is indeed the continuity conditions at the various interfaces of the materials constituting the guide and the boundary conditions that allow us to define these characteristics.

These conditions can be summarized as follows:

The tangential components of the electric and magnetic fields at the interface between two media with different properties are continuous, which is expressed by:

$$\begin{cases} \vec{n} \wedge \left(\overrightarrow{E_1} - \overrightarrow{E_2}\right) = \vec{0} \\ \vec{n} \wedge \left(\overrightarrow{H_1} - \overrightarrow{H_2}\right) = \vec{0} \end{cases} \quad \text{(I.16)}$$

Where $\vec{n}$ is a normal vector to the interface surface, directed from medium 2 to medium 1.

At the edge of a perfect electrical conductor, the condition is

$$\vec{n} \wedge \overrightarrow{E_1} = 0 \quad \text{(I.17)}$$

For a perfect magnetic conductor, we would have

$$\vec{n} \wedge \overrightarrow{H_1} = 0 \quad \text{(I.18)}$$

I.5.2. Classification of propagation modes

Three cases of modes can be isolated:

1- The electric and magnetic fields characterizing the mode have longitudinal components: the mode is called hybrid (EH or HE mode).

2- Only the longitudinal component of the electric field or the magnetic field is present. The mode is then called transverse magnetic (TM or E mode) or transverse electric (TE or H mode).

3- The fields are entirely transverse, the mode is called transverse electromagnetic (TEM).

The transverse dimension of the guides imposes propagation conditions. Generally, for each mode, there exists a cutoff frequency below which it cannot be propagated; the associated propagation constant is real, and the mode is said to be evanescent for certain modes that do not have a cutoff frequency, for example, the TEM mode.

I.8. Dispersion diagram

In a lossless waveguide, the propagation exponent takes the form:

$$\gamma = \alpha - j\beta = \sqrt{p^2 - k^2} = \sqrt{p^2 - \left(\frac{\omega}{c}\right)^2} \quad \text{(I.19)}$$

Where p and k are termed as wave numbers. With:

$$k = \omega\sqrt{\varepsilon\mu} = \frac{\omega}{c} \quad \text{(I.20)}$$

and p is a number dependent on the cross-section of the guide (shape and dimensions), as well as the distribution of the fields of the mode considered in the transverse plane, and not on the medium filling the guide. It is always real when the guide is homogeneous. The diagram representing β and α as a function of frequency is called a dispersion diagram.

I.9. Frequency bands, dominant modes, higher modes

In the dispersion diagram of a waveguide, from a practical standpoint, four frequency bands are distinguished:

•$f < f_{c1}$: No mode can propagate, and the fields decrease with distance. The guide will be used as an attenuator.

•$f_{c1} < f < 1.25f_{c1}$: Only one mode, the dominant mode, can propagate, but it exhibits significant dispersion, so this frequency band is generally not used for information transmission.

• $1.25f_{c1} < f < f_{c2}$: Only one mode propagates, which is the dominant mode. The dispersion is generally acceptable in this band.

• $f > 1.25f_{c2}$: Several modes can propagate, including the dominant mode and other modes, which have different attenuations and propagation velocities. This leads to signal distortion, making it impractical to operate in this frequency band[19].

I.10. Study of the rectangular waveguide

I.10.1. Rectangular waveguide

The separation of Maxwell's equations (I.1) to (I.6) into longitudinal and transverse components and their developments lead to the Helmholtz differential equations[11-15, 19]:

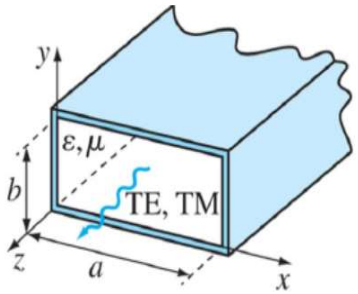

Figure I.5. Rectangular waveguide

For the TE mode

$$\nabla_t^2 H_z + \frac{\partial^2 H_z}{\partial z^2} + k^2 H_z = 0 \tag{I.21}$$

For the TM mode

$$\nabla_t^2 E_z + \frac{\partial^2 E_z}{\partial z^2} + k^2 E_z = 0 \tag{I.22}$$

The operator ∇_t^2 de notes the transverse part, by using variable separation, we have:

$$\begin{cases} \nabla_t^2 X_z + p^2 X_z = 0 \\ \frac{\partial^2 X_z}{\partial z^2} + \gamma^2 X_z = 0 \\ p^2 + \gamma^2 = k^2 \end{cases} \tag{I.23}$$

Where X represents H or E respectively

- For the TM mode:

$$\left(\frac{\partial^2}{\partial x^2} + \frac{\partial^2}{\partial y^2} + k^2\right)\Phi = 0 \tag{I.24}$$

With Φ (magnetic flux) = 0 on the walls.

- For the TE mode:

$$\left(\frac{\partial^2}{\partial x^2} + \frac{\partial^2}{\partial y^2} + k^2\right)\Psi = 0 \tag{I.25}$$

With:

$$\frac{\partial \Psi}{\partial n} = 0 \tag{I.26}$$

The derivative of the electric flux on the walls is zero.

I.10.2. Study of Transverse Magnetic Modes (TM)

Using the method of variable separation, we could write the previous equation in the form:

$$\Phi = X(x).Y(y) \tag{I.27}$$

Substituting (I.27) into (I.24) yields:

$$\frac{1}{x}\frac{\partial^2 X}{\partial x^2}+\frac{1}{Y}\frac{\partial^2 Y}{\partial y^2}+k^2=0 \tag{I.28}$$

Setting:

$$\frac{1}{x}\frac{\partial^2 X}{\partial x^2}=-\alpha^2,\frac{1}{Y}\frac{\partial^2 Y}{\partial y^2}=\beta^2 \tag{I.29}$$

We obtain the conditions:

$$\alpha^2+\beta^2=k^2 \tag{I.30}$$

The integration of equation(I.28) is immediate and yields:

$$\begin{cases} X=A_1\cos(\alpha x)+A_2\cos(\alpha x) \\ Y=B_1\cos(\beta x)+B_2\cos(\beta x) \end{cases} \tag{I.31}$$

Therefore:

$$\Phi(x,y)=(A_1\cos(\alpha x)+A_2\cos(\alpha x))(B_1\cos(\beta x)+B_2\cos(\beta x)) \tag{I.32}$$

The boundary conditions on the walls (Φ=0), as well as the normalization condition

$$\int_0^b\int_0^a \Phi^2(x,y)dxdy=\frac{1}{k^2} \tag{I.33}$$

Equation (I.22) allows us to determine the constants A_1 and A_2, B1 and B_2, α and β.

Finally, we obtain:

$$\Phi(x,y)=\frac{2}{\pi\left(m^2\frac{b}{a}+n^2\frac{a}{b}\right)^{1/2}}\sin\left(\frac{m\pi}{a}x\right)\sin\left(\frac{n\pi}{b}y\right) \tag{I.34}$$

Thus, neglecting losses, we obtain the components of the TM mode:

$$\begin{cases} E_{X_{mn}} = \pm j\beta & \frac{2}{\pi\left(m^2\frac{b}{a}+n^2\frac{a}{b}\right)^{1/2}}\left(\frac{m\pi}{a}\right)\cos\left(\frac{m\pi}{a}x\right)\sin\left(\frac{n\pi}{b}y\right)\exp(j\beta z) \\ E_{X_{mn}} = j\beta & \frac{2}{\pi\left(m^2\frac{b}{a}+n^2\frac{a}{b}\right)^{1/2}}\left(\frac{m\pi}{b}\right)\sin\left(\frac{m\pi}{a}x\right)\sin\left(\frac{n\pi}{b}y\right)\exp(j\beta z) \\ E_{Y_{mn}} = j\beta & \frac{2}{n\left(m^2\frac{b}{a}+n^2\frac{a}{b}\right)^{1/2}}\left(\frac{mn}{a}\right)\cos\left(\frac{m\pi}{a}x\right)\cos\left(\frac{n\pi}{b}y\right)\exp(j\beta z) \\ E_{Z_{mn}} = k^2 & \frac{2}{\pi\left(n^2\frac{b}{a}+n^2\frac{a}{b}\right)^{1/2}}\sin\left(\frac{m\pi}{a}x\right)\cos\left(\frac{n\pi}{b}y\right)\exp(j\beta z) \end{cases} \quad \text{(I.35)}$$

We have $H_{X_{mn}} = -\frac{1}{z_c}E_{Y_{mn}}, H_{X_{mn}} = \frac{1}{z_c}E_{X_{mn}} \text{et} H_{Z_{mn}} = 0$

And $\beta = \sqrt{p^2 + k^2}, Z_c = \frac{\beta}{a\varepsilon}, k = \left[\left(m\frac{b}{a}\right)^2 + \left(n\frac{a}{b}\right)^2\right]$

The indices m and n specify that there exists a double infinity of solutions, each of which characterizes a particular mode.

The cutoff wavelength will have the value [20, 21]:

$$\lambda_{c,mn} = \frac{2\pi}{k} = \frac{2\pi}{\left[\left(m\frac{b}{a}\right)^2+\left(n\frac{a}{b}\right)^2\right]^{1/2}} \quad \text{(I.36)}$$

Hence, the cutoff angular frequency is:

$$\omega_{c,mn} = \frac{2\pi c}{\lambda} = \frac{1}{\sqrt{\varepsilon\mu}}\left[\left(m\frac{b}{a}\right)^2 + \left(n\frac{a}{b}\right)^2\right]^{\frac{1}{2}} \quad \text{(I.37)}$$

I.11.3. Study of Transverse Electric Modes (TE)

This study is carried out in a similar manner starting from equation (I.23) and the boundary conditions at the walls, as well as the normalization condition; this leads

$$\text{to:}\begin{cases} H_{X_{mn}} = -j\beta \dfrac{2}{\pi\left(m^2\frac{b}{a}+n^2\frac{a}{b}\right)^{1/2}}\left(\frac{m\pi}{a}\right)\sin\left(\frac{m\pi}{a}x\right)\cos\left(\frac{n\pi}{b}y\right)\exp(j\beta z) \\ H_{Y_{mn}} = -j\beta \dfrac{2}{\pi\left(m^2\frac{b}{a}+n^2\frac{a}{b}\right)^{1/2}}\left(\frac{n\pi}{b}\right)\cos\left(\frac{m\pi}{a}x\right)\sin\left(\frac{n\pi}{b}y\right)\exp(j\beta z) \\ H_{Z_{mn}} = \beta \dfrac{2}{\pi\left(m^2\frac{b}{a}+n^2\frac{n}{b}\right)^{1/2}}\cos\left(\frac{m\pi}{a}x\right)\cos\left(\frac{n\pi}{b}y\right)\exp(j\beta z) \\ E_{Z_{mn}} = k^2 \dfrac{2}{\pi\left(m^2\frac{2}{a}+n^2\frac{a}{b}\right)^{1/2}}\sin\left(\frac{m\pi}{a}x\right)\cos\left(\frac{n\pi}{b}y\right)\exp(j\beta z) \end{cases} \quad \text{(I.38)}$$

We have $E_{X_{mn}} = Z_c H_{Y_{mn}}, E_{Y_{mn}} = -Z_c H_{X_{mn}}$ et$E_{Z_{mn}} = 0$

And $\beta = \sqrt{p^2 - k^2}, Z_c = \mu\omega, k = \left[\left(m\frac{b}{a}\right)^2 + \left(n\frac{a}{b}\right)^2\right]$

We see that the expression giving the cutoff frequency is the same as in the case of TM modes.

The dominant mode is the one that has the lowest cutoff frequency, which is the TE10 mode. In this case, we have: $\lambda_{c(10)} = 2a$

Therefore

$$\omega_{c(10)} = \frac{\pi}{\sqrt{\varepsilon\mu}a} \quad \text{(I.39)}$$

I.12. Standing Waves [19]

Let's consider a TE10 wave propagating in a medium characterized by a complex permittivity:

$$\varepsilon^* = \varepsilon_0(\varepsilon' - j\varepsilon'')$$

The field equations will be derived from (I.35) and are given by:

$$\begin{cases} E_y = E_0 \sin\left(\frac{\pi x}{a}\right)\exp(j\omega t - \gamma z) \\ E_y = 0 \\ E_z = 0 \end{cases} \quad \text{(I.40)}$$

The electric field is then constant along the y-axis (n= 0) and has a maximum along the x-axis (m=1). The coefficient is complex.

If a dielectric plate closes the waveguide, at z=0 for example, the incident wave will be partially reflected.

The incident wave propagates towards z >0, it will be characterized by:

$$E_y^i = E_0^i \sin\left(\frac{\pi x}{a}\right) exp(-\gamma z)\, exp(j\omega t) \tag{I.41}$$

The reflected wave propagates towards z <0 and similarly:

$$E_y^i = E_0^i \sin\left(\frac{\pi x}{a}\right) \exp(+\gamma z) \exp(j\omega t) \tag{I.42}$$

The plus signal $(+)$ indicates a reversal of the propagation direction on the terminal dielectric plate (at $z= 0$).

Γ is a complex reflection coefficient, which characterizes the terminal dielectric plate.

Let's define:

$$\Gamma = -\exp(-2w) = -\exp\big(-2(u + jv)\big) \tag{I.43}$$

Ahead of the terminal interface, the total field is:

$$E_y^t = E_y^i + E_y^r \tag{I.44}$$

Using equations (I.41) and (I.42) ultimately leads to:

$$E_y^t = 2E_0^i \sin\left(\frac{\pi x}{a}\right) \exp(-w)\, sh(w + \gamma z) \exp(j\omega t) \tag{I.45}$$

The propagation term in exp(-γz) has disappeared from this expression. We have a standing wave.

In practice, one cannot measure this field but its square value, which will be given by:

$$\left|E_y^t\right|^2 = \left(2E_0^i\right)^2 \sin\left(\frac{\pi x}{a}\right) exp(-2w)\, (sh^2(u + \alpha z) + sin^2(v + \beta z)) \tag{I.46}$$

We can distinguish three particular cases:

First case:

Propagation in vacuum ($\alpha = 0, \gamma = j\beta$) with a guide terminated by a short circuit($\rho = -1, w = 0$). So:

$$\left|E_y^t\right|^2 = 4\left(E_0^i)^2 \sin^2\left(\frac{\pi x}{a}\right) \sin^2(\beta z)\right) \tag{I.47}$$

Second case:

Propagation in vacuum ($\alpha = 0, \gamma = j\beta$) with a dielectric interface (Γ complex,$u \neq 0, w \neq 0$)

When moving along the z-axis,$\left|E_y^t\right|^2$varies sinusoidally.

The standing wave ratio (SWR) is defined as the ratio:

$$\theta = \frac{|E_t|_{max}}{|E_t|_{min}} \tag{I.48}$$

$$\theta = \frac{\left|sh^2(u)+1\right|^{1/2}}{sh(u)} = \frac{1}{th(u)} = \frac{1+\mathrm{e}\quad(2u)}{1-\exp(2u)} \tag{I.49}$$

This TOS is related to the reflection coefficient Γ by the formula:

$$\theta = \frac{1+|\Gamma|}{1-|\Gamma|} \tag{I.50}$$

Third case:

Propagation in the dielectric (γ complex) with a guide terminated by a short circuit ($\Gamma = -1, w = 0$)

$$\left|E_y^t\right|^2 = 4\left(E_0^i\right)^2 \sin^2\left(\frac{\pi x}{a}\right)(sh^2(\alpha z) + sin^2(\beta z)) \tag{I.51}$$

I.13. Coaxial line study

I.13.1. Coaxial Cable

Coaxial cable is very well known by television. It consists of two concentric conductors. The internal copper conductor (core) is used to transmit information (electromagnetic wave) in the form of a current or voltage. The latter, which is connected to the ground, can be made of copper or aluminum. It is presented either as a braid or as a coiled ribbon. It acts as a metal shield against interference signals and is covered with an insulating and protective plastic sheath. Figure (II.6).

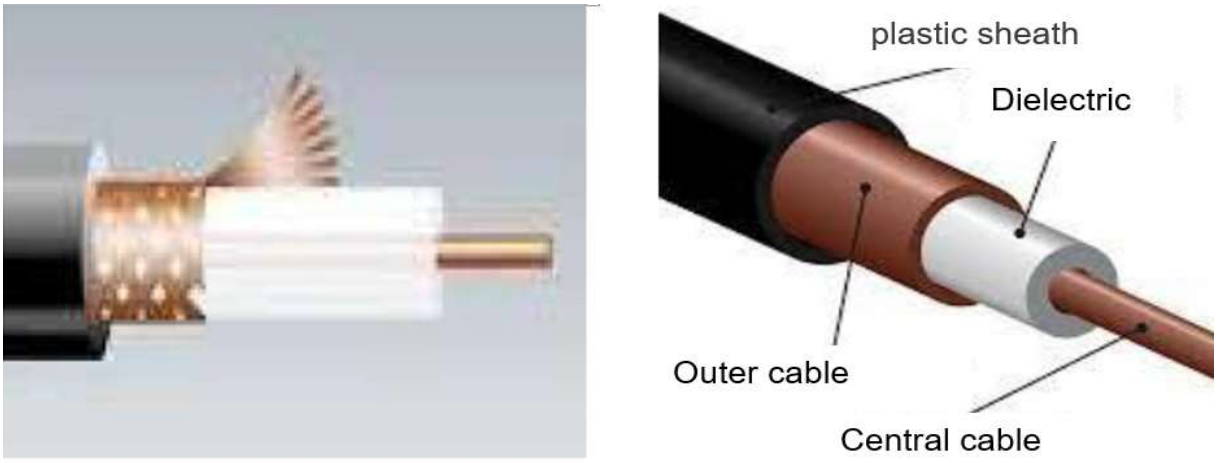

Figure I.6. Simplified diagram of a coaxial cable.

The coaxial cable is widely used in industry. It consists of two cylindrical conductors separated by a dielectric, as shown in Figure (I.7) Typically, the center conductor carries the signal, and the outer conductor serves as the ground.

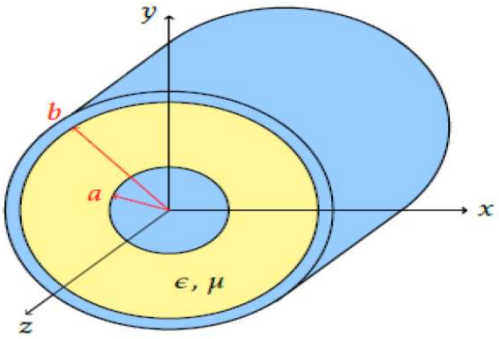

Figure I.7. Coaxial Cable.

I.12.2. Types of coaxial cables

Two types of coaxial cables are widespread; one with an impedance of 50 ohms (Ω) is frequently used in digital transmission installations, and the other 75 Ω is generally used in analog communication and cable television.

Due to its construction and shielding, a coaxial cable is characterized by a wide bandwidth and very good noise protection. The bandwidth depends on the quality of the cable, its length, and the signal-to-noise ratio. In modern cables, it is close to 1 GHz. This type of cable is still widely used in cable television and on networks

I.12.3. Scope of use of coaxial cable

Coaxial cable is widely used in both analog and digital data transmission networks, with its primary application being in radio and television systems. It is valued for its ability to efficiently carry high-frequency signals over long distances while minimizing interference. In addition to broadcasting, coaxial cables are also

commonly employed in telecommunications, internet connectivity, and CCTV systems. They're known for their durability and reliability, making them a preferred choice in various communication infrastructures.

I.12. 4. Advantages and disadvantages of coaxial cable

a) Benefits

- Immunity to electromagnetic noise.
- Transport digital (50 Ohms) and analog (75 Ohms) data.
- Ability to channel 10,000 channels of analog speech
- Several tens of Mbits/s.

b) Disadvantages

- Difficulty of installation and lack of adaptation to changes.
- Cost remains higher than twisted pair for now identical performance
- Has a significant mitigation.
- Largely surpassed by optical fibers for very high throughput.
- Supplanted by twisted pairs for average throughput (a few dozen Mbit/s) [22-23].

I.12.5. Study of Transverse Electromagnetic (TEM) Modes

Considering the straight section of the cable from an emetic math point of view, the domain between ame and shielding is doubly related and it can therefore be envisaged that a TEM wave, that is, such that $E_z = 0$ and $B_z = 0$ can propagate along the cable. The position of a current point will be located using the ρ, φ, and z. Explaining the Maxwell equations for a TEM wave in the inter-conductor medium, we obtain :

$$B_\rho = \frac{1}{j\omega}\frac{\partial E_\varphi}{\partial z}, B_\varphi = -\frac{1}{j\omega}\frac{\partial E_\rho}{\partial z}, 0 = \frac{\partial \rho E_\varphi}{\partial \rho} - \frac{\partial E_\rho}{\partial \varphi}$$

$$j\frac{\omega}{v^2}E_\rho = -\frac{\partial B_\varphi}{\partial z}, j\frac{\omega}{v^2}E_\varphi = \frac{\partial B_\rho}{\partial z}, 0 = \frac{\partial \rho B_\varphi}{\partial \rho} - \frac{\partial B_\rho}{\partial \varphi} \quad \text{(I.52)}$$

$$\frac{\partial \rho E_\rho}{\partial \rho} + \frac{\partial E_\varphi}{\partial \varphi} = 0, \frac{\partial \rho B_\rho}{\partial \rho} + \frac{\partial B_\varphi}{\partial \varphi} = 0$$

Where $v = C/n$ is the speed of wave propagation in the dielectric medium. Research only waves respecting the cylindrical symmetry. For these, we have $\partial\varphi = 0, E\varphi = 0$, and then $B\rho = 0$. The equations (I.52) simplify greatly:

$$\begin{aligned}&(a)\ \frac{\partial E_\rho}{\partial z} = -j\omega B_\varphi, \frac{\partial B_\varphi}{\partial z} = -j\frac{\omega}{v^2}E_\rho \\ &(b)\ \frac{\partial \rho E_\rho}{\partial \rho} = 0, \frac{\partial B_\varphi}{\partial \varphi} = 0\end{aligned} \tag{I.53}$$

From (I.53) (b) it is drawn that E_ρ must necessarily take the form

$$E_\rho(\rho, z, t) = \frac{F(z)}{\rho} e^{j\omega t} \tag{I.54}$$

Where F(z) is a function of z only. From (I.53) (a) it is easy to edit the equation to

which F(z) must meet: $\frac{d^2F}{dz^2} = -k^2F$ with $k = \frac{\omega}{v}$

The function F(z) is therefore of the form:

$$F(z) = F[e^{-jkz} + r\ e^{jkz}] \tag{I.55}$$

Where F and r are constants. Each of the terms of (16.53) is easily interpreted: the first represents a progressive wave propagating in the direction $\overrightarrow{Z'Z}$, while the second represents a retrograde wave, thus propagating in the opposite direction, which comes from a reflection of the first part on a possible obstacle in the cable. The constant r, which is the ratio of the second term to the first, can be interpreted as a reflection coefficient.

So now, omitting the temporal factor $e^{j\omega t}$, omitting the time factor,

$$E_\rho = \frac{F}{\rho}\left[e^{-jkz} + re^{jkz}\right], B_\varphi = \frac{F}{v\rho}\left[e^{-jkz} - re^{jkz}\right] \tag{I.56}$$

From these field expressions, we can deduce, by applying boundary conditions, the surface charge densities σ_a and σ_b and the currents J_a and J_b carried by the inner surface of the core and the inner surface of the shielding, respectively.

$$\sigma_a = \varepsilon E_\rho(\rho = a) = \frac{F\varepsilon}{a}\left[e^{-jkz} + re^{jkz}\right]$$

$$\sigma_b = -\varepsilon E_\rho(\rho = b) = -\frac{F\varepsilon}{b}\left[e^{-jkz} + re^{jkz}\right] \quad \text{(I.57)}$$

$$J_a = \frac{1}{\mu_0} B_\varphi(\rho = a) = \frac{F}{av\mu_0}\left[e^{-jkz} - re^{jkz}\right]$$

$$J_b = -\frac{1}{\mu_0} B_\varphi(\rho = b)(= -\frac{F}{bv\mu_0}\left[e^{-jkz} - re^{jkz}\right]$$

Note that the current densities are oriented according to z'z. From (16.58) charges are deducted Q_a, Q_b, and current intensities I_a, I_b carried by the soul and shielding, respectively:

$$Q_a = -Q_b = 2\pi a\sigma_a = 2\pi F\epsilon\left[e^{-jkz} + re^{jkz}\right]$$

$$I_a = -I_b = 2\pi a J_a = \frac{2\pi F}{v\mu_0}\left[e^{-jkz} - re^{jkz}\right] \quad \text{(I.58)}$$

Now let's look at possible expressions of V and $\vec{A}$ respecting the symmetry cylindrical. We have

$$E_\rho = -\frac{\partial V}{\partial \rho} - j\omega A_\rho, E_\varphi = 0 = -j\omega A_\varphi, E_z = 0 = -\frac{\partial V}{\partial z} - j\omega A_z$$

$$B_\rho = 0 = -\frac{\partial A_\varphi}{\partial z}, B_\varphi = \frac{\partial A_\rho}{\partial z} - \frac{\partial A_z}{\partial \rho}, B_z = 0 = \frac{1}{\rho}\frac{\partial \rho A_\varphi}{\partial \rho} \quad \text{(I.59)}$$

Where it appears that $A_\varphi = 0$ and one can choose $A_\rho = 0$, so that

$$E_\rho = -\frac{\partial V}{\partial \rho}, B_\varphi = -\frac{\partial A_z}{\partial \rho}, \frac{\partial V}{\partial z} = -j\omega A_z \quad \text{(I.60)}$$

By choosing (the time factor being part of)

$$V = F\ln\left(\frac{b}{\rho}\right)\left[e^{-jkz} + re^{jkz}\right], A_z = \frac{F}{v}\ln\left(\frac{b}{\rho}\right)\left[e^{-jkz} - re^{jkz}\right] \quad \text{(I.61)}$$

We obtain potentials that further satisfy the Lorenz gauge $\frac{\partial A_z}{\partial z} + j\frac{\omega}{v^2}V = 0$

The voltage U(z; t) between the core and the shielding for a given position z is obtained from the scalar potential:

$$U(z,t) = V(z,a,t) = F\ln\left(\frac{b}{a}\right)\left[e^{-jkz} + re^{jkz}\right]e^{j\omega t} \quad \text{(I.62)}$$

We can fix the constant F by giving the voltage to the dimension z = 0, either

$$U(0,t) = U_0 e^{j\omega t}$$

which gives

$$F = \frac{U_0}{(1+r)\ln\left(\frac{b}{a}\right)} \quad \text{(I.63)}$$

Taking this data into account, the voltage U(z; t) and the current intensity I_a(z; t) therefore have expressions

$$U(z,t) = \frac{U_0}{1+r}\left[e^{-jkz} + re^{jkz}\right]e^{j\omega t}$$

$$I_a(z,t) = \frac{1}{Z_c}\frac{U_0}{1+r}\left[e^{-jkz} - re^{jkz}\right]e^{j\omega t} \quad \text{(I.64)}$$

And

$$Z_c = \frac{1}{2\pi}\sqrt{\frac{\mu_0}{\epsilon}}\ln\left(\frac{b}{a}\right) \quad \text{(I.65)}$$

Is the characteristic impedance of the cable. The ratio U=I_a, which defines an "impedance" at position z, has the expression

$$Z(z) = Z_c\frac{e^{-jkz}+re^{jkz}}{e^{-jkz}+re^{jkz}} \quad \text{(I.66)}$$

The cable serves as a connecting element in a circuit, and therefore, the reflection coefficient r depends on the system to which it is connected. If Z0 is the input impedance of this system, we must impose the condition Z(h) = Z0. From this, we deduce:

$$r = \frac{Z_0 - Z_c}{Z_0 + Z_c}e^{-2jkh} \quad \text{(I.67)}$$

We conclude that to minimize wave reflection at the final connection of the cable, it is advantageous to ensure that the apparent impedance Z0 is equal to the characteristic impedance Zc. In this case, we say the cable is matched to the receiver. Numerically, for a = 1 mm, b = 4 mm, and n = 1.4, we find Zc to be approximately 60 ohms, which is a value close to those of common cable impedances ranging from 50 to 185 ohms.

It's interesting to recall here the expressions for capacitance C and self-inductance coefficient L per unit length of the cable:

$$\mathcal{C} = \frac{2\pi\epsilon_0 n^2}{\ln\left(\frac{b}{a}\right)}, \mathcal{L} = \frac{\mu_0}{2\pi}\ln\left(\frac{b}{a}\right) \tag{I.68}$$

Because we have the connections

$$Z_c = \sqrt{\frac{\mathcal{L}}{\mathcal{C}}} \text{ and } v = \frac{1}{\sqrt{LC}} \tag{I.69}$$

It is also interesting to note these other relationships

$$\frac{\partial I_a}{\partial z} = -C\frac{\partial U}{\partial t}, \frac{\partial U}{\partial z} = -L\frac{\partial I_a}{\partial t} \tag{I.70}$$

That we will find further by another method.

Even if the cable is connected to an appropriate characteristic impedance so that no wave reflection occurs at its termination in z = h, there may nevertheless be a wave reflection inside the cable, which may come from a dielectric fault. Let's model this defect as follows:

For z <ℓ< h, the permittivity of the medium is ε.

While for ℓ< z < h it takes another value ε'.

$$E_\rho^< = \frac{F}{\rho}\left[e^{-jkz} + re^{jkz}\right] \quad , \quad B_\varphi^< = \frac{F}{v\rho}\left[e^{-jkz} - re^{jkz}\right] \tag{I.71}$$

while for ℓ ≤ z ≤ h, we set:

$$E_\rho^> = \frac{F}{\rho}\tau\, e^{-jk'z}, \; B_\varphi^> = \tau\frac{Fk'}{\omega\rho}e^{-jk'z} \tag{I.72}$$

I.12.6. Higher Modes

The coaxial cable can also support TE and TM modes, in addition to the TEM mode. However, these modes are usually evanescent at the operating frequency of the guide. It is important, however, to know the cutoff frequency of the higher modes, to avoid mode superposition and therefore distortion in the signal transmitted over the cable.

The next mode to propagate on a coaxial cable (after the TEM mode) is the TE11 mode. Its cutoff frequency is given by:

$$f_c = \frac{ck_c}{2\pi\sqrt{\varepsilon_r}} \tag{I.73}$$

Where kc can be approximated by:

$$k_c \approx \frac{2}{a+b} \tag{I.74}$$

In practice, a safety margin of 5% is used for the operation of the coaxial guide***[24]***.

I.14.Conclusion

In this chapter, we have delved into the fundamental concepts and basic formulas essential for grasping guided propagation and waveguides., with a particular emphasis on the rectangular and coaxial guides, which are commonly encountered in engineering applications.

The distinction between waveguides that conform to transmission line theory and those that do not has been highlighted. While some waveguides exhibit transmission line behavior and can be analyzed using this theory, others require alternative approaches due to their unique characteristics.

Maxwell's equations have been instrumental in our understanding, serving as the theoretical foundation for describing electromagnetic wave propagation in waveguides. By examining these equations and the associated parameters, we have gained valuable insights into the underlying principles governing waveguide behavior.

Overall, this chapter provides a solid introduction to guided propagation and waveguides, laying the groundwork for further exploration and practical applications in fields such as telecommunications, microwave engineering, and optical communications. It serves as a foundational resource for engineers and researchers seeking to understand, analyze, and design waveguide systems.

References:

[1] Topal, Ugur, Husnu Ozkan, and Lev Dorosinskii. "Finding optimal Fe/Ba ratio to obtain single phase BaFe12O19 prepared by ammonium nitrate melt technique." Journal of alloys and compounds 428.1-2 (2007): 17-21.

[2] Liu, Ying, et al. "Efficiency and purity control in the preparation of pure and/or aluminum-doped barium ferrites by hydrothermal methods using ferrous ions as reactants." Journal of magnetism and magnetic materials 322.3 (2010): 366-374.

[3] Mattei, Elisabetta, et al. "Electromagnetic parameters of dielectric and magnetic mixtures evaluated by time-domain reflectometry." IEEE Geoscience and Remote Sensing Letters 5.4 (2008): 730-734.

[4] Bennia, Abdelhak, and Sedki M. Riad. "An optimization technique for iterative frequency-domain deconvolution." IEEE transactions on instrumentation and measurement 39.2 (1990): 358-362.

[5] G.Moradi, A. Abdipour. Measuring the Permittivity of Dielectric Materials Using STDR Approach. Progress In Electromagnetics Research, PIER 77,. 2007. pp. 357– 365.

[6] M. Shaarawi, S. M. Riad. Computing the complete fast Fourier transform of a step-like waveform. IEEE Transactions on instrumentation & measurement, Vol. IM-35, Nº. 1. March 1986.

[7] Samulon, H. A. "Spectrum analysis of transient response curves." Proceedings of the IRE 39.2 (1951): 175-186.

[8] SShaarawi, Amr M., and Sedki M. Riad. "Computing the complete FFT of a step-like waveform." IEEE transactions on instrumentation and measurement 1 (1986): 91-92.

[9] S. Orlowska. Design and prediction of dielectric characteristics of two and three-phase composite materials by modeling and experimental validation. PhD Thesis, Lyon, 2003.

[10] A. Balana. Study of the electromagnetic behavior of heterogeneous media in centimeter waves, modeling. PhD Thesis, University of Bordeaux I, 1990.

[11] A. Celzard. Contribution to the study of the percolation phenomenon in composites with anisotropic properties. PhD Thesis, June 1995.

[12] J. Aubic, A. M. Bottreau. Use of TDR for the Study of Moisture Transfers in Permeable Porous Media. Journal of Hydrology, 57. 1982. pp. 337-357.

[13] A. Benhamouda, J.M. Fornies-Marquina, N. Bouzit, N. Bourouba. Dielectric behavior of ternary composites of epoxy/BaTiO3/(CuO or MgO). Eur. Phys. J. Appl. Phys. 46, 20404. 2009.

[14] H. Bakhti, N.Bouzit, J.M. Fornies-Marquina, N.Bourouba, A.Benhamouda. Low-frequency experimental analysis of the dielectric constant variation of a bi-titanate composite as a function of concentrations. Proceeding JIPMA'07 – Annaba. 2007.

[15] H. Bakhti, N.Bouzit, J.M. Fornies-Marquina, N.Bourouba, A.Benhamouda. Measurements of the dielectric permittivity of a mixture of (CuO – BaTiO3 – Epoxy Resin) in the frequency band from 0 to 5 GHz. Proceeding JIPMA'07 – Annaba. 2007.

[16] Parruck, S. M. Riad. TDR, Step response, and 'S' parameters measurements in the time domain. Picosecond pulse labs AN-3044, Revision 1, 5/89. 1989.

[17] N.E. Hager. Broadband Time-Domain-Reflectometry Dielectric Spectroscopy Using Variable-Time-Scale Sampling. Dielectric Spectroscopy, Rev. Sci. Instrum. Vol. 65, Nº. 4. April 1994.

[18] S. Ahire, A. Chaudhari, M. Lokhande, S. C. Mehrotra. Complex Permittivity Spectra of Binary Pyridine-Amide Mixtures Using Time Domain Reflectometry. Journal of Solution Chemistry, vol. 27, no 11, 1998.

[19] Bakhti, Haddi, and Nacerdine Bouzit. "Experimental study of dielectric and functional properties of polymer matrix/cu2o/batio3 heterogeneous composites in broad band frequency." 14th International Multidisciplinary Scientific GeoConference SGEM 2014. 2014.[20] B. K. Diefenderfer. Development and Testing of a Capacitor Probe to DetectDeterioration in Portland Cement Concrete. Master's Thesis, 1998.

[21] D. Hamzaoui. Study by frequency domain spectroscopy of the evolution of complex permittivity as a function of charge and frequency. Application to polyester loaded with ceramics: BaTiO3 and SrTiO3. Magister Thesis, Sétif, 1998.

[22] Dr. A Hamouda., "Chargé de Cour and TD of Chapter 02 and 03, module: electromagnetism, transmission line, Université Larbi Ben Mhidi- OEM", 2020.

[23] Chehami Fadhila., «Study of subwavelength waveguides in the form of (c) for the design of optical nano-couplers»,(Master, in physics, University Mouloud Mammeri-Tizi-Ouzou),2017.

[24] Christian Carimalo. Chapitre 16: Guides d'ondes et lignes de transmission. Electromagnétisme, pp. 507-511.

Measurement Technique (Wideband and X-Band).

Chapter 2 Measurement Technique (Wideband and X-Band).

II.1 Introduction

In this chapter, we embark on an exciting journey into the heart of measurement techniques, highlighting two distinct approaches: wideband and X-band technologies. We begin with a thorough analysis of material characterization methods, a fundamental element of our investigation. By leveraging essential tools such as Time Domain Reflectometry (TDR) and fixed-frequency measurement benches, we explore the foundations of these techniques and their relevance in the field of electronics. This introduction marks the starting point of an immersive dive into the subtleties and potentials offered by these measurement advances, promising insight into future innovations to come. Measurement techniques, true pillars of scientific and technological research, play a central role in understanding and characterizing physical phenomena.

II.2 Measurement Techniques

Several techniques exist for extracting electromagnetic characteristic properties, each having its advantages and disadvantages, and the choice of method depends on several factors such as the bandwidth, the required measurement accuracy, the material to be measured (dispersive, homogeneous, sample size, material state, and so on).

Generally speaking, characterization techniques are divided into two groups [1]:

- Wideband Measurement Techniques, such as (Network Analyzer in the frequency domain and Time Domain Reflectometry in the temporal domain TDR)
- X-Band Measurement Techniques, such as (Fixed-Frequency Measurement Bench **MTB)**

II.2.1 Network Analyzer

The network analyzer is used to determine the S-parameters of a two-port or four-port network. There are two main families of network analyzers: scalar analyzers, which measure only the magnitude of the S-parameters [2], and vector analyzers, which measure both the magnitude and the phase [3].

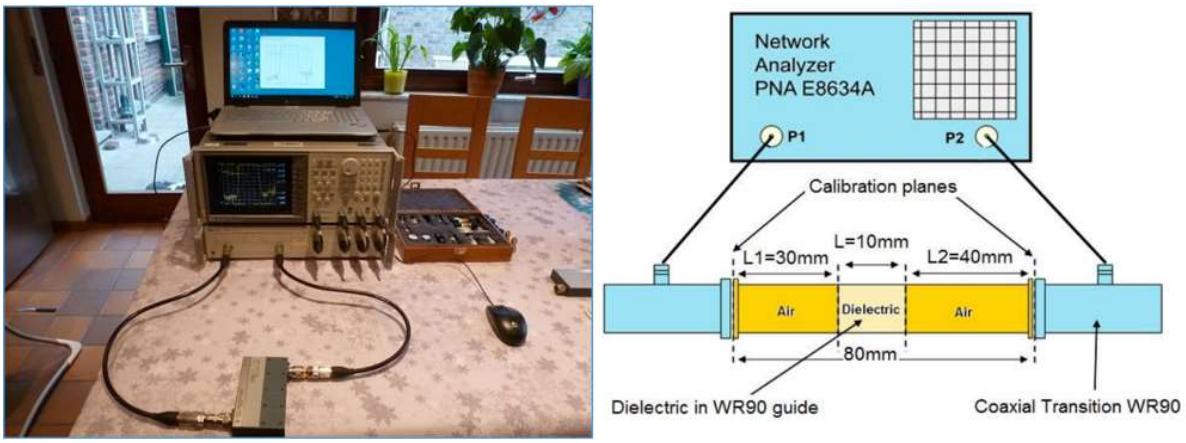

Figure II.1. Vector network analyzer connected to a PC for data processing.

Chapter 2 Measurement Technique (Wideband and X-Band).

The principle of a network analyzer involves exciting the DUT through its ports using a sinusoidal signal of constant amplitude and automatically variable frequency, and then measuring the signals reflected and transmitted by the DUT. By successively exciting all the ports, we obtain the scattering matrix terms as a function of the swept frequency. The system allows the source signal to be directed from port 1 to port 2, and then from port 2 to port 1. When a port is excited, the system must split the signal into two parts. The first part is directed to the test path and serves as the source for the DUT. The second part serves as a reference signal to which the reflected and transmitted signals by the DUT are compared. [4]

III.3 Time Domain Reflectometry

Among the methods for material characterization, we have opted for the Time Domain Reflectometry (TDR) technique. This method focuses on analyzing the behavior of an electromagnetic wave emitted into the studied medium. It exploits the propagation velocity of this wave, which depends on the permittivity of the medium, and the reflection at each discontinuity or impedance change in the transmission line. The wave is a short-duration electrical impulse or step function, thus of very high frequency, delivered by a step generator (Figure II.2).

This wave travels along a coaxial line, at the end of which the sample of the material under study is placed. Measuring the round-trip time of the wave using an ultra-fast oscilloscope allows us to deduce the permittivity. The measurement device used for this purpose consists of a step generator, a coaxial line, a sampling oscilloscope, and a microcomputer for data acquisition and processing [5,6,7].

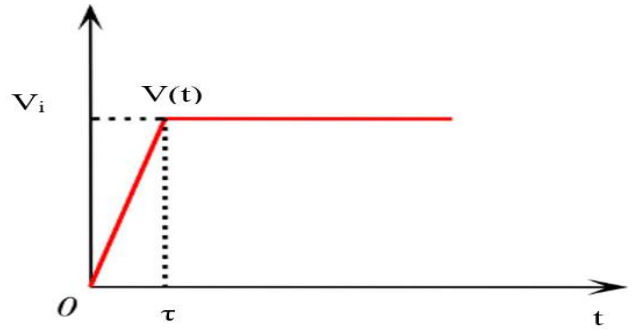

Figure II.2: Voltage step signal

The characteristics of the voltage step signal

$$\begin{cases} V(t) = 0 & \text{for} \quad t =\leq 0 \\ V(t) = \frac{Vi}{\tau} t & \text{for} \quad 0 \leq t \leq \tau \\ V(t) = Vi & \text{for} \quad t \geq \tau \end{cases} \qquad \text{(II.1)}$$

The complex amplitude in the frequency domain is given by:

$$V(\omega) = \int_{-\infty}^{+\infty} V(t)e^{-j\omega t}dt = \frac{V_i}{\tau}.\frac{1-e^{-j\omega\tau}}{\omega^2} \quad \text{(II.2)}$$

For very small τ, we obtain:

$$V_{t\to 0}(\omega) = \frac{V_i}{j\omega} \quad \text{(II.3)}$$

Which is simply the Fourier transform of the step function, and its spectral density is:

$$I(\omega) = V(\omega).V^*(\omega) = 2V_i^2\frac{2V_i^2}{\tau^2}\left(\frac{1-\cos(\omega\tau)}{\omega^4}\right) \quad \text{(II.4)}$$

Similarly, as τ tends towards zero:

$$I_{t\to 0}(\omega) = \frac{V_i^2}{\omega^2} \quad \text{(II.5)}$$

From the equations, it is clear that the spectral density attenuates much more rapidly for longer rise times. The shorter rise time, the slowerspectral density attenuates, hence the interest in using increasingly shorter rise times thanks to the advent of fast recovery diodes which allow reaching frequencies of over 10 GHz. In our case, the spectrometer we used delivers a voltage step of amplitude 200mV, with a rise time on the order of 28 ps, which will cover, after Fourier transformation, a bandwidth extending from DC up to 12.5 GHz.
This step signal propagates in the coaxial line with characteristic impedance Z_0. When it encounters the sample, located at the end of the line and having an impedance Z, a portion of the incident signal is reflected. The reflection coefficient is given by:

$$R = \frac{Z-Z_0}{z+Z_0} \quad \text{(II.6)}$$

We can then, knowing R and Z_0 = 50 Ω, obtain Z and consequently characterize the cause of this impedance change. It may be due, as we have already mentioned, to a change in the guide's standard, a line defect, or the presence of a sample in the line. This latter aspect is the basis for the development of the work presented here.

The electromagnetic characteristics (dielectric ε', ε''; electrical σ; and possibly magnetic μ', μ'') of a material are then determined as a function of frequency, either by treating the reflection coefficient R(ω) or by passing through the characteristic admittance of the medium Y(ω) (or its impedance $Z(\omega) = \frac{1}{Y(\omega)}$) [8, 9] .

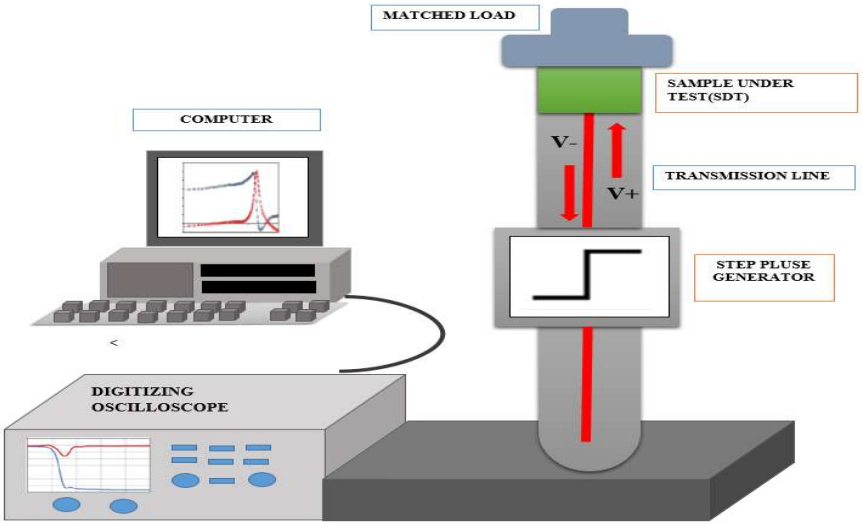

Figure II.3. Time Domain Reflectometry Measurement Setup (TDR)

II.3.1 Main Methods Used in Time Domain Spectroscopy.

II.3.1.1 General Expression of the Reflection Coefficient (Optical Approach).

In this approach, we analyze the response of a sample by studying the reflection coefficients at the interfaces, considering each reflection individually. This is possible because, in our time-domain reflectometry setup, the reflected waves arrive staggered in time. The overall reflection coefficients are subsequently calculated using a method commonly employed by optical and microwave engineers[10].

Consider a dielectric slab with thickness d and dielectric constant ε_2 placed between two different mediums of infinite lengths and relative permittivities ε_1 and ε_3. Then, generally, we have:

$$p_i = \frac{Z_{i+1} - Z_i}{Z_{i+1} + Z_i} = \frac{n_i - n_{i+1}}{n_i + n_{i+1}} \quad \text{(II.7)}$$

Where :$n_i = \sqrt{\varepsilon_i}$.

At the upstream side of the first interface, we obtain:

$$p_1 = \frac{Z_2 - Z_1}{Z_2 + Z_1} = \frac{n_1 - n_2}{n_1 + n_2} \quad \text{(II.8)}$$

However, on the downstream side, we have:

$$p_2 = \frac{Z_2 - Z_3}{Z_2 + Z_3} = \frac{n_2 - n_3}{n_2 + n_3} \quad \text{(II.9)}$$

The system can be represented by the following(Figure II.4):

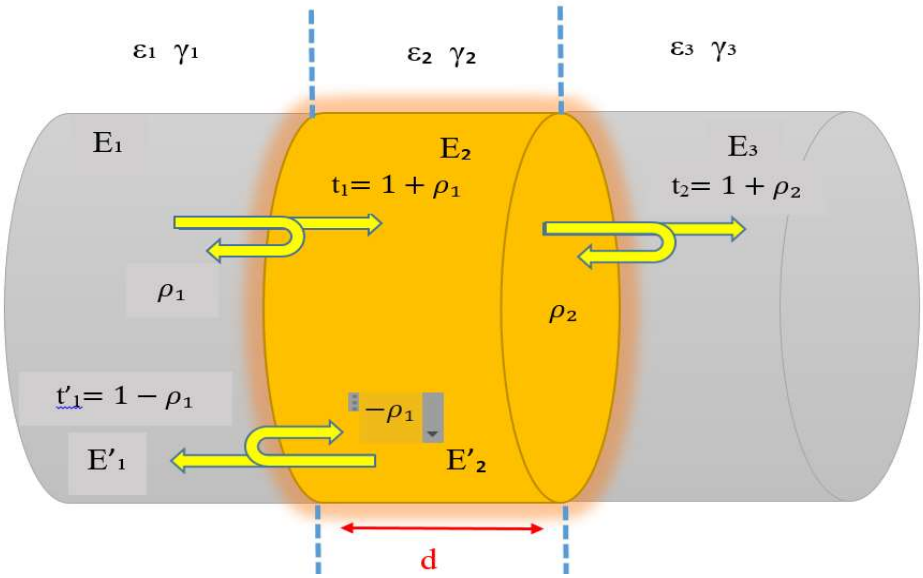

Figure II.4 Multiple reflections in a dielectric

Where :

γ:propagation constant in the studied dielectric

E_1: incident field on the first interface

E'_1: total reflected field at the first interface

E_2: total field at the first interface inside the dielectric

E'_2: total reflected field at the second interface and inside the dielectric

E_3: total transmitted field

E'_2: total field reflected at the second interface and inside the dielectric

E_3: total transmitted field

ρ_1: reflection coefficient at the first interface

t_1: transmission coefficient at the first interface

ρ_2: reflection coefficient at the second interface

t2: transmission coefficient at the second diopter

The following relationships between field expressions can then be established [11,12]:

$$\begin{cases} E_2 = (1+\rho_1)E_1 - \rho_1 E_2' \exp(-\gamma_2 d) \\ E_3 = (1+\rho_2)E_2 \exp(-\gamma_2 d) \\ E'_2 = \rho_2 E_2 \exp(-\gamma_2 d) \\ E_1' = \rho_1 E_1 + (1-\rho_1)E_2' \exp(-\gamma_2 d) \end{cases} \quad \text{(II.10)}$$

From this system of linear equations, the general expressions of the global reflection coefficient R and the global transmission coefficient T:

$$R = \frac{E_1'}{E_1} \text{ and } T = \frac{E_3}{E_1} \quad \text{(II.11)}$$

Either :

$$R = \frac{E_1'}{E_1} = \frac{\rho_1 + \rho_2 \exp(-2\gamma d)}{1 + \rho_1 \rho_2 \exp(-2\gamma d)} \quad \text{(II.12)}$$

for the reflection coefficient

$$T = \frac{E_3}{E_1} = \frac{(1+\rho_1)(1+\rho_2)\exp(-2\gamma d)}{1 + \rho_1 \rho_2 \exp(-2\gamma d)} \quad \text{(II.13)}$$

For the transmission coefficient.

The experimental protocols that will be implemented in time spectroscopy will be defined from these two fundamental relationships. Their advantages and disadvantages will be presented and the choice of those retained in our work will be exposed.

There are two categories of methods: the first reflection method and the multiple reflection method.

II.3.1.2 T he First ReflectionMethod .

It was the first to be implemented in time-domain spectroscopy. The figure below shows that only the reflection from the air/sample interface is taken into account. However, it is necessary to use a sample of

sufficient length so that all the information carried by the reflection of the first interface is obtained before the second reflection due to the second interface appears [13-15]. (Figures II.5 and II.6) present respectively the experimental device and a schematization of the corresponding signals.

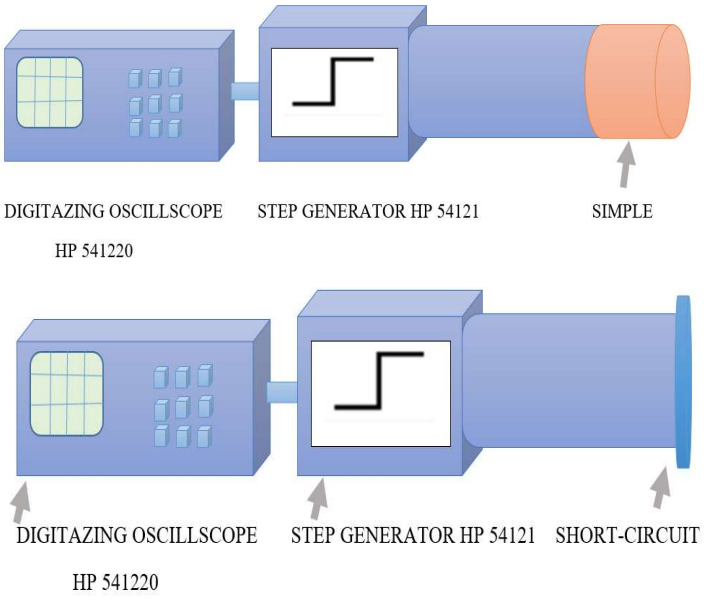

Figure II.5. Experimental device used in the first reflection

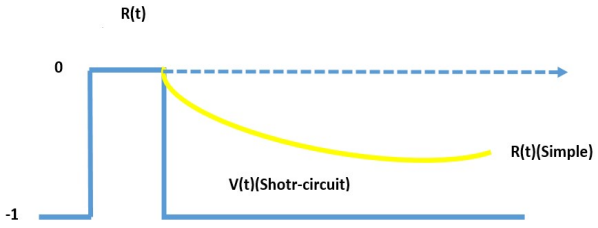

Figure II.6. Representation of reflected signals for the first reflection method

The time signals obtained by the first reflection method for a hexanol sample are shown in Figure (II.7.) [16].

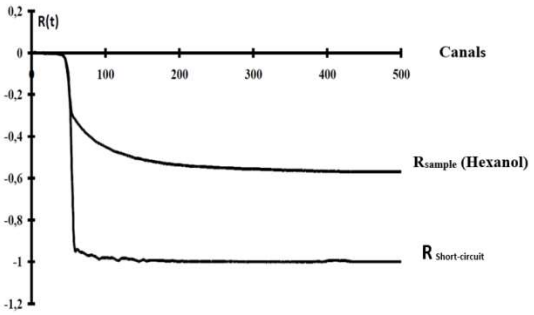

Figure II.7. Real signals obtained by the first reflection method.

In this two-step experiment, the $R_{ec}(t)$ signal reflected by the air/dielectric interface is recorded first. Then it is the signal $R_{cc}(t)$, reflected by the short circuit placed at the place precisely occupied by the front face of the material, which is recorded Thus, the signals $R_{ec}(t)$ and $R_{cc}(t)$ are located relative to the same origin of times. Reflection is given by the relationship[10]:

$$\rho(\omega) = -\frac{\int_{-c}^{+\infty} R_{ec}(t)\exp(-j\omega t)dt}{\int_{-c}^{+\infty} R_{cc}(t)\exp(-j\omega t)dt} = -\frac{R_{ec}(\omega)}{R_{cc}(\omega)}\frac{H(\omega)}{H(\omega)} \quad \text{(II.14)}$$

As $Z = \frac{Z_0}{\sqrt{\varepsilon}}$Where Z represents the characteristic impedance of the material and Z0 is the characteristic impedance of the coaxial airline, this leads to:

$$\mathrm{R} = \rho = \frac{Z-Z_0}{Z+Z_0} = \frac{1-\sqrt{\varepsilon}}{1+\sqrt{\varepsilon}} \quad \text{(II.15)}$$

Complex permittivity is thus simply obtained by:

$$\varepsilon = \left(\frac{1-\rho}{1+\rho}\right)^2 \quad \text{(II.16)}$$

This method is characterized by extreme simplicity and ease of implementation. This makes it a method of choice for the study of liquids for which we can obtain sufficiently long samples [11].

However, this method has several disadvantages, three of which seem to be the most fundamental:

1- The sample must be the longer we are in the presence of low-frequency relaxations to take into account the decay of the temporal response curve.

2- In the general case where one cannot separate permittivity and permeability because then we only have information:

$$\frac{\varepsilon}{\mu} = \left(\frac{1-\rho}{1+\rho}\right)^2 \quad \text{(II.17)}$$

However, for magnetic field studies [13] where permittivity does not vary based on B: $\varepsilon(B \neq 0) = \varepsilon(B = 0)$, allows us to study the variations of:

$$\mu = \varepsilon\left(\frac{1+\rho}{1-\rho}\right)^2 \quad \text{(II.18)}$$

3- Finally, the main drawback of this method lies in the control of a possible shift in the origin of time. Indeed, the dynamics of the phases is extremely weak considering that:

$$\rho = \frac{1-\sqrt{\varepsilon}}{1+\sqrt{\varepsilon}} = \frac{1-n'+jn''}{1+n'-jn''} \tag{II.19}$$

where $n=\sqrt{\varepsilon}$ =n'- jn" is the electromagnetic index of the medium. We can write the reflection coefficient also in the form of:

$$\rho = R(\rho) + jI(\rho) = |\rho| \exp(-j\phi) \tag{II.20}$$

With

$$\phi = \text{Artg}\left(\frac{n''}{n'-1}\right) - \text{Artg}\left(\frac{n''}{n'+1}\right) \tag{II.21}$$

In our case n" is much lower than n' which implies that always remains weak hence the difficulty of experimentation. Even a very small variation in the origin of times will result in a parasitic phase variation which can be of the same order of magnitude as ϕ. Indeed, if we consider the reference signal R_{cc} (t) (corresponding to the measurement of a short circuit) and the time signal given by the sample shifted by a quantity t, the response obtained after the use of a Fourier transform is given by:

$$R_{shif}(\omega) = \frac{TFD[V(t+\delta t)]}{TFD[R_{cc}(t)]} = \frac{\Delta t \sum_0^N V(t+\delta t)\exp(-jt\omega)}{\Delta t \sum_0^N R_{cc}(t)\exp(-j\omega t)} \tag{II.22}$$

where $R_{shif}(\omega)$represents the obtained signal, we still have:

$$R_{shif}(\omega) = \frac{\sum_0^N V(t)\exp(-j\omega t)\exp(-j\delta\omega t)}{\sum_0^N R_{cc}(t)\exp(-jt\omega)} \tag{II.23}$$

Thus, it follows that $R_{shif}(\omega) = R(\omega)\exp(-j\omega\delta t)$ where R(ω) is the desired signal. There is a phase correction term $\exp(-j\omega\delta t)$ between the two expressions. Even for extremely small values of δt, this correction can become significant at the high-frequency limits of the band of interest, particularly for materials with low losses. This problem is no longer a constraint because the new generation of spectrometers allows for the definition of time t=0 with excellent precision from an experimental point of view.

This method, which is perfectly suited for liquids (long samples), could not be adopted in this work (short samples). Therefore, we have tried to determine the protocols best suited to our research by using the properties of multiple reflections.

II.3.1.3 Multi-Reflection Methods

When using these methods, we assume that the waves propagate in a perfect air line upstream of the sample. Unlike the previous method, it is not necessary to use long samples to characterize them. Several protocols that allow the definition of the electromagnetic parameters of the material are presented, each time considering its thickness d, its permittivityε , and its terminal load impedance Z_tEach protocol will be critically examined regarding its application domains for magnetic or non-magnetic, conductive or non-conductive materials, in order to choose the most suitable method for the present work.

II.3.1.3.1 The Short-Circuited Line Method

On the oscilloscope, the generated step is visualized, and after a duration T, an inverted polarity pulse with attenuation depending on the length and losses of the cable is observed. In practice, this can correspond to an accidental cut or crushing of a cable that has created a short circuit.

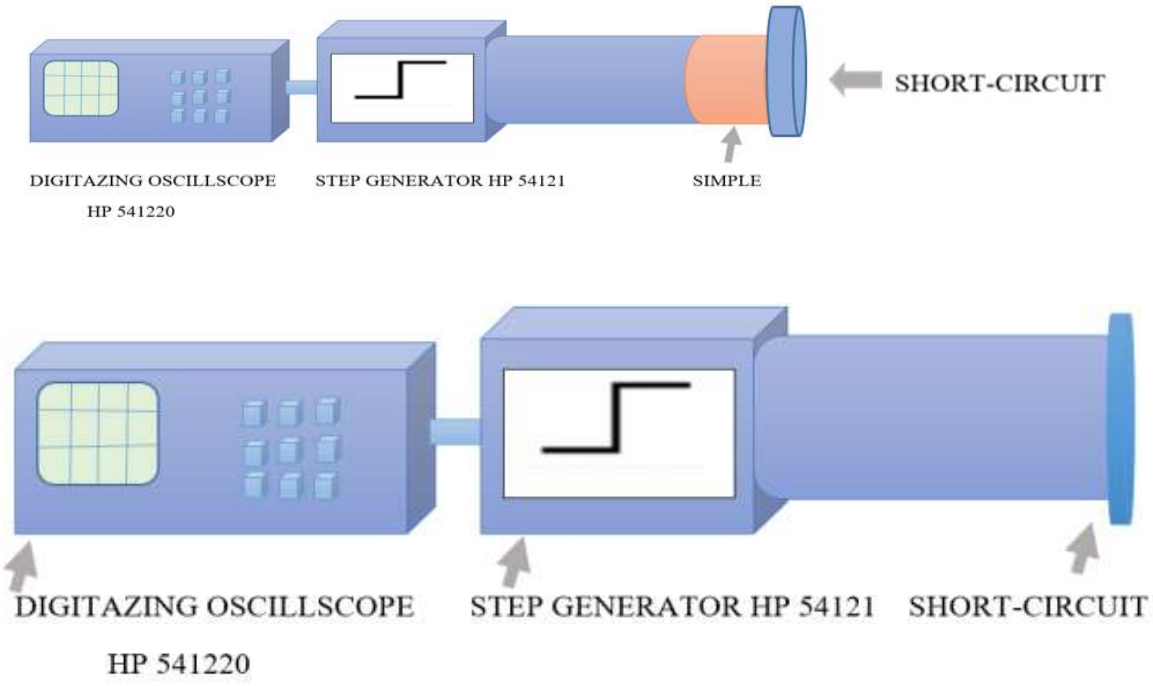

Figure II.8. Representation of the measurement setup for a short-circuited line

(Figure II.9) shows the multiple reflections in the sample and their influences on the time-domain signal.

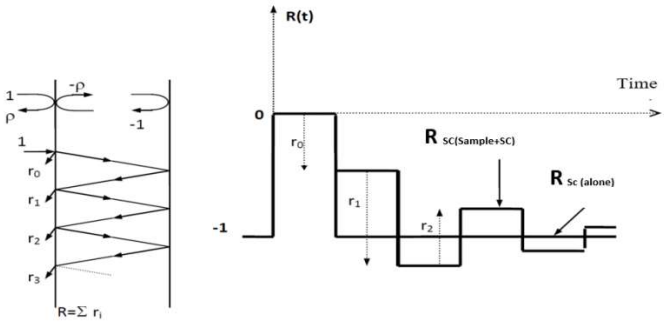

Figure II.9. Representation of multiple reflections for the short-circuited line method

(Figure II.10) shows an example of real signals obtained with and without the sample in the time domain.

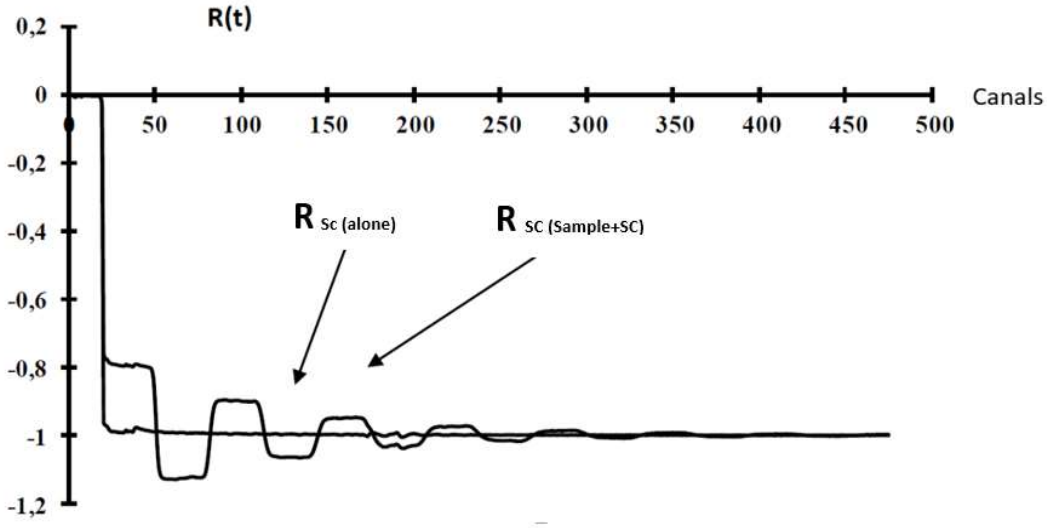

Figure II.10. Representation of reflected signals obtained by the short-circuited line method (for a dielectric medium)

This method has been the subject of numerous studies and articles in the laboratory [8, 17, 18, 19]. It consists of setting $Z_t = 0$, that is to say $\rho = -1$. Under these conditions, we obtain:

$$\rho_1 = \rho = \frac{1-\sqrt{\varepsilon}}{1+\sqrt{\varepsilon}} \qquad \text{(II.24)}$$

From (II.24), the overall reflection coefficient is expressed as:

$$R_c(\omega) = \frac{\rho - \exp(-2\gamma d)}{1-\rho \exp(-2\gamma d)} \qquad \text{(II.25)}$$

with, of course, $T_c(\omega) = 0$.

This method, widely used for specific frequencies, seems less interesting for characterizing dielectric materials over a wide band. To convince ourselves of this, let us calculate the impedance of the material plus the terminal load combination. It results in:

$$Z = \frac{1+\mathbf{R_c}}{1-\mathbf{R_c}} = [\frac{1+\rho}{1-\rho}] \frac{1-\exp(-2\gamma \mathbf{d})}{1+\exp(-2\gamma \mathbf{d})} = \sqrt{\frac{\mu}{\varepsilon}}\,\mathrm{th}(\gamma \mathrm{d}) \qquad \text{(II.26)}$$

At low frequency, when γd << 1, we can expand this expression to the first order as follows:

$$\mathbb{Z} \cong \sqrt{\frac{\mu}{\varepsilon}}(j\frac{\omega}{c}\sqrt{\varepsilon\mu}d) = j\mu\frac{\omega}{c}d \qquad \text{(II.27)}$$

As a result, the permittivity of the material to be studied becomes difficult to determine at low frequencies for thin samples, as the dependence on ε only appears in the second order. In fact, this method will mainly be used for permeability measurements on magnetic materials or materials of considerable length.

Another inherent difficulty with this method is that the equation to solve for permittivity from Rc is transcendental, which requires the use of an iterative method. However, a simple solution can be obtained if one has a material with two thicknesses that are double each other. In this case, the expressions for the impedances for the two thicknesses are:

$$\mathbb{Z}_1 = \sqrt{\frac{\mu}{\varepsilon}}\,\mathrm{th}\left(\mathrm{j}\frac{\omega}{c}\mathrm{d}\sqrt{\varepsilon\mu}\right) \qquad \text{(II.28)}$$

$$\mathbb{Z}_2 = \sqrt{\frac{\mu}{\varepsilon}}\,\mathrm{th}\left(\mathrm{j}\frac{\omega}{c}2\mathrm{d}\sqrt{\varepsilon\mu}\right) \qquad \text{(II.29)}$$

If we then set $\mathrm{p} = \frac{Z_1}{Z_2}$ and $\mathrm{x} = \exp(-2\mathrm{j}\frac{\omega}{\mathrm{c}}\mathrm{d}\sqrt{\varepsilon\mu})$ we obtain

$$\mathbf{p} = \left(\frac{1-\mathbf{x}}{1+\mathbf{x}}\right)\left(\frac{1+\mathbf{x}^2}{1-\mathbf{x}^2}\right) = \frac{1+\mathbf{x}^2}{(1+\mathbf{x})^2} \qquad \text{(II.30)}$$

thus, finally, knowing x, we obtain $C_1 = \sqrt{\varepsilon\mu}$, which we substitute into the expression for \(Z_1 \), and we have: $C_2 = \sqrt{\frac{\mu}{\varepsilon}}$. Thus, finally $\varepsilon = \frac{C_1}{C_2}$ And $\mu = C_1 C_2$

Another method involves using the method of the movable short-circuit (Figure II.11): the short-circuit can occupy any position behind the sample, and one can thus determine the overall reflection coefficient R_m, which also leads to solving a transcendental equation. However, the major difficulty lies in maintaining electrical contact between the guide and the short circuit as it is moved.

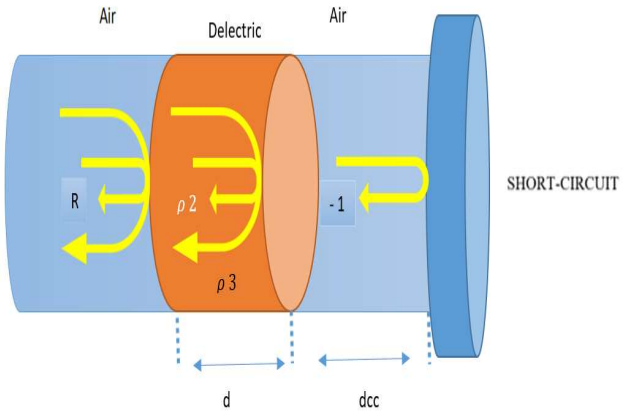

Figure II.11. Measurement setup for the movable short-circuit method.

II.3.1.3.2 The Matched Line Method (ZT = Z0)

The material is placed in an airline, terminated by its characteristic impedance *Z*0 (50 Ohms); in this case, the overall wave transmitted through the sample cannot return to it. We provide the experimental setup used in (Figure II.12) below[20].

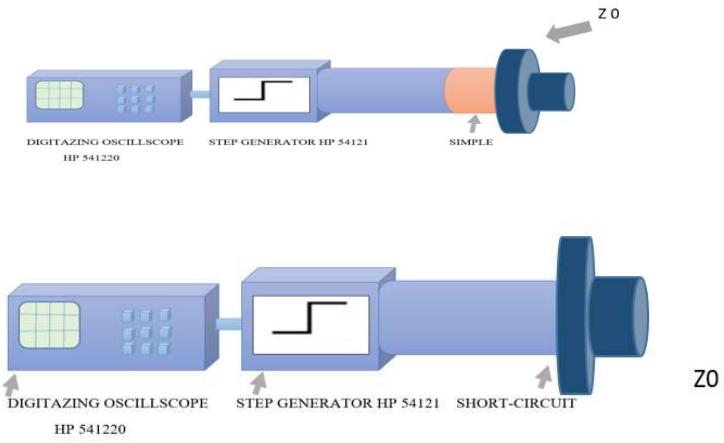

Figure II.12. Representation of the measurement setup of a matched line

The corresponding signals are schematically represented below for the transmission Tca and the reflection Rca:

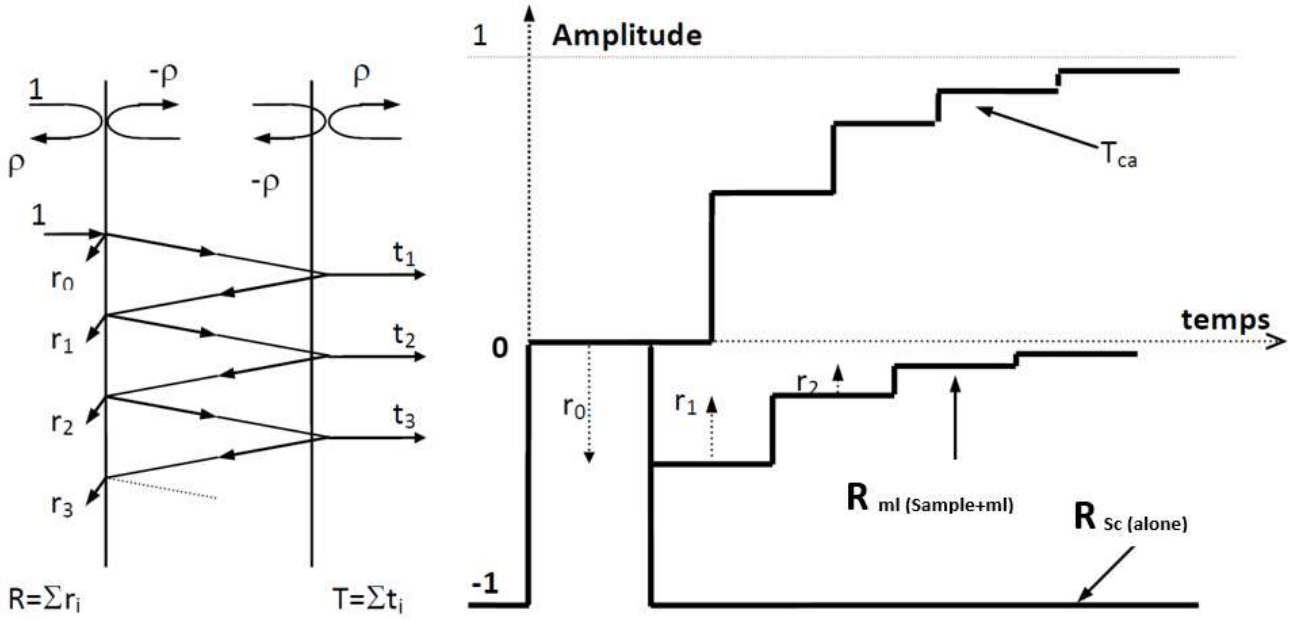

Figure II.13. Representation of multi-reflections for the matched line method

We also present in the following figures the different real signals obtained during measurements on materials exhibiting the following characteristics:

- A pure dielectric medium, PVC ($\sigma = 0$, $\mu = 0$), whose real signals are shown in Figure II.14.
- A material exhibiting non-zero conductivity ($\sigma \neq 0$ and $\mu = 0$), specifically non-deionized water, whose real signals are shown in Figure II.15.
- Lastly, a magnetic material, a ferrite ($\mu \neq 0$ and $\sigma = 0$), whose real signals are given in Figure II.16.
- Finally, we present in Figure II.17 a synthesis of the different behaviors observed previously.

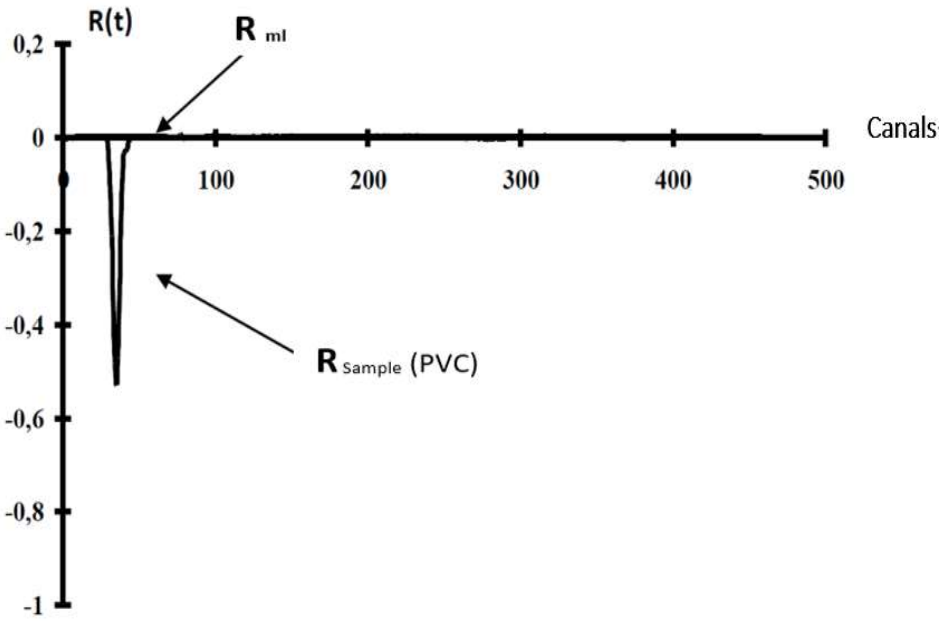

Figure II.14. Representation of reflected signals for the matched line method (for a pure dielectric medium: PVC)

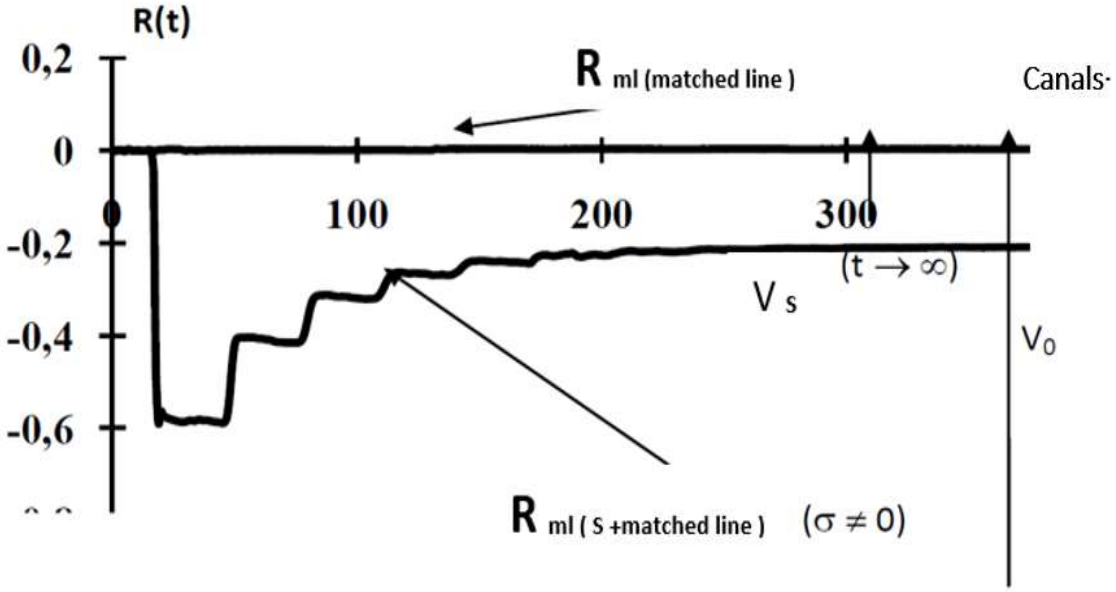

Figure II.15. Representation of reflected signals for the matched line method (for aconductive dielectric medium).

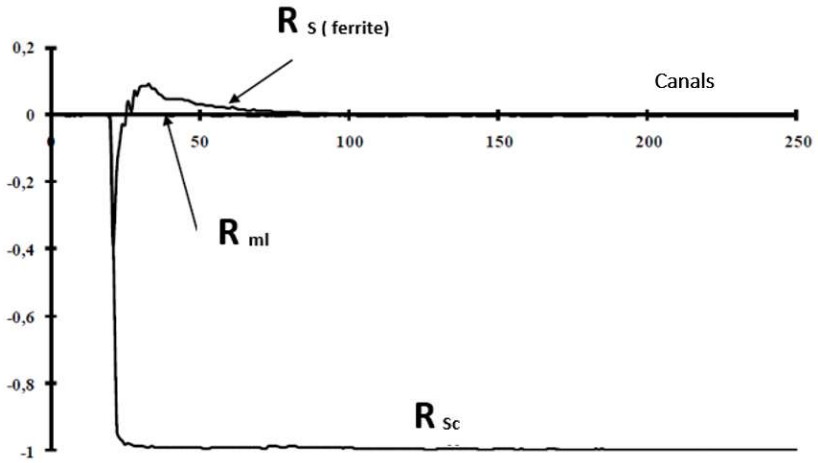

Figure II.16. Representation of reflected signals for the matched line method for a magnetic dielectric medium (ferrite)**.**

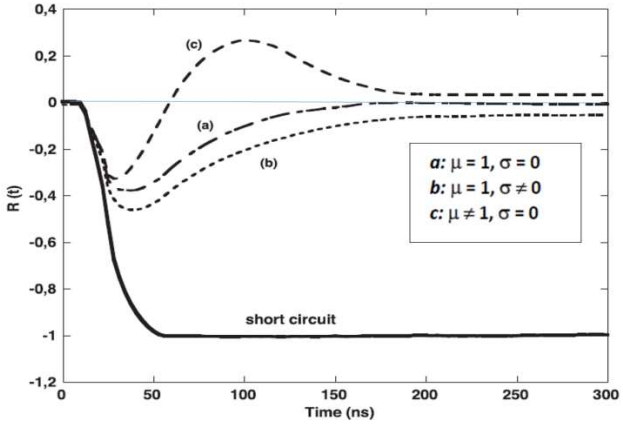

Figure II.17. Schematic representation of the different time responses in matched lines according to the electromagnetic characteristics of the material

Figure (II.17) shows that this experimental protocol allows directly visualizing on the oscilloscope screen the properties of the material, thus enabling the selection of the most suitable method for studying a material with undefined characteristics a priori.

For this experimental protocol, at the level of the first interface:

$$\rho_1 = \rho = \frac{1-\sqrt{\varepsilon}}{1+\sqrt{\varepsilon}} \qquad \text{(II.31)}$$

While at the second interface, we will have:

$$\rho_2 = \frac{\sqrt{\varepsilon}-1}{\sqrt{\varepsilon}+1} = -\rho \qquad \text{(II.32)}$$

The expressions giving the reflection and transmission coefficients are then of the form, with $\gamma_1 = \gamma_3 = \gamma_0$ and $\gamma_2 = \gamma$, the propagation coefficient of the studied medium:

$$R = \frac{\rho(1-\exp(-2\gamma d))}{1-\rho^2 \exp(-2\gamma d)} \quad \text{(II.33)}$$

$$T = \frac{(1-\rho^2)\exp(-\gamma d)}{1-\rho^2 \exp(-2\gamma d)} \quad \text{(II.34)}$$

From the expression of the reflection coefficient, we can deduce the admittance of the sample plus terminal load combination. Indeed:

$$Y = \frac{1}{Z} = \frac{1-R}{1+R} \quad \text{(II.35)}$$

So we have directly:

$$Y = \left[\frac{1-\rho}{1+\rho}\right] \frac{1+\rho\exp(-2\gamma d)}{1-\rho\exp(-2\gamma d)} \quad \text{(II.36)}$$

The first term of this expression corresponds to the admittance of the input interface of the sample (air/material), and the second term corresponds to the contribution of multiple reflections within the sample. In the general case where the sample has a non-zero permeability, it follows:

$$Y = \sqrt{\frac{\varepsilon}{\mu}} \frac{\sqrt{\mu}+\sqrt{\varepsilon}+(\sqrt{\mu}-\sqrt{\varepsilon})\exp(-2j\frac{\omega}{c}d\sqrt{\varepsilon\mu})}{\sqrt{\mu}+\sqrt{\varepsilon}-(\sqrt{\mu}-\sqrt{\varepsilon})\exp(-2j\frac{\omega}{c}d\sqrt{\varepsilon\mu})} \quad \text{(II.37)}$$

So, furthermore:

$$Y = \sqrt{\frac{\varepsilon}{\mu}} \frac{\sqrt{\mu}\left(1+exp(-2j\frac{w}{c}d\sqrt{\varepsilon\mu})\right)+\sqrt{\varepsilon}\left(1-exp(-2j\frac{w}{c}d\sqrt{\varepsilon\mu})\right)}{\sqrt{\mu}\left(1-exp(-2j\frac{w}{c}d\sqrt{\varepsilon\mu})\right)+\sqrt{\varepsilon}\left(1+exp(-2j\frac{w}{c}d\sqrt{\varepsilon\mu})\right)} \quad \text{(II.38)}$$

Which finally becomes:

$$Y = \sqrt{\frac{\varepsilon}{\mu}} \frac{1+\sqrt{\frac{\varepsilon}{\mu}}\text{th}\left(j\frac{w}{c}d\sqrt{\varepsilon\mu}\right)}{\text{th}\left(j\frac{w}{c}d\sqrt{\varepsilon\mu}\right)+\sqrt{\frac{\varepsilon}{\mu}}} \quad \text{(II.39)}$$

If we consider the particular case where μ= 1, the previous relation simplifies, and we obtain:

$$Y = \sqrt{\varepsilon} \frac{1+\sqrt{\varepsilon}\text{th}\left(j\frac{\omega}{c}d\sqrt{\varepsilon}\right)}{\text{th}\left(j\frac{\omega}{c}d\sqrt{\varepsilon}\right)+\sqrt{\varepsilon}} \quad \text{(II.40)}$$

This equation is transcendental, and its solution requires computational processing, which we will develop later.

However, as we have seen previously, this method has the great merit of defining, through simple observation of temporal signals, the type of materials we are dealing with (Figure 2.19), thus allowing a choice of the protocol to use. Furthermore, if we perform an asymptotic expansion at long times considering that the quantity γd is very small ($\gamma d << 1$), we obtain for $t \to \infty (\omega \to 0)$:

$$exp(-2\gamma d) = 1 - 2\gamma d \quad \text{(II.41)}$$

Under these conditions, the reflection coefficient becomes equal to:

$$R(\omega \to 0) = \frac{2\rho\gamma d}{1-\rho^2+2\rho^2\gamma d} \quad \text{(II.42)}$$

So by replacing it with its value, we obtain:

$$R(\omega \to 0) = \frac{(1-\varepsilon)2j\frac{\omega}{c}d\sqrt{\varepsilon}}{4\sqrt{\varepsilon}+(1-\sqrt{\varepsilon})^2 2j\frac{\omega}{c}d\sqrt{\varepsilon}} = \frac{(1-\varepsilon)j\frac{\omega}{c}d}{2+(1-\sqrt{\varepsilon})^2 j\frac{\omega}{c}d} \quad \text{(II.43)}$$

If we consider a sample with conductivity, the permittivity is written in the form $\varepsilon = \varepsilon' - j\varepsilon'' - j\sigma/(\omega\varepsilon_0)$, and we will have:

$$R(\omega \to 0) = \frac{(1-\varepsilon'+j\varepsilon''+j\frac{\sigma}{\varepsilon_0\omega})j\frac{\omega}{c}d}{2+\left(1-\sqrt{\varepsilon'-j\varepsilon''-j\frac{\sigma}{\varepsilon_0\omega}}\right)^2 j\frac{\omega}{c}d} \quad \text{(II.44)}$$

For $\omega = 0$, we obtain:

$$R(\omega = 0) = -\frac{\frac{\sigma}{c\varepsilon_0}d}{2+\frac{\sigma}{c\varepsilon_0}d} \quad \text{(II .45)}$$

which leads to:

$$\frac{\sigma}{\varepsilon_0} = -\frac{c}{d}\frac{2R(\omega=0)}{1+R(\omega=0)} = -\frac{c}{d}\frac{2R(t\to\infty)}{1+R(t\to\infty)} \quad \text{(II.46)}$$

Another advantage of this method is to simply obtain the DC conductivity of the material from the asymptotic value of $R_{ec}(t)$. In our experiments, we will use as a reference the difference between the value of the signal at long times given by a short circuit $R_{cc}(\omega) = 1$ and that given by the matched line $R_{la}(\omega) = 0$. By associating with the reflection, the transmission coefficient, as well as Nicolson's method, we can obtain ϵ and μ. This is a derivative of the method commonly used with network analyzers[8].

II.3.1.3.3 The Open Line Method (ZT = ∞ and YT = 0).

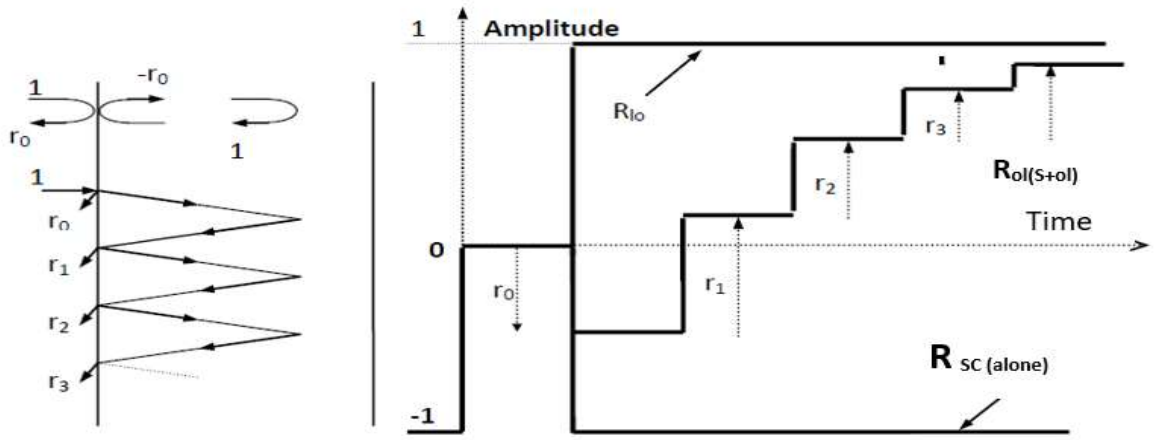

Figure II.18. Representation of multi-reflections for the open-line method

This figure shows the real signals obtained for the open line alone, and then with a material exhibiting high conductivity and a Teflon plate ($\varepsilon' \cong 2{,}1$). It can be observed that the signals of the open line and the Teflon are practically overlapping in the time domain, making them difficult to model using other techniques (such as TLM) and highlighting the importance of harmonic analysis.

The difficulty of this method lies in achieving a null terminal admittance (ideal line). Indeed, for a fixed frequency in guided measurement, it is relatively easy to satisfy this requirement by placing a short circuit at $\frac{\lambda}{4}$the back face of the sample. However, it is much more challenging to achieve such experimental

conditions in broadband devices. This is because, as shown by Markuvitz through variational treatment[8,21] in his work, the phase reference is shifted downstream.

At the Laboratory, A. Merzouki [22,23] developed this open line technique by working with a coaxial (propagation line) - circular cutoff (measurement cell) transition, establishing the modal equations related to propagation and their connection to the evanescent waves generated in the cylindrical cell. Then, A. Boutaudon [24] addressed the issue of planar probes, which, beyond solving the modal equations in the coaxial part, must be connected to integral equations governing propagation in free space (field continuity). These are extremely difficult problems to tackle rigorously, especially in planar probes, for which it becomes essential to establish charts allowing the complex permittivity to be obtained from the complex impedance provided by the measurement. A complete bibliography of the studies conducted on the open line can be found in the theses of A. Merzouki and A. Boutaudon [21,24]. Here, we have highlighted some of them that appeared to be the most significant from the authors' perspective [25,].

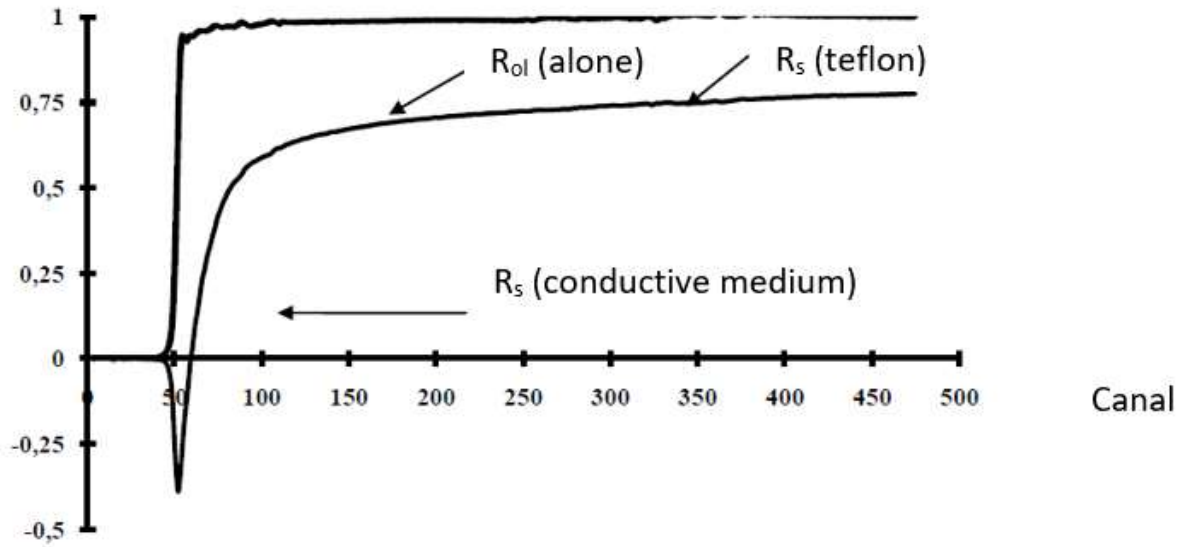

Figure II.19. Representation of reflected signals for the open line method

In the case of the ideal open line (terminal admittance null without presenting any phase shift), which is never the case but a good approximation, at low frequency and to grasp the problem, the reflection at the dielectric interface / terminal load is equal to $\rho_2 = 1$. Since the sample is always placed in a lossless airline, we have:

$$\rho_1 = \rho = \frac{1-\sqrt{\varepsilon}}{1+\sqrt{\varepsilon}} \qquad \text{(II.47)}$$

The reflection coefficient is then given by:

$$R = \frac{\rho + \exp(-2\gamma d)}{1 + \rho \exp(-2\gamma d)} \quad \text{(II.48)}$$

Which finally leads to the overall admittance of the system:

$$Y = \frac{1-R}{1+R} = \left[\frac{1-\rho}{1+\rho}\right] \frac{1-\exp(-2\gamma d)}{1+\rho \exp(-2\gamma d)} \quad \text{(II.49)}$$

Which is finally:

$$Y = \frac{1-R}{1+R} = \frac{1-\rho}{1+\rho} \text{th}(\gamma d) \quad \text{(II.50)}$$

Which can also be written considering the general case where ε and μ are non-zero:

$$Y = \sqrt{\frac{\varepsilon}{\mu}} \text{th}\left(j \frac{\omega}{c} d \sqrt{\varepsilon \mu}\right) \quad \text{(II.51)}$$

If we perform a series expansion of the hyperbolic tangent at low frequency, we obtain:

$$Y \cong \sqrt{\frac{\varepsilon}{\mu}} j \frac{\omega}{c} d \sqrt{\varepsilon \mu} \quad \text{(II.52)}$$

So that:

$$Y \cong j \frac{\omega d}{c} \varepsilon \quad \text{(II.53)}$$

The variation of the admittance is of the first order in ε, while the dependence on μ only appears at higher orders. Therefore, this method is particularly well-suited for studying dielectric materials, but it is not effective for measurements of magnetic materials.

It is also worth noting that this method is valuable for studying conductivities σ. Indeed, by expanding the above formula, we obtain:

$$Y(\omega \to 0) = j \frac{\omega}{c} d\left(\varepsilon' - j\varepsilon'' - j \frac{\sigma}{\omega \varepsilon_0}\right) \quad \text{(II .54)}$$

So when: $\omega = 0(\mathrm{t} \to \infty)$: $\mathrm{Y}(\omega = 0) = \frac{\sigma}{\varepsilon_0}\frac{\mathrm{d}}{\mathrm{c}} = \mathrm{Y}(\mathrm{t} \to \infty)$

$$\sigma = \frac{\varepsilon_0 c}{d}\mathrm{Y}(\mathrm{t} \to \infty) \quad \text{(II.55)}$$

II.4 .RECTANGULAR WAVEGUIDE

The principle of electromagnetic characterization of dielectric materials using a rectangular waveguide. We will describe two approaches to follow: one uses a fixed-frequency measurement bench, and the other uses a network analyzer to cover the bandwidth of the waveguide's dominant mode.

III.4.1 Fixed-Frequency Measurement Bench

Fixed-frequency measurements are carried out using a device consisting of a microwave generator based on a Gunn diode [25]. Downstream, the measurement line is composed of a unidirectional line, preventing the source from being disturbed by reflections. Next, there is a modulator and another unidirectional line. Following this is the measurement device, which consists of a line for measuring the Standing Wave Ratio (SWR). Finally, we have the measurementsIn this method, two measurements are performed: one without the sample and one with the sample in the shape of the waveguide and of thickness, which is placed inside the waveguide against the short circuit.

The port of the waveguide is excited by a microwave signal. This signal propagates inside a rectangular waveguide until it encounters the upstream interface of the sample. Part of the energy is reflected, while the other part continues to propagate through the sample, with or without attenuation depending on whether the material is absorptive or not. Finally, the part that reaches the short circuit is completely reflected. ent cell, which ends with a short circuit.

II.4.2. Determination of Electrical Permittivity

For the propagation of the TE01 mode in a rectangular waveguide filled with lossy dielectric, the general propagation equation is written as [27-29]:

$$\Delta\mathrm{E} - \varepsilon_1\mu_1\frac{\delta^2\mathrm{E}}{\delta\mathrm{t}^2} = 0 \quad \text{(II.56)}$$

ε_1 :complex electrical permittivity (absorbing dielectric).

μ_1 :real magnetic permeability($\mu_1 = \mu_0$ for non-magnetic medium).

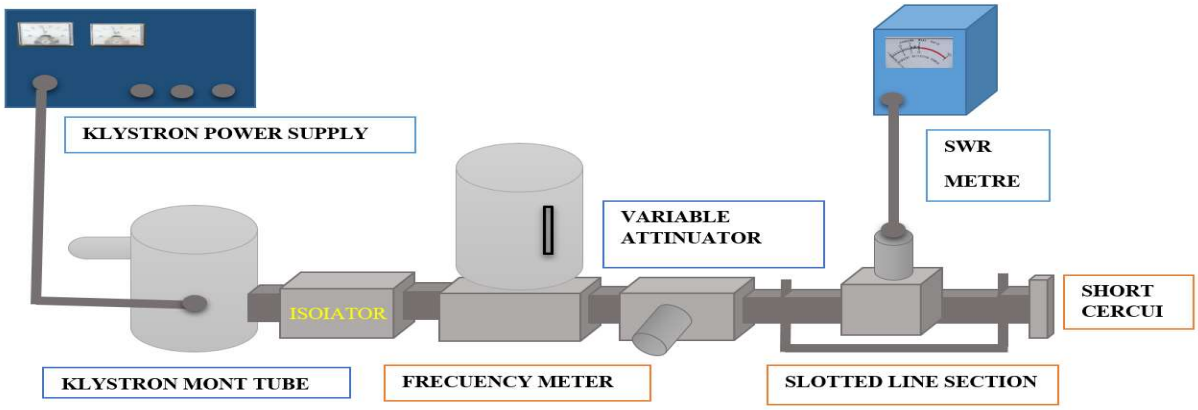

Figure II.20. Rectangular waveguide

By analogy with free propagation, taking into account the boundary conditions, we can seek a solution of the form:

$$E_y = E_0 Cos\frac{\pi x}{a} Exp(j\omega t - \gamma_{1g} z) \quad \text{(II.57)}$$

$$E_x = 0 \quad \text{(II.58)}$$

$$E_z = 0 \quad \text{(II.59)}$$

Where b is the dimension of the long side of the waveguide, and γ is the guided propagation constant in the dielectric filling the waveguide.

$$\gamma_{\lg} = \alpha_{\lg} + j\beta_{\lg} \quad \text{(II.60)}$$

$\alpha_{\lg}$:attenuation constant of the line.

$\beta_{\lg} = \frac{2\pi}{\lambda_{\lg}}$:phase constant.

The electric field $\bar{E}$ is parallel to the axis Oy. Calculating the Laplacian of the field involves writing $E_y = E$ as:

$$\Delta E = \frac{-\pi^2}{a^2} E + \gamma_{\lg}^2 E \quad \text{(II.61)}$$

When writing $\frac{\delta^2 E}{\delta t^2} = -\omega^2 E$, equation (II.56) thus becomes:

$$\gamma_{\lg}^2 = 4\pi^2 \left[\frac{1}{4a^2} - \frac{\varepsilon_1 \mu_1}{T^2}\right] \quad \text{(II.62)}$$

T:The period of the radio frequency signal.

$$\varepsilon_1 \mu_1 = \mu_r \mu_0 \varepsilon_r \varepsilon_0 = \frac{\mu_r \varepsilon_r}{c^2} \quad \text{(II.63)}$$

C: The speed of light in a vacuum. and $\mu_r = 1$ from where $\frac{\varepsilon_1 \mu_1}{T^2} = \frac{\varepsilon_r}{c^2 T^2} = \frac{\varepsilon_r}{\lambda_0^2} = \frac{\varepsilon_r' - j\varepsilon_r''}{\lambda_0^2}$

λ_0 :The wavelength in vacuum in free space.

Furthermore, the cutoff wavelength of the waveguide is given by:$\lambda_c = 2a$

$$\left(\alpha_{\lg} + j\beta_{\lg}\right)^2 = 4\pi^2 \left[\frac{1}{\lambda_c^2} - \frac{\varepsilon_r' - j\varepsilon_r''}{\lambda_0^2}\right] \quad \text{(II.64)}$$

Separating real and imaginary parts, we obtain:

$$\varepsilon_r' = \frac{\lambda_0^2}{\lambda_c^2} + \frac{\lambda_0^2}{4\pi^2}\left[\beta_{\lg}^2 - \alpha_{\lg}^2\right] \quad \text{(II.65)}$$

$$\varepsilon_r = \frac{\lambda_0^2}{4\pi^2}\left[2\alpha_{\lg}\beta_{\lg}\right] \quad \text{(II.66)}$$

As the parameters ($\alpha_{\lg}$ and $\beta_{\lg}$) are not directly accessible to measurement, we must use a measurement technique based on the measurement of the standing wave ratio (SWR) in the empty part of the guide and

the measurement of the abscissas, the minimum, and the maximum of the field. These measurements allow us to determine the electrical permittivity.

II.4.2.1. Short-circuited line method

Consider a waveguide closed by a metallic mirror. If only the short circuit were present, a system of standing waves with zero minima would be obtained. One of the main variants of the short-circuited line

method consists of modifying the phenomenon of standing waves by placing a parallel-faced dielectric slab of the studied material against the short circuit inside the waveguide [27; 30; 31]

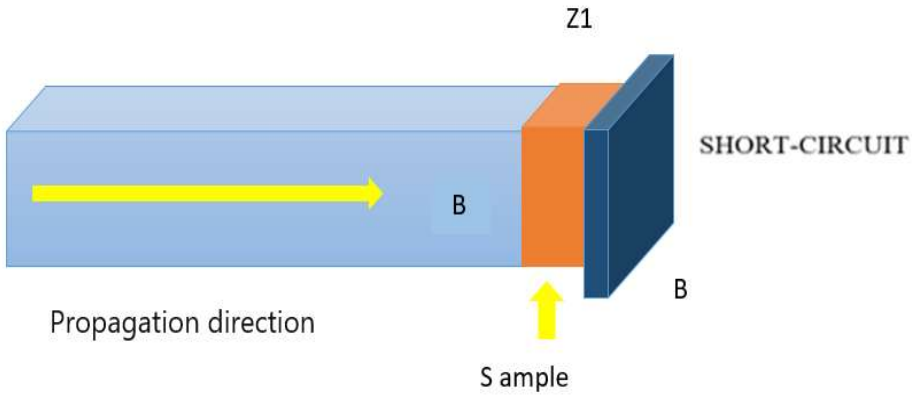

Figure III.21. Waveguide loaded by the sample and the short circuit

The determination of the standing wave ratio (SWR) and the position of a minimum ahead of the sample allows for the deduction of the complex reflective impedance ahead of B [27]. This complex reflective impedance is related to $\gamma_{\lg}$, indeed:

- The impedance reduced at the short circuit level A is zero.$z_2 = 0$
- The impedance reduced at B relative to the medium (1) is:

$$z_{\mathrm{B}} = th(\gamma_{\lg} e) \tag{II.67}$$

The reflective impedance at B is then:

$$z_1 = \frac{z_{\lg} th(\gamma_{\lg} e)}{z_{0\mathrm{g}}} \tag{II.68}$$

$\mathbb{Z}_{\lg}$ and Z_{0g} are the characteristic impedances of media (1) and (0).

Due to the invariance of the product $z_{lg}\gamma_{lg}$ and taking into account that $\mu_r = 1$ we can write:

$$z_{\lg}\gamma_{\lg} = z_{0g}\gamma_{0g} = z_{0g}\left(j\frac{2\pi}{\lambda_{0g}}\right) \tag{II.69}$$

$$\left(\beta_{0g} = j\frac{2\pi}{\lambda_{0g}} \text{ in a vacuum}\right)$$

$$\frac{z_{1g}}{z_{0g}} = z_{1g} = \frac{j2\pi}{\lambda_{0g}} \frac{1}{\gamma_{1g}} \quad \text{(II.70)}$$

And

$$z_1 = \frac{j2\pi}{\lambda_{0g}} \frac{th(\gamma_{1g}e)}{\gamma_{1g}e} \quad \text{(II.71)}$$

We are thus led to perform the following two operations:; measure z_1; solve equation (II.71)

II.4.2.3 Measurement Technique

The reflective impedance Z_1 is deduced from the study of the standing wave system existing in front of the dielectric. This study is done using the measurement of the standing wave ratio θ and d_m related to Z_1 by the formula:

$$z_1 = \frac{1+j\theta tg(\beta_{0g}d_m)}{\theta+jtg(\beta_{0g}d_m)} \quad \text{(II.72)}$$

Where θ is the standing wave ratio (SWR). and d_m represents the difference between minima.

II.4.2.3.1. Determination of dm

The d_m is determined as follows:

We locate a minimum when the sample is present. Let X_m be the reading (the rule is positively graduated towards the source).

The sample is removed. We locate the first minimum encountered by moving from X_m towards the source. Let X'_m be the reading.

d_m is calculated by:

$$d_m = X'_m - X_m + e. \quad \text{(II.73)}$$

e : is the thickness of the sample.

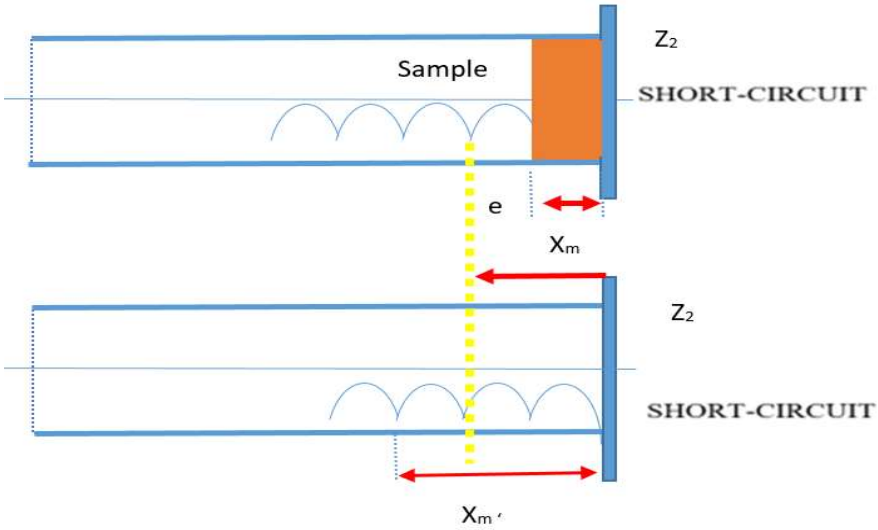

Figure II.22. Principle of measuring the distance to the minimum (in the presence and absence of the sample).

II.4.2.3.2 Determination of θ

a- Direct method for low T.O.S.

θ is the ratio of the field amplitude at a maximum to the field amplitude at a minimum. If the response of the detector crystal is quadratic, the detected current is proportional to the square of the field modulus:

$$\theta = \frac{|E|_{max}}{|E|_{min}} \tag{II.74}$$

b- Double Minimum Method for a High T.O.S.

Positions on either side of the minimum where the detected current is double the minimum current are noted. Let Δx be the corresponding displacement; from this, for a quadratic response law of the detector, we deduce [27] [32]:

$$\theta = \frac{\lambda_{0g}}{\pi \Delta x} \tag{II.75}$$

c- Corrections to be Applied to T.O.S Measurements

For a line of length **l**, with characteristic impedance $\mathbb{Z}_c$, terminated on $\mathbb{Z}_t$; the normalized input impedance is:

$$z_0 = \frac{z_t + th(\gamma l)}{1 + z_t th(\gamma l)} \tag{II.76}$$

The reflection coefficient at the input:

$$\rho = \frac{z_0-1}{z_0+1} = \frac{1-th(\gamma l)}{1+th(\gamma l)}\frac{z_t-1}{z_t+1} = \rho_v \frac{1-th(\gamma l)}{1+th(\gamma l)} \quad \text{(II.77)}$$

ρ_v is the true reflection coefficient of z_t: if $z_t = 0, \rho_v = -1$, and:

$$\rho_{cc} = -\frac{1-th(\gamma l)}{1+th(\gamma l)} \quad \text{(II.78)}$$

ρ_{cc} is the reflection coefficient at the input of the short-circuited line.

Let's write:

$$|\rho_m| = \frac{\theta_m - 1}{\theta_m + 1}$$

$$|\rho_{cc}| = \frac{\theta_{cc} - 1}{\theta_{cc} + 1}$$

$$|\rho_v| = \frac{\theta_v - 1}{\theta_v + 1}$$

ρ_m is the measured reflection coefficient at the input:

$$|\rho_m| = |\rho_v|.|\rho_{cc}|$$

$$\frac{\theta_v - 1}{\theta_v + 1} = \frac{\theta - 1}{\theta + 1}\frac{\theta_{cc} + 1}{\theta_{cc} - 1}$$

So:

$$\frac{\theta\theta_{cc} - 1 + \theta - \theta\theta_{cc}}{\theta\theta_{cc} - 1 - \theta + \theta_{cc}} = \frac{\theta_v - 1}{\theta_v + 1}$$

$$\theta_v = \frac{\theta\theta_{cc} - 1}{\theta_{cc} - \theta} \quad \text{with} \quad \theta\theta_{cc} >> 1$$

This leads to the simple relationship [33]:

$$\frac{1}{\theta_v} = \frac{1}{\theta_m} - \frac{1}{\theta_{cc}} \quad \text{(III.79)}$$

II.5. conclusion:

In conclusion, this chapter delves deeply into the realm of measurement techniques, emphasizing the wideband and X-band technologies that are crucial for material characterization. By employing tools like Time Domain Reflectometry (TDR) and fixed-frequency measurement benches, we uncover the underlying principles and applications of these methods in electronics. These measurement techniques, fundamental to scientific and technological research, not only enhance our understanding of physical phenomena but also pave the way for future innovations. Through this exploration, we gain valuable insights into the intricacies and potential of advanced measurement technologies, underscoring their pivotal role in the ongoing advancement of the field.

References :

[1]N.jebbor, S.Bri,A.M.Sanchez,M.Chaibi :"Microwave characterization of low-loss solid dielectric materials using rectangular waveguide." International Journal of Emerging Sciences ISSN 2222-4254, Volume: 2; Issue: 4; PP.: 526-532; 2012. (2012).

[2] Agilent, Network Analysis: Applying the 8510 TRL Calibration for Non-Coaxial Measurements, Product Note 8510-8A, 2001.

[3] F. Djerfaf, Doctoral Dissertation, University Ferhat Abbas Sétif, 2012.

[4] https://www.electronics-notes.com/articles/test-methods/rf-vector-network-analyzer-vna/what-is-a-vna.php 2024

[5]M. Abdelguerfi, A. Soualmia. Utilisation des Techniques Fréquentielles et Temporelles pour l'Analyse Diélectrique. B4-*5, 17ème Colloque International Optique Hertzienne & Diélectrique*. Calais, 2003.

[6] M. Sabi. Etude de la Permittivité et de la Perméabilité des Matériaux Hétérogènes en espace libre aux Hyperfréquences. Mémoire de Magister, D. B. Leeson. Waves & Impedances on Transmission Lines. Tl Waves & Impedances, EEE 194 Rf.. 1998.

[7] R. H. Mitchell. Perovskites - Modern & Ancient. Almaz press. 2002

[8] N. Bouzit , Caractérisation Diélectrique de Matériaux Hétérogènes par Spectroscopie Temporelle: Application à l'Etude de composites Polyesters Chargés par des Titanates. Thèse de Doctorat. Université Ferhat Abbas Sétif, 2002.

[9] D. B. Leeson. Waves & Impedances on Transmission Lines. Tl Waves & Impedances, Eee 194 Rf

[10] A. M. Bottreau. Conférence C2 et C3, Ecole d'été du Trégor, (1978).

[11] A. Sugget. J. Phys. E, 8, 327, (1975).

[12]G. Raoult, "Les Ondes Centimétriques"*Ed.Masson Paris* (1958).

[13] A. M. Bottreau, Y. Dutuit et J. Morceau. J.Chem. Phys., 66, 3331, (1977).

[14] Y. Dutuit. Thèse d'Etat présentée à l'Université de Bordeaux, (1980).

[15] H. W. Loeb, G. M. Young, P. A. Quickenden et A. Sugget, J. Phys. Chem., 75, 1155, (1971).

[16]A. R. Von Hippel. *"Les diélectriques et leurs applications",* Dunod Paris (1961).

[17]A. Balana, Thèse présentée à l'Université de Bordeaux, (1990).

[18] G. Vicq. Thèse présentée à l'Université de Bordeaux, (1968).

[19]A. M. Bottreau et G. Vicq. J. Mol. Liq., 34,233, (1988).

[20] M. Stuchly, M. Brady, S. Stuchly et G. Gadga, Equivalent circuit of an open-ended coaxial line in a lossy dielectric d,. IEEE Trans. Instrum. Meas.IM- 31,116, 899, (1982).

[21]N. Markuvitz. Waveguide Handbook, Mc Graw Hill, (1951).

[22] A. Merzouki, Thèse d'Etat présentée à l'Université de Bordeaux I, (1992).

[23] A. M. Bottreau et . Merzouki,. Broadband measurement method using the admittance change between two standards. IEEE Trans. Instrum. Meas.IM 42,5, 899, (1993).

[24] A. Boutaudon. Thèse de l'Université de Bordeaux I, Décembre (1992).

[25] P. de Langhe. Thèse présentée à l'Université de Gent (Belgique) , Décembre (1994).

[26] A. Boutaudon, Doctoral Dissertation, University of Bordeaux I, December 1996

[27] A. Merzouki, Activity Report, University of Bordeaux I, 1980.

[28] P. F. Combes, Microwaves Vol. 1: Lines and Cavities, pp. 241-248, Dunod, 1996.

[29]S. Ramo, J. R. Winnery, T. Van Duzer, Fields Waves in Communication Electronics, p 411-518, 2èmeEd John Wiley & Sons, 1984.

[30] S. Baazizi, Master's Thesis, Institute of Electronics, University of Sétif, 1996.

[31] D. Hamzaoui, Master's Thesis, Institute of Electronics, University of Sétif, 1998

[32]H. Chaloupka, MTS 7.4.4 Microwave Technology III, LEYBOLD, 1991

[33] A. M. Bottreau, G. Vicq, and A. Balana, Journal of Molecular Liquids, vol. 33, pp. 311-324, 1987.

Dielectric Materials and Mixing Laws

III.1. Introduction

Dielectric materials play a pivotal role in numerous fields, serving as the foundation for many technological advancements. This chapter delves into the intricate world of dielectrics, exploring their behavior under the influence of electric fields and the phenomenon of polarization. Understanding how dielectric materials respond to electric fields is fundamental across a spectrum of applications, ranging from electronics to materials science. By comprehending the underlying principles of polarization, researchers,and engineers can harness the unique properties of dielectrics to develop innovative technologies and materials.

At its core, polarization elucidates how dielectric materials interact with electric fields, resulting in the alignment of their constituent electric dipoles. This alignment contributes to various electrical phenomena, including capacitance, energy storage, and the propagation of electromagnetic waves. Through a thorough examination of polarization mechanisms, we aim to unravel the intricacies of dielectric behavior and its implications for practical applications.

Furthermore, this chapter explores the laws of mixing, which govern the combined properties of different dielectric materials when they are brought into proximity or mixed. By elucidating these laws, we gain insights into the synergistic effects that arise from the interaction between different dielectric components. Such insights are invaluable for optimizing material properties and designing tailored solutions for specific engineering challenges.

In essence, this chapter serves as a comprehensive guide to dielectric materials, offering a deep dive into their fundamental principles and practical implications. By embarking on this exploration, readers will gain a profound understanding of how dielectrics shape the landscape of modern technology and pave the way for future innovations.

III.2. Dielectric Materials

Ideal dielectric materials are substances that are not conductors of electric current because they do not contain free charges in their structure. Unlike conductive materials such as metals, the strong ionic and covalent bonds that hold atoms together do not allow electrons to move freely through the material under the influence of an electric field. The charges of different signs in the atoms and particles of dielectrics are bound. When these charges are subjected to forces induced by an electric field, some of these bonds do not break, but only

slight elastic displacements occur. The material becomes electrically polarized, with its internal positive and negative charges separating somewhat and aligning parallel to the axis of the electric field. All positive charges move in the direction consistent with that of the field, and negative charges in the opposite direction, create polarization of the dielectric. When used in a capacitor, this polarization acts to reduce the resistance of the electric field maintained between the electrodes, which in turn increases the amount of charge that can be stored [1].

Real dielectric materials contain a certain volume of free charges originating from impurities. Thus, in dielectrics, one can also observe very slight conduction, detectable especially at low frequencies. All phenomena in dielectrics subjected to an electric field depend on the frequency of the field, temperature, and the structure of the dielectric.

III.3 Phenomenon of Polarization in Matter

The effect of dielectric polarization was discovered by Michael Faraday in 1837. Different polarization mechanisms are more or less significant depending on the frequency of the polarizing field. Five main types of dielectric polarization mechanisms are distinguished: electronic, ionic, dipolar, and interfacial (or Maxwell-Wagner type), (Figure III.1). These polarizations can coexist or appear separately. Also, they can be classified into two groups according to their characteristics: elastic (or resonance) polarization and relaxation polarization. Total polarization is the sum of the different types of polarization [2].

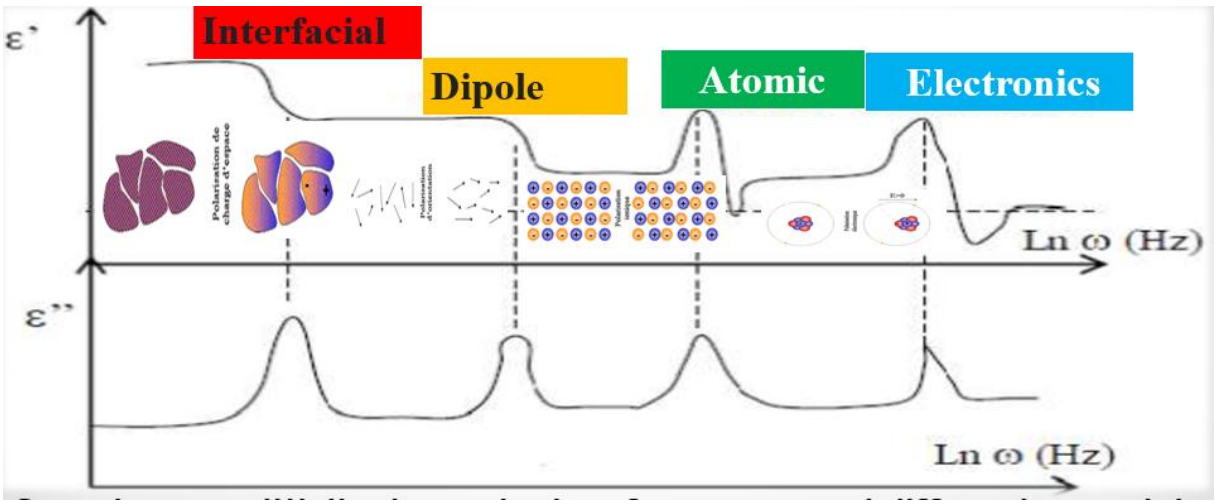

Figure III.1 Contribution of different polarizations in a dielectric material

III.3.1 Electronic Polarization

Electronic polarization is present in all dielectrics, without exception. It results from the displacements of the outer electronic orbits relative to the nucleus of the atom. Electronic polarization is established in about 10^{-15} seconds; therefore, it is independent of frequency up to the ultraviolet range. Electronic polarization is due to the deformation of the electron cloud surrounding each atom: the center of gravity of the electrons of each atom in the material shifts and no longer coincides with that of the protons (Figure III.2). This effect is relatively weak and has a very short establishment time (10^{-15} seconds). It occurs in the frequency range of ultraviolet (between 10^{14} and 10^{16} Hz). This polarization is noted :

$$\vec{P}_e = N.\alpha_e.\vec{E}_{locally} \qquad \text{(III .1)}$$

N is the number of particles per unit volume

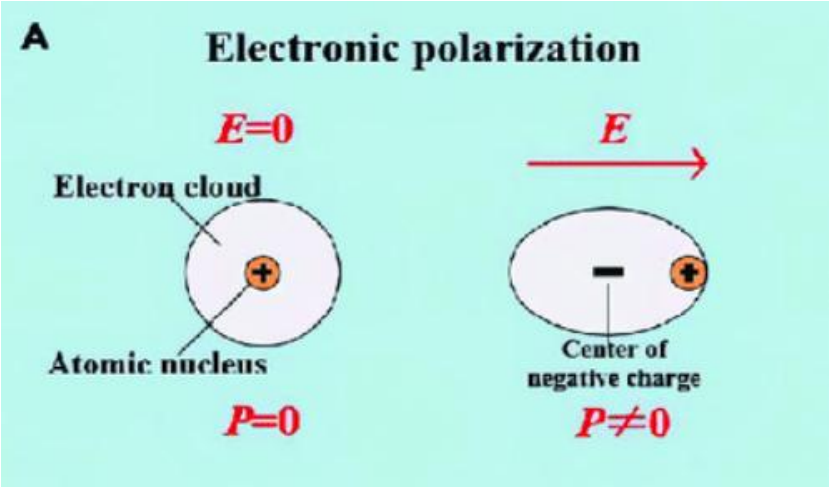

Figure III.2 Schematic representation of electronic polarization

The deformation of the orbit accompanying it is elastic, meaning that the work required for its appearance is not converted into heat but stored in the electric field. The elastic electronic polarization as well as the induced dipoles disappear when the field is removed [3].

III.3.2 Ionic Polarization

Ionic polarization (or atomic) results from the displacement of atoms bound within molecules by ionic bonds. In the case of ionic bonds, valence electrons travel through shared orbits with other atoms. This process is similar to the previous one (concerning electrons and protons), but it occurs with anions and cations. It occurs in the frequency range of infrared (10^{12} - 10^{16} Hz). Ionic bonds are encountered in most non-organic solid dielectrics with a crystalline structure (ionic crystals). Due to the inertia of relatively heavy ions, this type of polarization is established in about 10^{-13} seconds, thus slower than electronic polarization, and depends on the charge of the ion as well as the forces of mutual ionic bonds (Figure III.3). This polarization is given by:

$$\vec{P}_i = N.\alpha_i.\vec{E}_{locally} \qquad \text{(III.2)}$$

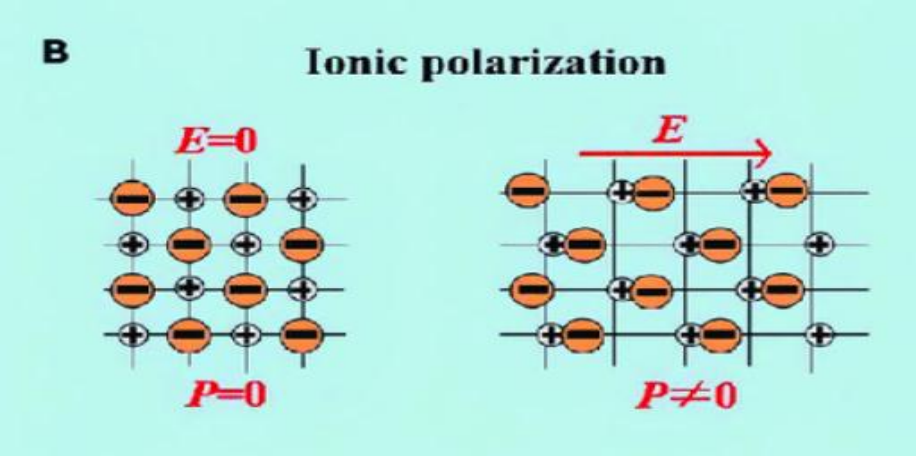

Figure III.3 Schematic representation of ionic polarization

III.3.3 Dipolar Polarization

Dipolar polarization (or orientation) consists of the alignment of dipolar molecules under the action of an electric field, namely those that possess a permanent dipole moment. In the absence of an external field, the dipole moments of different molecules are randomly oriented, resulting in a net zero. In the presence of an excitation, there is a preferred orientation, and the resultant is non-zero. Dipolar polarization depends on temperature and occurs in gases, liquids, and highly viscous amorphous bodies. It occurs in the high-frequency range, between 10^8 and 10^{11} Hz (Figure III.4). The expression of this polarization is given by:

$$\vec{P}_0 = N.\alpha_0.\vec{E}_{locally} \qquad \text{(III. 3)}$$

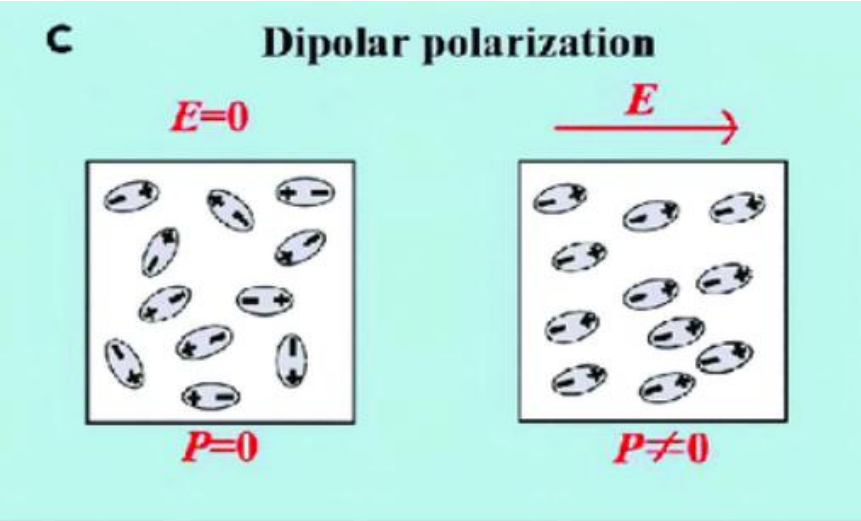

Figure III.4 Schematic representation of dipole polarization

The structure of these molecules is asymmetrical: the resulting center of gravity of all the negative charges of such a molecule does not coincide with that of all its positive charges - the molecule is an electric dipole. The dipolar character is generally inherent to molecules of chemical compounds with ionic bonds, but also to compounds with covalent bonds that have an asymmetrical structure (for example, H_2O).

III.3.4 Interfacial Polarization

Interfacial polarization (or Maxwell-Wagner-Sillars effect) [4] occurs in non-homogeneous dielectrics. This phenomenon occurs in heterogeneous materials and results from the accumulation of charges at the interface of two materials, i.e., at the boundary of two mediums with different conductivity and/or dielectric permittivity (Figure III.5). The total polarization in a material is given by the sum of these four types:

$$\vec{P} = \overrightarrow{P_e} + \vec{P}_i + \overrightarrow{P_0} + \overrightarrow{P_h} \quad \rightarrow \quad \vec{P} = N.\alpha.\vec{E}_{locally} \tag{III.4}$$

Where $\alpha = \alpha_e + \alpha_i + \alpha_0 + \alpha_h$ represents the total polarizability in the material. Depending on the nature of the material medium and the operating frequency, this quantity may be reduced to only$(\alpha_e + \alpha_i)$ or to $(\alpha_e + \alpha_i + \alpha_0)$

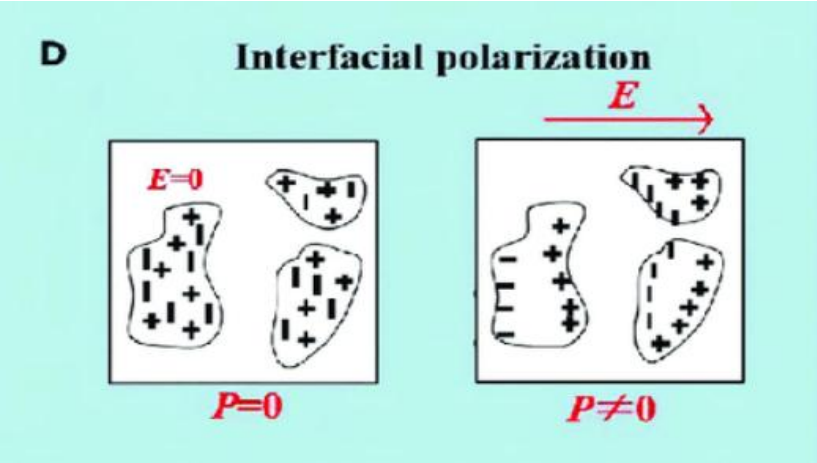

Figure III.5 Schematic representation of interfacial polarization

This type of polarization also exhibits a relaxation characteristic; the relaxation time increases as the conductivity decreases. Generally, interfacial polarization weakens at frequencies higher than acoustic frequencies in the low and medium frequency ranges, below 108 Hz [5].

III. 4. Dielectric Susceptibility

Starting from equations of Local Electric Field and (III.4):

$$\begin{cases} \vec{P} = N.\alpha.\vec{E}_{locally} \\ \vec{E}_{locally} = \vec{E}_{ext} + \frac{\vec{P}}{3\varepsilon_0} \end{cases} \quad \rightarrow \quad \vec{P} = N.\alpha.(\vec{E}_{ext} + \frac{\vec{P}}{3\varepsilon_0}) \qquad \text{(III .5)}$$

$$\rightarrow \quad \vec{P} = \frac{3\varepsilon_0.N.\alpha}{3\varepsilon_0 - N.\alpha} . \vec{E}_{ext} \qquad \text{(III.6)}$$

Such as $\vec{P} = \varepsilon_0 \chi \vec{E}_{ext}$

So, we obtain:

$$\varepsilon_0 \chi = \frac{3\varepsilon_0.N.\alpha}{3\varepsilon_0 - N.\alpha} \qquad \text{(III.7)}$$

$$\chi = \frac{3.N.\alpha}{3\varepsilon_0 - N.\alpha} \qquad \text{(III.8)}$$

χ is called dielectric susceptibility

III.4.1. Dielectric Permittivity-Susceptibility Relation

By definition, we have [6, 7][1.3]:

$$\vec{D} = \varepsilon . \vec{E}_{ext} \tag{III.9}$$

As:

$$\vec{D} = \varepsilon_0 . \vec{E}_{ext} + \vec{P} \tag{III.10}$$

By replacing the polarization vector with its expression, we will find:

$$\vec{D} = \varepsilon_0 . \vec{E}_{ext} + \varepsilon_0 \chi \vec{E}_{ext} \tag{III.11}$$

Or alternatively:

$$\vec{D} = \varepsilon_0 (1 + \chi) . \vec{E}_{ext} \tag{III.12}$$

By comparison with (III.9), we find that: $\varepsilon = \varepsilon_0 (1 + \chi)$

The ratio between ε and ε₀ defines the relative dielectric permittivity:

$$\varepsilon_r = (1 + \chi) \tag{II.13}$$

III.5. Clausius-Mossotti Relation

According to equations (III.8) and (III.12), we can arrive at the formula:

$$\frac{\varepsilon_r - 1}{\varepsilon_r + 2} = \frac{N.\alpha}{3\varepsilon_0} \tag{II.14}$$

This formula is known as the 'Clausius-Mossotti relation', which relates the relative dielectric permittivity ε_r to the polarizability α.

III.6. Dynamic Behavior of Dipole Polarization

When an electric field E is applied to a molecular system, all dipoles, individually, tend to orient themselves in the direction of the field, in order to decrease the potential energy of the system. However, since molecules are subject to thermal interaction, molecular agitation tends to oppose the orientation of dipoles induced by the field. The transition from

the non-polarized state in the absence of the electric field to a polarized state in equilibrium with the field is not an instantaneous phenomenon. Indeed, there is a certain delay in the establishment of polarization due to the inertia of dipole movement. This phenomenon is called dielectric relaxation.

III.6.1. Debye Model

Dipolar relaxation in the Debye sense is a purely viscous process without elastic restoring force and thus of the first order. The typical equation for such a phenomenon is, for instance, the one describing the motion of a particle with non-negligible mass after the application of a constant force in a viscous medium that exerts a braking force on the particle. By analogy, one can write that the dipole polarization P of a set of dipoles in thermal equilibrium obeys the equation [8,9-12,13,14]:

$$\frac{dP_d}{dt} = \frac{1}{\tau}[\varepsilon_0(\varepsilon_s - \varepsilon_\infty)E(t) - P_d(t)] \quad \text{(III.15)}$$

Here τ represents the unique dipolar relaxation time.

Let's now imagine that the dipoles (or, by analogy, the particles) are in an alternating field of the form:

$$E^* = E_0 e^{j\omega t} \quad \text{(III.16)}$$

In alternating current, all variables, and in particular the polarization P, oscillate sinusoidally with angular frequency ω, such that we can write:

$$P_d^* = |P_{d_0}|e^{(j\omega t+\varphi)} \quad \text{(III.17)}$$

And we can directly obtain the solution of equation (II.15):

$$P_d^* = \frac{\varepsilon_0(\varepsilon_s-\varepsilon_\infty)E^*}{1+j\omega\tau} \quad \text{(III.18)}$$

Sachant que :

$$P_d^* = \varepsilon_0(\varepsilon^* - \varepsilon_\infty)E^*$$

So, it is possible to determine the complex relative dielectric constant:

$$\varepsilon^*(\omega) = \varepsilon_s + \frac{(\varepsilon_s - \varepsilon_\infty)}{1+j\omega\tau} \tag{III.19}$$

This relationship is the Debye model.

Par convention :

$$\varepsilon^*(\omega) = \varepsilon'(\omega) - j\varepsilon''(\omega)$$

$$\begin{cases} \varepsilon'(\omega) = \varepsilon_s + \frac{(\varepsilon_s - \varepsilon_\infty)}{1+(\omega\tau)^2} \\ \varepsilon''(\omega) = \frac{(\varepsilon_s - \varepsilon_\infty)\omega\tau}{1+(\omega\tau)^2} \end{cases} \tag{III.20}$$

The variations of these two parameters as a function of the excitation frequency are presented in Figure (III. 6):

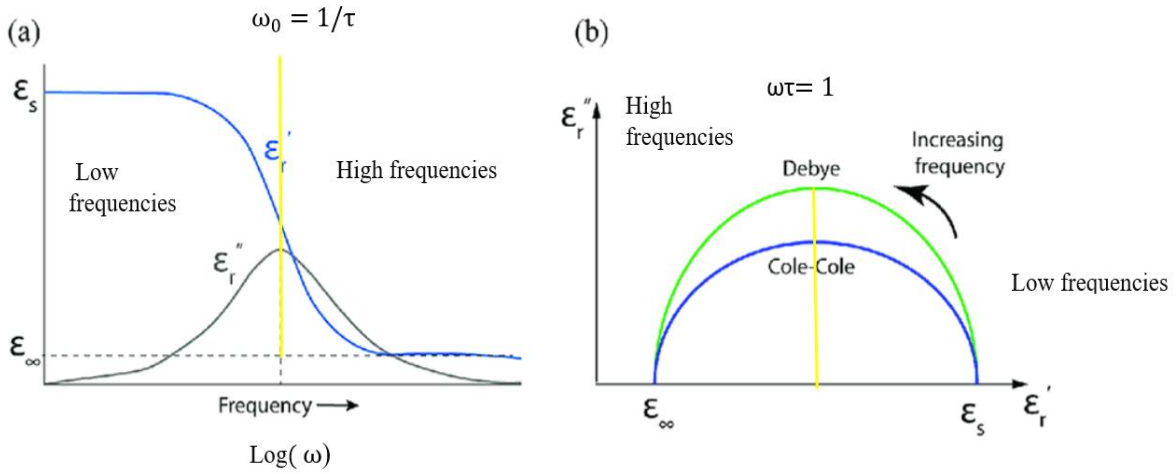

Figure III.6. (a) Variations of the functions ε' and ε'' as a function of the angular frequency ω, and (b) the Cole-Cole diagram of the Debye model.

This single relaxation time model is characterized by a dielectric response whose half-width at peak height $\omega_D = 1.144$ decades on a logarithmic scale. The representation of this equation in the complex plane, called the Argand diagram or more commonly the Cole-Cole diagram when referring to the (ε', ε'') diagram, is a semicircle of radius($\frac{(\varepsilon_s - \varepsilon_\infty)}{2}$)and whose center is placed on the ε' axis at an ordinate of ($\frac{(\varepsilon_s + \varepsilon_\infty)}{2}$). Therefore, the permittivity can vary

with temperature, frequency, and amplitude of the excitation electric field, external constraints, etc.

By defining the cyclic relaxation frequency $\omega_r = 1/\tau$, we can rewrite equation (III.I8) as:

$$\varepsilon^*(\omega) = \varepsilon_s + \frac{(\varepsilon_s - \varepsilon_\infty)}{1+j\frac{\omega}{\omega_r}} \quad \text{(III.21)}$$

For a material with non-zero conductivity, the term for losses due to conductivity must be added to the model. Thus, we obtain:

$$\varepsilon^*(\omega) = \varepsilon_s + \frac{(\varepsilon_s - \varepsilon_\infty)}{1+j\frac{\omega}{\omega_r}} - j\frac{\sigma}{\omega\varepsilon_0} \quad \text{(III.22)}$$

In this case, the imaginary part of the permittivity becomes:

$$\varepsilon''(\omega) = \frac{\tau\omega(\varepsilon_s - \varepsilon_\infty)}{1+(\tau\omega)^2} + \frac{\sigma}{\omega\varepsilon_0} \quad \text{(III.23)}$$

It represents dielectric losses (first term) and losses known as ionic conductivity losses. These two terms are equal when ω is equal to:

$$\omega = \sqrt{\frac{\omega_r^2\sigma}{(\varepsilon_s - \varepsilon_\infty)\omega_r\varepsilon_0 + \sigma}} \quad \text{(III.24)}$$

III.7 Theory of Local Electric Field

The theoretical approach to calculating the dielectric permittivity of dielectric mixtures requires the calculation of the local electric field $\overrightarrow{E}_{\text{locally}}$ defined by the field prevailing at the location of a given dipole. It is the result of the applied macroscopic field and the fields created by all the other dipoles $\vec{E}_j$[15].

$$\left(\overrightarrow{E}_{locally}\right) = \vec{E} + \sum_{J\neq i}\vec{E}_j \quad \text{(III.25)}$$

$\overrightarrow{E}_{\text{locally}}$ is the field "actually seen" by the inclusion and is different from the applied field $\vec{E}$. A good definition was provided by Guillot [16]: the local field is the field "that would exist at the location where the inclusion is located if it were removed before its surroundings have had time to realize its disappearance"

Consider a dielectric material placed in an electric field (E), and the particles of the dielectric are located within a macroscopic spherical cavity (FigureI II.6).

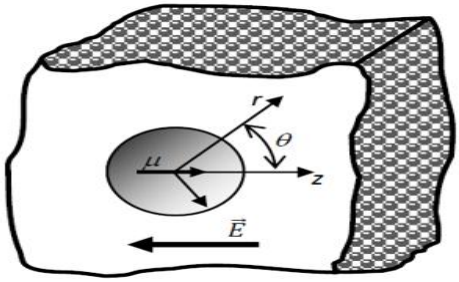

Figure III.6 Macroscopic cavity situated in an external electric field $\overrightarrow{E}$

The field prevailing inside the cavity will be the resultant of the external macroscopic field $\overrightarrow{E}$, of the macroscopic field $\vec{E}_1$ arising from the induced charges on the surface of the cavity, hence from the uniformly polarized continuous medium by the polarization vector$\vec{P}$, representing the number of dipoles per unit volume, and the field.$\vec{E}_2$ represents the sum of the individual fields created by the dipoles (particles) located inside the cavity. The local electric field of this dielectric will then be:

$$\overrightarrow{E}_{locally} = \overrightarrow{E} + \vec{E}_1 + \vec{E}_2 \qquad \text{(III.26)}$$

Lorentz assumed that the electric fields created by the particles filling the spherical cavity of the dielectric cancel each other inside this cavity $(\vec{E}_2 = 0)$.

$$\overrightarrow{E}_{locally} = \overrightarrow{E} + \vec{E}_1 \qquad \text{(III.27)}$$

If the cavity is spherical, this field is determined by elementary electrostatic calculation:

$\vec{E}_1 = \vec{P}/_{3\varepsilon_0}$, the factor $\vec{1}/_{3\varepsilon_0}$ being the depolarization coefficient of a sphere(ε0 is the permittivity of vacuum) :

$$\overrightarrow{E}_{locally} = \overrightarrow{E} + \frac{\vec{P}}{3\varepsilon_0} + \frac{\acute{\varepsilon}+2}{3}\overrightarrow{E} \qquad \text{(III.28)}$$

The Lorentz local field model is therefore only applicable in the case of non-polar dielectrics with spherical particles.

III.8 Dielectric Permittivity

In purely dielectric materials, an external electric field polarizes the bound charge carriers, causing them to undergo a slight displacement from their equilibrium position: all positive charges move in the direction aligned with the field, while negative charges move in the opposite direction, creating dielectric polarization. Electrical conduction is therefore negligible, but the density of dipoles aligning with the external electric field can be significant.

The dielectric permittivity ε, The dielectric permittivity is a tensor quantity where each term of the tensor is a complex parameter. ($\varepsilon = \acute{\varepsilon} - j\acute{\varepsilon}$). The real part represents the ability of the dielectric to store electrical energy, while the imaginary part represents dielectric losses. In the case of a homogeneous isotropic material, the dielectric permittivity reduces to a scalar.

The induction vector$\vec{D}$ can be written as indicated in the equation :

$$(\vec{D} = \varepsilon_0 \vec{E} + \vec{P}) \qquad \text{(III.29).}$$

Generally, electric polarization is proportional to the electric field experienced by the charges. It can be written in the following form:

$$\vec{P} = N\alpha \ \overrightarrow{E}_{locally} \qquad \text{(III.30)}$$

Where N is the concentration of dipoles and α is the polarizability of atoms or molecules. The field $\overrightarrow{E}_{locally}$ experienced by the dipoles may not necessarily be identical to the electric field $\overrightarrow{E}$ that prevails within the dielectric but depends on the internal structure of the material. By using the relationships (III.29) and (III.30), we obtain:

$$\varepsilon = \varepsilon_0 \varepsilon_r = \left(1 + \frac{N\alpha}{\varepsilon_o} \frac{E_{locally}}{E}\right) \qquad \text{(III.31)}$$

This equation shows that the permittivity depends on the number and polarizability of the elements in the microstructure (atoms or molecules), the field experienced by the dipoles, and the average field prevailing within the dielectric. The local field is influenced by the presence of neighboring dipoles when the medium is dense. However, we can assume that the external field is the same as that experienced by each dipole when the dipole concentration is low.

The polarizability α, The polarizability, a microscopic quantity, depends on various polarization mechanisms. It varies depending on the medium involved and changes with frequency. The effective permittivity, or macroscopic permittivity ε_{eff} , defined as the ratio of the displacement to the electric field.

$$\vec{D} = \varepsilon_0 \overrightarrow{E} + \vec{P} = \varepsilon_{eff} \overrightarrow{E} \quad \text{(III.32)}$$

The polarization $\vec{P}$ is the sum of all induced multipole moments and is related to the polarizability α by the following equation:

$$\vec{P} = \sum_k N_k \alpha_k (\overrightarrow{E})_k \quad \text{(III.32)}$$

N_K the number of dipoles. *K* par unité de volume and $\vec{E}$ is the inducing field that polarizes the dipole. This equation allows us to relate the microscopic and macroscopic characteristics of the medium. By substituting (III.31) into (III.32), we have:

$$(\varepsilon_{eff} - \varepsilon^0)\overrightarrow{E} = \sum_k N_k \alpha_k (\vec{E}_{localy})_k \quad \text{(III.33)}$$

III.9 Electrical conductivity

Electrical conductivity σ is the quantity characterizing the ability of a material to allow the passage of electric current, meaning to enable electric charges, free charges, to move in a given direction within it when an electric field is applied. In the case of good conductors, the drift velocity of charge carriers in the presence of an electric field is proportional to the amplitude of this field, and the direction of movement is the same as that of the field.

This is expressed by the equation:

$$\vec{j} = \sigma \vec{E} \quad \text{(III.34)}$$

which relates the current density vector $\vec{J}$, the electric field $\vec{E}$, and the conductivity of the medium σ.

If we revisit Maxwell's equation, assuming that the electric field is sinusoidal ($\frac{\partial \vec{D}}{\partial t} = j\omega\varepsilon\vec{E}$).

We obtain:

$$rot\vec{H} = \nabla \times \vec{H} = \vec{J} + \frac{\partial \vec{D}}{\partial t} = \sigma\vec{E} + j\omega\varepsilon\vec{E} = j\omega(\varepsilon + \frac{j\sigma}{\omega})\vec{E} \qquad \text{(III.35)}$$

The conductivity is now combined with the permittivity and contributes through an imaginary term. Generally σ , is a second-order tensor that reduces to a scalar if the medium is The conduction current is in phase with the electric field, resulting in energy loss from the field.

III.10 Dispersion

The polarization mechanism of the material strongly depends on the temporal variation of the excitation, which is why the permittivity also depends on the frequency of the electric field: this is called dispersion. Figure III.8 shows the typical dispersion curve of a material for different types of polarization.

The dielectric permittivity of a real material is maximum under direct current, and it also depends on the frequency of the applied field oscillation. It decreases in steps with frequency because each polarizing entity has its own time constant. Thus, as the frequency increases, only lighter entities can follow, leading to a decrease in polarization. Moreover, the material's polarization does not respond instantaneously to the electric field, resulting in a phase difference. Therefore, dielectric permittivity is generally treated as a complex function.

$$\boldsymbol{\varepsilon^*(\omega)} = \acute{\varepsilon}(\omega) - j\acute{\varepsilon}(\omega) \qquad \text{(III.36)}$$

With:

$\acute{\varepsilon}$: the real part of the permittivity, which is related to the energy stored in the medium.

$\acute{\varepsilon}$: the imaginary part of the permittivity, which is related to the energy loss in the medium

III.11 Dielectric Losses

Dielectric losses are generally expressed in terms of the dielectric loss tangent defined as the ratio of the imaginary part to the real part of the complex permittivityε^* :

$$tan\delta = \frac{\acute{\varepsilon}}{\acute{\varepsilon}} \quad \text{(III.37)}$$

Where δ also represents the phase angle between the voltage applied to the dielectric and the resulting current. These losses are also expressed by the quality factor Q [17]:

$$Q = \frac{1}{tan\delta} \quad \text{(III.38)}$$

III. 12. Overview of Heterogeneous Mixtures

III.12.1.The mixture

Mixture [39] of divided solids (powders, granular media) is a key operation for many industrial sectors (pharmacy, food processing, cement, plastics, etc.), ensuring homogeneity at the required scale, often that of packaging. It is indeed primarily responsible for meeting the specifications and usage properties of formulated products. However, the concept of homogeneity in solid mixtures, inseparable from the scales of observation and segregation, remains difficult to achieve through measurement.

In most cases, estimation must be done through sampling, which poses technical and statistical challenges. The current development of non-intrusive, online measurement methods should soon allow for better definition and control of homogeneity. Achieving a certain quality of the mixture is mainly due to dynamic aspects, which are themselves related to the mechanisms that govern particle movement: convection, shear, and diffusion.

These mechanisms are influenced not only by the flow properties of the products but also by the technological capabilities of the mixing equipment. From this perspective, the mixers used in the industry fall into three main types, depending on whether the agitation is produced by an internal moving part, (convective mixers), by rotating the drum (drum mixers), or by the material's own flow (static mixers). Both continuous and batch mixing processes can be employed, with the choice depending on production constraints and the specific requirements of different industries.

As with other unit operations involving divided solids, basic scientific knowledge is still lacking to clearly explain the phenomenology of mixing. This is likely due to the mesoscopic nature of these materials and the lack of models to describe them at this scale. Within a systemic and thus macroscopic approach, considering the reactor scale, it is possible to account for certain classic dynamic aspects in process engineering (mixing kinetics, residence time distribution, power consumption, etc.) and to model the operation globally.

Finally, it is necessary to consider that the concept of mixing quality must be integrated at the overall process level. The presence of steps that induce segregation (transportation, storage) can affect the homogeneity of a mixture beyond the mixer itself.

III.12.2.Mixing Mechanisms

There are three categories of mixing mechanisms [40]:

III.12.2.1 Diffusion Mixing

This involves the individual movement of particles initiated by collisions, resulting in the individual redistribution of particles. This mechanism is quite slow. The term "diffusion" is somewhat improper by analogy with molecular diffusion, as in the case of powders, an input of energy is necessary.

III.12.2.2 Convective Mixing

In this case, a group of particles is set in motion by a moving part within the mixer. This usually requires the intervention of an external force, such as an agitation blade, to impart significant energy to the divided solid.

III.12.2.3 Shear Mixing

In this case, sliding planes of particle layers appear within the mixture under mechanical action. The relative movement of these planes involves the mixing of particles with efficiency intermediate between the previous two mechanisms. It is often difficult to separate these three mechanisms. The predominance of one mechanism over another is determined by the type of mixer used as well as the nature of the particles. The mixer favors a mechanism according to its mechanical action. Only qualitative notions can be provided to evaluate the effect of powder characteristics on the type of mechanism.

III.12.3 Homogeneous and Heterogeneous Mixtures

III.12.3.1 Homogeneous Mixture

Homogeneous mixtures [41] are those in which the constituents cannot be distinguished from one another. These mixtures have a uniform composition, and their properties do not depend on spatial variables but remain constant throughout the mixture. This type of mixture has a unique and periodic structure, and the substances are physically combined, not chemically bonded or combined.

III.12.3.2 Heterogeneous Mixture

A heterogeneous mixture [42] is an aggregate formed from grains of one or more constituents distributed within a continuous medium. It is characterized by its compactness or the volume fraction of the grains, given by the following relation:

$$P = \frac{V_{grain}}{V_{aggregate}} \tag{III.39}$$

Where:

- P: The volume fraction of the grains,
- V_{grain}: Volume of the grains,
- $V_{aggregate}$: Volume of the aggregate.

Such a mixture's dielectric response depends on several parameters, including:

- The intrinsic permittivity of the constituents.
- Their compactness.
- The shape of the grains and their orientation within the load.
- The spatial distribution of the inclusions.

III.12.4 Types of Mixtures

The permittivity of such a mixture depends on the intrinsic permittivity of the constituents, their volume proportions, the shape of the grains, and their orientations. Mixtures can be classified into two categories [38]:

III.12.4.1 Lattice Mixtures

These mixtures are composed of grains that have the same shape, size, and orientation. To ensure weak interactions, the grains must have a simple shape and the mixtures must be sufficiently diluted. These media present purely theoretical benefits.

III.12.4.2 Statistical Mixtures

These mixtures consist of grains with arbitrary shapes and sizes distributed randomly. These mixtures are of great interest in almost all fields. They are mostly synthesized to produce materials that meet the dielectric requirements of a specification established by their application domain. However, ...the lack of information about this type of material prevents us from embarking on a potentially unpleasant venture during the possible fabrication of such a mixture. It is therefore necessary to resort to predictive laws that describe the dielectric behaviors of these mixtures and to choose those that are most suitable for a specific need. Numerous mixing laws have been developed in this regard, for modeling dielectric behavior and addressing issues related to heterogeneity, random particle size distribution, and others. However, some laws are considered more effective than others, so we will limit ourselves to the most commonly used ones in the following.

III.12.5.Homogenization

Homogenization methods are widely used in the field of materials science to effectively determine their characteristics (notably dielectric) for macroscopic needs. Many domains demand the implementation of experimental and/or numerical tools for material design: applications in metrology, geosciences, antennas and propagation, and electromagnetic compatibility (EMC) naturally come to mind. In this context, the proposed works aim to describe the interesting properties of composite materials through various formalisms, specifically for solid/gas, solid/liquid, and solid/solid mixtures.

There are numerous methods to describe effective properties based on effective medium theories (EMT); details on the available formalisms are accessible, along with elements highlighting the difficulty in establishing their limits of validity [43].

Crystalline materials are composed of atoms that are regularly spaced and periodically repeated in space, forming a specific lattice. In most crystals, the distance between the nearest neighboring nodes is on the order of angstroms or tens of angstroms. To get an idea of the spectral range in which macroscopic Maxwell's equations correctly describe the electromagnetic behavior of a crystal, we can evaluate the number of atoms in the crystal per wavelength.

Crystalline materials are composed of atoms that are regularly spaced and periodically repeated in space, forming a specific lattice. In most crystals, the distance between the nearest neighboring nodes is on the order of angstroms or tens of angstroms. To get an idea of the spectral range in which macroscopic Maxwell's equations correctly describe the

electromagnetic behavior of a crystal, we can evaluate the number of atoms in the crystal per wavelength.

Let's take the example of a common crystal, salt (or sodium chloride), where the distance between the nearest neighbors is $a = 5.6\text{Å}$. The number of atoms per wavelength, for illumination in the blue spectrum ($\lambda = 500\text{nm}$), is:

$$\frac{\lambda}{a} \approx \frac{500\times10^{-9}}{5\times10^{-10}} = 1000 \qquad \text{(III.40)}$$

Thus, each incident wavelength excites the response of approximately 1000 atoms. Such a response is therefore a collective response and justifies the use of macroscopic Maxwell's equations. The generally accepted upper limit for considering a medium homogeneous enough to apply macroscopic Maxwell's equations is $\mathrm{d} < \frac{\lambda}{10}$ (where d is the size of the particles or the inter-particle distance). For typical crystals, this corresponds to minimum wavelengths of about 10 nm (X-rays). Below this limit, microscopic details (such as the structure of the electromagnetic field between atoms) and diffraction phenomena must be taken into account (the study of crystal structure by X-ray diffraction is a well-known example of this) [44].

The characterization of a heterogeneous medium by these dielectric functions is not straightforward, as one must know the exact geometric arrangement of the material's constituents. However, if the wavelength of the electromagnetic radiation is much larger than the dimension of the individual constituents, the medium can be approximated as homogeneous, allowing the use of effective medium theories to describe its macroscopic properties.

If the wavelength of electromagnetic radiation is much larger than the dimension of the particles, classical theories of non-homogeneous media assume that the material can be treated as a homogeneous substance with an effective dielectric function (Figure III.7). The challenge then is to relate the average permittivity, known as the effective permittivity, to those of the various constituents. This quantity depends on the properties of the constituents, as well as their volume fractions, shapes, and sizes. Homogenization thus involves replacing the heterogeneous medium with an effective medium that has the same dielectric properties [45].

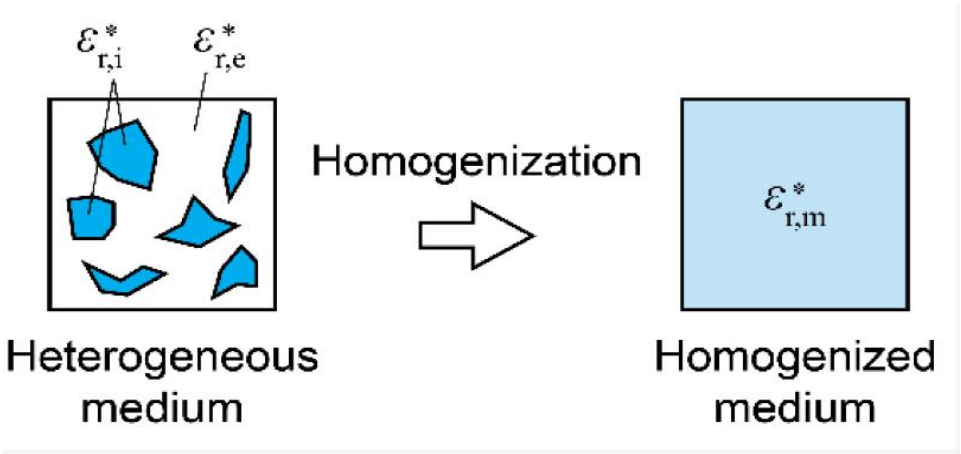

Figure III.7: Representation of a heterogeneous medium and its homogeneous equivalent.

III.12.6. Theory of Heterogeneous

The first version of the dielectric model of a heterogeneous mixture with two phases was proposed by Mossotti and Clausius. In 1848, the astronomer Mossotti [46] observed that the behavior of dust composed of identical particles can be described by the quantity $N_k\alpha_k/3\varepsilon_0$ proportional to the dust density (where N_k is the number of particles per unit volume and $\alpha_k$is the polarizability of each particle). In 1879, the thermodynamicist Clausius [47] showed that the ratio $(\varepsilon-\varepsilon_0)/(\varepsilon+2\varepsilon_0)$ was proportional to the density, where ε is the macroscopic permittivity. Eventually, the two descriptions, microscopic (Mossotti) and macroscopic (Clausius), were combined into a single one, now called the Clausius-Mossotti relation [48]:

$$\frac{\Sigma_k N_k\alpha_k}{3\varepsilon_0}=\frac{\varepsilon-\varepsilon_0}{\varepsilon+2\varepsilon_0} \qquad \text{(III.41)}$$

This theory, developed in the late 19th century, establishes a relationship between the macroscopic parameters of the material and the individual electric polarizability α_k of the atoms or molecules constituting it. From this unique Clausius-Mossotti relation, all major classical theories of the effective medium dielectric function can be derived. For each of these theories, it is sufficient to define the medium in which the inclusions are immersed.

III.13. Mixing Laws

Dielectric modeling of a mixture is a mathematical tool that allows the prediction of the dielectric constant of a mixture based on the parameters of its constituents. In the specialized scientific literature, several models and laws addressing this subject can be found, each based on different considerations. Some models take into account the geometric or granular aspect of the inclusions, the way they are dispersed in the host medium, or the physical nature of the mixture itself (gas, liquid, or solid). However, the majority of these models require a characteristic parameter of any mixture, which is the volumetric fractions of the different phases.

In a mixing law, the dielectric constant of a composite is often expressed in terms of the permittivities of each constituent and its volumetric fraction. There are numerous mixing laws, but we will focus on the most commonly used ones.

III.13.1 The Rayleigh Model

This model is given by the expression:

$$\frac{\varepsilon_m-1}{\varepsilon_m+2}=\sum_{i=1}^{n} f_i\frac{\varepsilon_i-1}{\varepsilon_i+2} \qquad \text{(III.42)}$$

ε_m: represents the dielectric constant of the mixture.

ε_i : represents the dielectric constant of the constituent.

f_i : represents the volume fraction of the constituent.

III.13.2 Böttcher's Model

The equation proposed by Böttcher is intended to calculate the dielectric constant of a binary mixture and is given by:

$$f_1\cdot\frac{\varepsilon_1-\varepsilon_m}{\varepsilon_1+2\varepsilon_m}+f_2\cdot\frac{\varepsilon_2-\varepsilon_m}{\varepsilon_2+2\varepsilon_m}=0 \qquad \text{(III.43)}$$

The inclusions for this model are assumed to be spherical. Boersma and Van Turnhout proposed a general form of the Böttcher equation for a multi-phase system, given by:

$$\sum_{i=1}^{n} f_i \frac{\varepsilon_i - \varepsilon_m}{\varepsilon_i + 2\varepsilon_m} = 0 \quad \text{(III.44)}$$

III.13.3 Berentsveig Model

The model proposed by Berentsveig has proven its effectiveness for wideband characterization (from 1 to 10 GHz) for a "Sandy Clays" composite. It is expressed by the relationship:

$$\varepsilon_m = \bar{\varepsilon} + \frac{\sum_{i=1}^{n} f_i \frac{\varepsilon_i - \bar{\varepsilon}}{\varepsilon_i + 2\bar{\varepsilon}}}{\sum_{i=1}^{n} f_i \frac{1}{\varepsilon_i + 2\bar{\varepsilon}}} \quad \text{(III.45)}$$

$\bar{\varepsilon}$ is the average permittivity defined by: $\bar{\varepsilon} = \sum_{i=1}^{n} f_i \varepsilon_i$ Another form of this model is given by the equation:

$$\sum_{i=1}^{n} f_i \frac{\varepsilon_i - \varepsilon_m}{\varepsilon_i + 2\bar{\varepsilon}} = 0 \quad \text{(III.46)}$$

It resembles the generalized Böttcher model but in this form, ε_m m is replaced by $\bar{\varepsilon}$ in the denominator[17,18,19,23-36].

III.13.4 Wiener's Law

Wiener proposed a model for describing the effective permittivity of a composite with n constituents given by:

$$\varepsilon_m^c = \sum_{i=1}^{n} f_i \varepsilon_i^c \quad \text{(III.47)}$$

We notice the introduction of a parameter noted as C called the shape factor or depolarization factor. This parameter is between -1 and +1. Two limiting cases arise:

$C = -1$: In this case, the model describes the dielectric constant of a composite formed by n layers arranged in series between two flat plates of a capacitor Figure (III.7). (a). This is Wiener's indirect model.

$C = 1$: In this case, the model describes the dielectric constant of a composite formed by n layers arranged in parallel between two flat plates of a capacitor Figure (III.7).(b). This is Wiener's direct model.

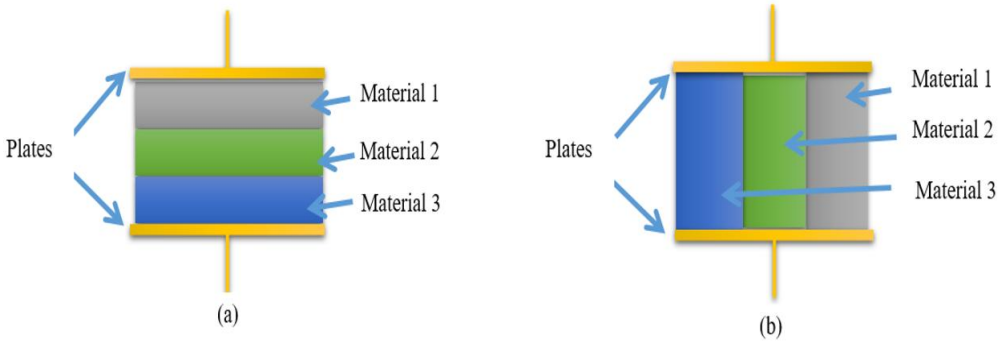

Figure III.8: The schematization of the extreme cases of Wiener's model for a composite

III.13.5 Lichtenecker-Rother Model

Lichtenecker and Rother proposed a mathematical model for the determination of the dielectric constant of a mixture composed of n constituents (1924). This model is given by [21]:

$$\varepsilon_m^c = \sum_{i=1}^{n} f_i \varepsilon_i{}^c \qquad \text{(III.48)}$$

expression:

$$\ln(\varepsilon) = \sum_{i=1}^{n} f_i \ln(\varepsilon_i) \qquad \text{(III .49)}$$

This form has proven its validity in several studies and for various types of materials [19-35]. If we start from the formula for two constituents:

$$\ln(\varepsilon) = V_1 . \ln(\varepsilon_1) + V_2 . \ln(\varepsilon_2) \qquad \text{(III.50)}$$

Where ε represents the effective value of the permittivity of the mixture. We can therefore consider this new mixture as being a single material characterized by ε. If we add to this another constituent having a permittivity ε_3, Lichtenecker's binary law remains valid, and then we write ;

$$\ln(\varepsilon_m) = V.\ln(\varepsilon) + V_3.\ln(\varepsilon_3) \quad \text{(III.51)}$$

Where ε₃ represents in this case the effective permittivity of the new material.

Since: $\ln(\varepsilon) = V_1.\ln(\varepsilon_1) + V_2.\ln(\varepsilon_2)$

We can expand it as follows:

$$\ln(\varepsilon_m) = V.(V_1.\ln(\varepsilon_1) + V_2.\ln(\varepsilon_2)) + V_3.\ln(\varepsilon_3) \quad \text{(III.52)}$$

Still with: $V_1 + V_2 = 1 \text{et} V + V_3$

We will finally have:

$$\ln(\varepsilon_m) = f_1.\ln(\varepsilon_1) + f_2.\ln(\varepsilon_2)) + f_3.\ln(\varepsilon_3) \quad \text{(III.53)}$$

Where: $f_1 = V.V_1, f_2 = V.V_2$ and $f_3 = V_3$

This formula expresses the permittivity of the ternary mixture from the parameters of each of its constituents.

III.13.6 Complex Refractive Index Method

In 1974, Birchak proposed the method known as CRIM (Complex Refractive Index Method) for calculating the dielectric permittivity of a binary mixture, assuming that the size of the inclusions is small compared to the wavelength. This method is given by the formula[27]:

$$\sqrt{\varepsilon_m} = f_1\sqrt{\varepsilon_1} + f_2.\sqrt{\varepsilon_2} \quad \text{(IIi.54)}$$

For the case of a multi-phase system, Wharton proposed a generalized formula:

$$\sqrt{\varepsilon_m} = \sum_{i=1}^{n} f_i\sqrt{\varepsilon_i} \quad \text{(III.55)}$$

This model is a special case of the Lichtenecker-Rother law when $C = 0.5$.

III.13.7 Bruggeman-Hanai Model

One of the most widely used models is the Bruggeman-Hanai model, given by the relationship:

$$\frac{\varepsilon_m-\varepsilon_i}{\varepsilon_h-\varepsilon_i}\left(\frac{\varepsilon_h}{\varepsilon_m}\right)^{\frac{1}{2}} = 1 - f_i \qquad \text{(III.56)}$$

ε_h and ε_i represent respectively the dielectric constants of the host medium and the inclusions.

This model has proven its effectiveness in several published works. A general form was given by Sen by introducing a depolarization factor denoted as L, which varies from 0 to +1[18]:

$$\frac{\varepsilon_m-\varepsilon_i}{\varepsilon_h-\varepsilon_i}\left(\frac{\varepsilon_h}{\varepsilon_m}\right)^{L} = 1 - f_i \qquad \text{(III.57)}$$

When L=0, the model becomes that of Lichtenecker-Rother for c=1. When L=1, it becomes that of Lichtenecker-Rother for c=-1. Sherman [9] estimated that this parameter essentially depends on the porosity, conductivity, and value of the host matrix used.

III.13.8. Looyenga Model

Looyenga starts from the observations of Van Beek, who noticed that the formulas of Bruggeman and Böttcher, respectively, give approximately the same results despite their different origins and forms. Looyenga then considers a sphere of radius a containing a mixture with a dielectric constant $(\varepsilon\_m\text{-}\Delta\varepsilon)$ and volume fraction (1-f), where at its center, small particles with a radius b containing a dielectric constant $(\varepsilon\_m+\Delta\varepsilon)$ and volume fraction P are added. The dielectric constant of the resulting mixture is then $\bar{\varepsilon}\_m$. By using the Taylor series for the calculation of the compactness P and using Böttcher's equation, he arrives at the following formula:

$$f = \frac{\varepsilon_m^{1/3}-\varepsilon_1^{1/3}}{\varepsilon_2^{1/3}-\varepsilon_1^{1/3}} \qquad \text{(III .58)}$$

Which can also be written in the following form:

$$\varepsilon_m^{1/3} = (1-f)\varepsilon_1^{1/3} - f\varepsilon_2^{1/3} \qquad \text{(III.59)}$$

In his calculations, Looyenga did not introduce the shape of the particles, hence the application of this law to all kinds of homogeneous mixtures.

III.13.9 Maxwell-Garnett Law

The Maxwell-Garnett law has been primarily applied to composites based on metallic inclusions encapsulated in an insulating matrix and for a low filling fraction (concentration). Subsequently, it has proven its validity without restrictions for any type of composite. This law is given by the expression[36]

:

$$\varepsilon = \varepsilon_m + 3f\varepsilon_m \frac{\varepsilon_i - \varepsilon_m}{\varepsilon_i + 2\varepsilon_m - f(\varepsilon_i - \varepsilon_m)} \quad \text{(III.60)}$$

III.13.10 Bottreau's Law

Certain dielectric composites that exhibit the phenomenon of percolation or have non-spherical granular structures did not conform to Lichtenecker's law. For this reason, Bottreau made a graphical representation of the logarithm of the permittivity as a function not of the volume fraction of the filler, but as a function of its logarithm on one hand and that of the matrix on the other hand. Based on numerous measurements, he first proposed taking Ln (V_i)as the origin, where V_i is the volume fraction of the filler at the inflection point. The curves obtained resemble hyperbolic tangents provided that, on one hand, in the first case $Ln((V_2)/V_i)$ is used, and on the other hand, in the second case $Ln((1V_i)/V_1)$is used. Then, he performs a new change of origin and obtains, under these conditions, the final abscissas, which serve as the basis for his work and become functions of $Ln((V_2)/V_i)$[37]:

$$Ln\left(\frac{V_2}{V_1}\right) - Ln\sqrt{\left(\frac{V_2V_1}{V_1(1-V_i)}\right)} = Ln\sqrt{\left(\frac{(1-V_i)V_2}{V_1V_i}\right)} \quad \text{(III .61)}$$

Then, depending on $Ln((1-V_i)/V_1)$ the two abscissas will be identical, allowing signals to be treated as a whole using the same axis system. This variable is set equal to LnV_N, a normalized variable; it is then sufficient to normalize the variations of e Ln between ±1. Consequently, a hyperbolic tangent is obtained, for which we must determine the slope at the origin, which Bottreau called α, Thus, the final relation of Bottreau's modeling is obtained, expressed as:

$$Ln(\varepsilon_N) = \frac{2Ln(\varepsilon) - Ln(\varepsilon_1\varepsilon_2)}{\ln(\varepsilon_1/\varepsilon_2)} = Tanh(\frac{\alpha}{2}LnV_N) \quad \text{(III .62)}$$

With $V_N = \frac{(1-V_i)V_2}{V_1 V_i}$

This leads to:

$$Ln(\varepsilon_N) = \frac{V_N^{\alpha}-1}{V_N^{\alpha}+1} \quad \text{(III.63)}$$

So we will have:

$$V_N^{\alpha} = \frac{Ln(\varepsilon)-Ln(\varepsilon_1)}{\ln(\varepsilon_2)-\ln(\varepsilon)} \quad \text{(III.64)}$$

After expansion, we obtain:

$$n(\varepsilon) = p_1 Ln(\varepsilon_1) + p_2 Ln(\varepsilon_2) \quad \text{(III.65)}$$

$$p_1 = \frac{\left(\frac{V_1}{1-V_i}\right)^{\alpha}}{\left[\left(\frac{V_2}{V_i}\right)^{\alpha}+\left(\frac{V_1}{1-V_i}\right)^{\alpha}\right]} = \frac{1}{1+V_N^{\alpha}} \quad \text{(III.66)}$$

$$p_2 = \frac{\left(\frac{V_2}{V_i}\right)^{\alpha}}{\left[\left(\frac{V_2}{V_i}\right)^{\alpha}+\left(\frac{V_1}{1-V_i}\right)^{\alpha}\right]} = \frac{V_N^{\alpha}}{1+V_N^{\alpha}} \quad \text{(III.67)}$$

We notice that for $V_i = 0{,}5 \; and \; \alpha = 1$, we rediscover the logarithmic law of Lichtenecker:

$$\varepsilon_i^2 = \varepsilon_1 \varepsilon_2 \quad \text{(III.68)}$$

III.14. Conclusion

In wrapping up our exploration of dielectric materials, it's clear that these substances stand as indispensable pillars in the realms of science and technology. Through our examination of their behavior under electric fields and the intricate phenomenon of polarization, we've unearthed a wealth of knowledge regarding their foundational principles and practical applications.

The understanding of how dielectric materials interact with electric fields is paramount across a diverse spectrum of endeavors, spanning from cutting-edge developments in electronics to innovative pursuits in materials science. The alignment of electric dipoles within dielectrics, as elucidated through polarization, serves as the bedrock for a myriad of electrical phenomena, including but not limited to capacitance, energy storage, and the propagation of electromagnetic waves.

Furthermore, our exploration of the laws governing the mixing of different dielectric materials has provided invaluable insights into the synergistic effects that arise from their combination. Armed with this understanding, engineers and researchers are equipped to optimize material properties and craft bespoke solutions tailored to address specific engineering challenges with precision.

As we draw the curtains on our journey through the realm of dielectric materials, it becomes abundantly clear that they occupy a central position in shaping the contemporary technological landscape and propelling innovations forward. With a deep-seated comprehension of dielectric behavior and its real-world implications, we stand poised to push the boundaries of technological advancement and chart a course toward future breakthroughs in science and engineering.

References

[1] https://www.britannica.com/technology/capacitor-dielectric

[2] Arthur von Hippel, Dielectrics and Waves, Artech House, Boston London, 1995.

[3] Robert Fournié, Roland Coelho, Dielectrics: Theoretical Foundations, Techniques de l'Ingénieur, Electrical Engineering Treatise, D2300.

[4] K. W. Wagner, "Explanation of the dielectric fatigue phenomenon on the basis of Maxwell's concept," Arkiv für Electrotechnik - Edition Shering H. Berlin: Springer-Verlag, 1914.

[5] R. Sillars, "The properties of a dielectric containing semiconducting particles of various shapes," Journal of Institution of Electrical Engineers, Vol. 80, pp. 378-394, 1937.

[6]. N.Bouzit. "Dielectric Characterization of Heterogeneous Materials by Time-Domain Spectroscopy: Application to the Study of Polyester Composites Loaded with Titanates." Doctoral thesis, UFAS, 2002.

[7] D. Hamzaoui. "Study by frequency domain spectroscopy of the evolution of complex permittivity as a function of charge and frequency. Application to polyester loaded with ceramics: BaTiO3 and SrTiO3." Master's thesis, Sétif, 1998.

[8] A. Benhamouda. "Electromagnetic Characterization of Composites by Time-Domain Spectroscopy." Master's thesis, UFAS, 2004.

[9] A. Celzard. "Contribution to the Study of Percolation Phenomenon in Composite Materials with Anisotropic Properties." Doctoral thesis, June 1995.

[10] J. Aubic, A. M. Bottreau. Utilisation de la TDR pour l'Etude des Transferts d'Humidité en Milieux Poreux Perméable. *Journal of Hydrology, 57.* 1982. pp. 337-357.

[11] A. Benhamouda, J.M. Fornies-Marquina, N. Bouzit, N. Bourouba. Dielectric behavior of ternary composites of epoxy/BaTiO3/(CuO or MgO). *Eur. Phys. J. Appl. Phys. 46, 20404.* 2009.

[12] H. Bakhti, N.Bouzit, J.M. Fornies-Marquina, N.Bourouba, A.Benhamouda. Experimental Analysis of Low-Frequency Variation of the Dielectric Constant of a Bi-Titanate Composite as a Function of Concentrations. Proceedings of JIPMA'07 – Annaba, 2007.

[13] S. Ramo, J. R. Whinnery, T. Van Duzer. Fields & Waves In Communication Electronics. *Second Edition John Wiley & Sons.* 1984.

[14] J. J. Makosz, P. Urbanowicz. Relaxation and resonance absorption in dielectrics. *Zeitschrift fur Naturforschung. 57 a, 119-125.* 2002.

[15] S. Berthier, Optics of Composite Media, Polytechnica, Paris 1993.

[16] T. Guillot, Contribution to the modeling of electromagnetic properties of random mixtures of dielectric/conductor type, Thesis of the University of Paris VI, 1992.

[17] A. PriouMaterials in Electromagnetism: Characterization of Composite Materials.

Engineering Techniques AF3373. 1999.

[18] S.Orlowska. "Design and prediction of dielectric characteristics of two and three-phase composite materials through modeling and experimental validation. PhD Thesis, Lyon. 2003".

[19] K. Lichtenecker, K. Rother. *Physik. Zeitschr., 32,255.* 1931.

[20] Tarik, Zakri"Contribution to the Study of Dielectric Properties of Porous Materials for the Estimation of Their Water Content: Mixture Models and Experimental Results. PhD Thesis, National Polytechnic Institute of Grenoble. France: unpublished, 1997."

[21] A. Lonjon. "Polymer/Metallic Nanowires Conductive Nanocomposite: Elaboration and Analysis of Physical Properties. PhD Thesis, June 2010."

[22] J. Aubic, A. M. Bottreau. "Utilization of Time Domain Reflectometry for the Study of Moisture Transfer in Permeable Porous Media. Journal of Hydrology, 57. 1982. pp. 337-357."

[23] H. Bakhti, N.Bouzit, J.M. Fornies-Marquina, N.Bourouba, A.Benhamouda. "Measurements of the dielectric permittivity of a mixture of (CuO – BaTiO3 – Epoxy Resin) in the frequency range of 0 to 5 GHz. Proceedings of JIPMA'07 – Annaba. 2007."

[24] N. Bouzit, J.M. Fornies-Marquina, A. Benhamouda, N. Bourouba. Modeling and dielectric behavior of ternary composites of epoxy (BaTiO3/CaTiO3). *Eur. Phys. J. Appl. Phys. 38, 147-152.* 2007.

[25] N. Bouzit, J.M. Fornies-Marquina, A. Benhamouda, N. Bourouba. "Dielectric behavior of an Epoxy - BaTiO3 - CaTiO3 mixture. Proceedings of ICMM'06, Sétif. 2006."

[26] H.Bakhti, N.Bouzit,N.Bourouba,and JP Martinez Jiménez.Dielectric behavior of a sintered heterogeneous ternary composite resin/BT/Cu2O.Eur.Phys.J.Appl.Phys.80,20202.

[27] H. Bakhti, N. Bouzit . Experimental study of dielectric and functional properties of polymer matrix/Cu2O/BaTiO3 heterogeneous composites in broadband frequency. 14th International Multidisciplinary Scientific GeoConference SGEM 2014, www.sgem.org, SGEM2014 Conference Proceedings, ISBN 978-619-7105-21-6 / ISSN 1314-2704, June 19-25, 2014, Book 6, Vol. 2, 169-176 pp

[28] F. Sischka. Characterization Handbook. TDR. 2002.

[29] S. Ramo, J. R. Whinnery, T. Van Duzer. Fields & Waves In Communication Electronics.

Second Edition John Wiley & Sons. 1984.

[30] J. J. Makosz, P. Urbanowicz. Relaxation and resonance absorption in dielectrics. *Zeitschrift fur Naturforschung. 57 a, 119-125.* 2002.

[31] Appendix B & C. Debye Equation & Review of Dielectric Mixture Rules.

[32] T. Samiha, Bishay. Numerical Methods for Calculation of Cole-Cole Parameters. *Egypt J. Sol., Vol. 23, N°2.* 2000.

[33] Zhi Yu et Chen Ang. Maxwell-Wagner Polarization in Ceramic Composites BaTiO3-(Ni0.3 Zn0.7)Fe 2.1O4. *Journal of Applied Physics.* January 2002. Vol. 91, 2.

[34] P. Debye. Polar Molecules. *Chemical Catalog Co., New York.* 1929.

[35] K.S. Cole, R.H. Cole. *J. Chem. Phys. 9, 341.* 1941.

[36] J.C. Maxwell-Garnett. *Philos. Trans. R. Soc. London Ser. A, 203, 385,.* 1904.

[37] J. P. Faroux, J. "Renault. Electromagnetism 2: Maxwell's equations and induction phenomena. DUNOD Edition. 1998."

[38]Haddi BAKHTI, "Dielectric characterization of a mixture of titanate and oxide (Epoxy resin, BaTiO3, Cu2O) sintered as a function of frequency," PhD Thesis in Electronics, Ferhat Abbas University of Sétif, 2018.

[39] Maxwell-Garnett, J. C. "Colours in metal glasses and metallic films." Philosophical Transactions of the Royal Society 203 (1904): 385-420.

[40] Demeyre, Jean-François. "Characterization of powder mixing homogeneity and agitation in a triaxial mixer." Doctoral thesis in process engineering and environment, National Polytechnic Institute of Toulouse, 2007.

[41] Sabri, N. "Study of the phenomenon of rotary polarization." Magisterial thesis, Abou Bekr Belkaid University of Tlemcen, 2001.

[42] Reddaf, Abdelmalek. "Study and simulation of the behavior of dielectric materials at fixed frequency." Magisterial thesis in instrumentation, Ferhat Abbas University of Sétif, 2009.

[43] S. Lalléchère, S. Girard, Analyse de matériaux composites aléatoires à l'aide d'outils tridimensionnels de simulation électromagnétique, Journal International de Technologie, de l'Innovation, de la Physique, de l'Energie et de l'Environnement 2(1) (2016) 1 - 16.

[44] R. Landauer, Electrical conductivity in inhomogeneous media, AIP Conf.Proc.-ETOPIM 40(2) (1978) 2 - 45.

[45] Ari Sihvola, "Electromagnetic mixing formulas and applications," The Institution of Engineering and Technology (IET): London, United Kingdom, 2008.

[46] O.F. Mossotti, Discussione analitica sull influenza che l'azione di un mezzo dielettrico ha sulla distribuzione dell'ellettricta alla superficie di più corpi elettici disseminati in esso, Mem. Math. Fisica Modena 24 (1850) 49 - 74.

[47] R. Clausius, Die mechanische behandlung der elektrizität. Die mechanische wärmtheorie, Braunschweig : Vieweg 2 (1879) 62 - 97.

[48] M.T. Prinkey, A. Lakhtakia, B. Shanker, On the extended Maxwell-Garnett and the extended Bruggeman approaches for dielectric-in-dielectric composites, Optik 96 (1) (1994) 25 - 30.

Modeling of Dielectric Composite

IV. Introduction

In this chapter, we address two parts. In the first part, we examine a composite made from epoxy resin (ER) in a liquid state, combined with barium titanate (BT) in powder form, at room temperature. This composite is prepared using a mixing method, with innovative molds created in the scientific instrumentation laboratory. This approach allowed us to minimize the losses of titanate and resin by accurately calculating the volume and weight needed to create a sample of the composite. We extract several dielectric parameters, including dielectric permittivity, dielectric losses, electric modulus, static conductivity, and dissipation factors. These parameters vary according to the concentration of barium titanate and the frequency of the characterization bench, which ranges from a few MHz to several tens of GHz.

To better validate the experimental results, two experimental characterization methods are employed: one covering a wide frequency range and the other at a fixed frequency, to determine the dielectric parameters of the composite. The first method is time-domain spectroscopy (TDS) using coaxial waveguides, while the second is conducted using a fixed-frequency X-band test bench (MTB) made from rectangular waveguides. Additionally, various empirical mixing laws are applied to estimate the dielectric permittivity of the composites. The results indicate that increasing the concentration of BT enhances the effective dielectric permittivity, supported by different empirical mixing models. These findings have significant implications for the development of electrical devices such as sensors, wave absorbers, resonators, and antennas. The research presented in this chapter contributes to the advancement of materials designed for efficient energy storage and other related applications.[1]

In the second part, we discuss my topic, which I presented at a conference: characterization of dielectric materials in heterogeneous multilayers at microwave frequencies. This work involves studying heterogeneous multilayer dielectric materials at microwave frequencies. We employ a fixed frequency measurement characterization technique. The multilayer dielectric materials (CaTiO3), resulting from stacking heterogeneous layers, create a new medium with unique properties that differ from standard constants. Composite materials demonstrate superior performance compared to homogeneous materials, making them very promising for applications. The permittivity of heterogeneous mixtures has been studied by several researchers, and numerous theories and empirical formulas have been proposed and developed to model the dielectric behavior of composites.

The main objective is to propose a new approach to characterize a specific layer that is part of a multilayer structure. We start from the following principle: for a multilayer stacking of different materials, the effective dielectric permittivity essentially depends on the permittivities of the materials and their thickness (or volume). Thus, measuring the effective permittivity allows us to determine the permittivity of a specific layer by knowing the thicknesses and constituents of each layer. Moreover, we also aim to highlight the effect of each layer on the effective permittivity of the entire structure.[2]

IV.1 .PART 1

IV.1. 1 . Sample Preparation Procedure

Based on previous work, the authors found that most errors are related to the sample preparation method. Therefore, in this section, we will emphasize the technique for producing the different samples. Furthermore, we found it very useful to outline the procedure for preparing these samples using the newly manufactured molds. We will use two materials: first, liquid epoxy resin, which acts as a matrix (or support) to encapsulate and bind the grains of the fillers, which are expected to be ellipsoidal, and second, barium titanate (BT) in the form of white powder with a particle size ranging from 0.1 to 1.5 µm.

IV.1.1.2. Host Matrix: (Epoxy Resin)

The term "epoxy resin" refers both to the pre-polymer and its system of hardened resin and hardener. Before the epoxy is cured, the resin has an unlimited shelf life. The ability to transform from a liquid state to a hard thermosetting solid is one of the valuable properties of epoxy resins. Solidification is achieved through the addition of a chemical reagent known as a hardening agent or hardener. The polymerization reaction can be conducted at room temperature.

Figure IV.1 La résine et le durcisseur

IV.1.1.2.1 Types of Resins

There are two types of resins available on the market: epoxy resins and polyurethane resins. Generally, the concept of resin as a binder involves a base resin combined with a hardener, resulting in a completely rigid material. This application requires proper preparation of the binder and must follow specific proportionality guidelines, considering conditions such as temperature, humidity, and lighting. Epoxy resin is regarded by professionals as the standard for resins. It offers excellent mechanical resistance and significant customization options through the addition of color pigments, which can create a color palette. It's important to note that incorporating mineral fillers and various additives can affect both the strength and the properties of the resin itself. [3]

Its main component is bisphenol A, which may be combined with bisphenol F to achieve better resistance. The most commonly used hardener is cycloaliphatic amine. The polyurethane resin is noted for being more flexible and versatile. While this solution is less economical, it offers greater versatility. Its base consists of synthetic polyols or polyalcohols, a polyether backbone, and a hardener known as isocyanate, which is quite common. Its primary advantage lies in its flexibility, while still maintaining hardness due to the resin.

IV.1.1.3 Barium titanate (BT)

Barium titanate is a polar ferroelectric ceramic powder produced by a solid-state reaction of barium carbonate ($BaCO_3$) with titanium dioxide (TiO_2) or by precipitation from an intermediate, such as barium oxalate (BaC_2O_4) [4]. BT comes in five varieties, based on the temperature used in its manufacturing process.

It finds varied applications in the electronics industry due to its exceptionally high permittivity, as well as its piezoelectric and ferroelectric properties.

Its dielectric constant is highly dependent on the applied potential and temperature; it can vary from 1200 at 25°C to 10000 at 130°C for a frequency of 1kHz. Therefore, BT is generally modified in combination with other materials (Figure IV.2). This allows its characteristics to be manipulated, resulting in a wide variation of its properties. Among the ceramic components based on BT, we can mention sensors, microwave capacitors, resonators, measuring instruments, and more [5].

Figure IV.2 Barium titanate (BT).

IV.1.1.3.1 Crystallographic Study of BT

The ABO3 type ferroelectrics have a perovskite structure and are widely used in the microelectronics industry due to their high dielectric constant materials. The most significant example of ferroelectrics is barium titanate (BT) [6]. Barium titanate possesses a face-centered cubic crystal structure, which explains its high permittivity at elevated temperatures.

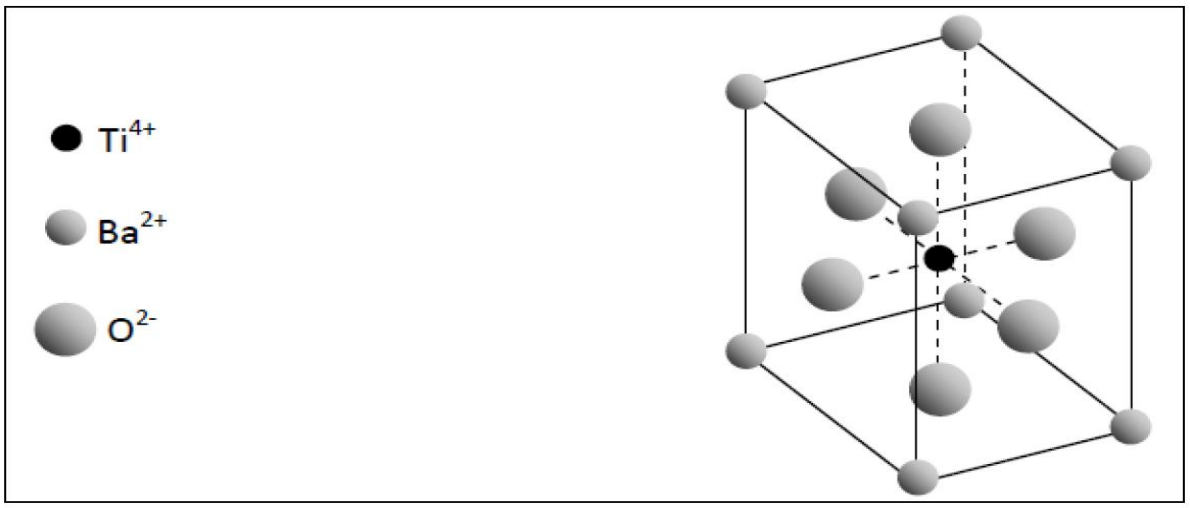

Figure IV.3 Crystal structure of barium titanate (BT), of the face-centered cubic type.

IV.1.1.4 Sample Preparations.

IV.1.1.4.1 Development of resin matrix composite materials

The processes for implementing composite materials involve three essential steps. The first step is the association and impregnation of the reinforcement with the resin. The second step involves maintaining the shape of the sample, and the final step is the thermal solidification of the material, which can occur either through cooling for thermoplastic

matrices or through polycondensation or crosslinking for thermosetting matrices (at increasing temperatures), known as polymerization.

There are various processes, but the most commonly used is the molding process. Molding can be performed in an open mold with an exposed surface or in a closed mold. We utilized epoxy resin (RE) as the matrix medium, which binds the particles of the fillers and eliminates air pores. The included fillers vary in volume fraction from 0% to 30%, with a step of 5%. Table (IV.1) lists the designation and composition of the samples.

Table IV.1: Composition used for sample preparation

Material Designation	Sample code	Epoxy Resin (RE) (%)	Barium Titanate (BT) (%)
100 RE_0 BT	RB0	100	0
95 RE_5 BT	RB1	95	5
90 RE_10 BT	RB2	90	10
85 RE_15 BT	RB3	85	15
80 RE_20 BT	RB4	80	20
75 RE_25 BT	RB5	75	25
70 RE_30 BT	RB6	70	30

IV.1.1.4.2 Determination of volume fractions

Since the mixing laws depend on volume fractions, it is essential to work with volumes. For titanates in powder form, direct measurement of volume is not feasible, so we must weigh the exact masses that correspond to specified volumes. The conversion from volume to mass is performed as follows: First, we establish the total volume "V_{tot}" of a sample (based on the mold dimensions); then, we determine the volume fraction "F_{matrix}" of the matrix (epoxy resin), and we calculate the required volume of the matrix using the equation (IV.1).

$$V_{matrix} = V_{tot}. F_{matrix} \quad \text{(IV .1)}$$

Next, we establish the volumetric fraction "Vcharge" of a given charge (for example BT) and calculate the volume corresponding to this volumetric fraction using equation (IV .2)

$$\mathbf{V_{charge}} = \mathbf{V_{tot}}. \text{Fcharge} \quad \text{(IV .2)}$$

Finally, the mass M, the charge of this volume, is deduced using the charge density, denoted as D charge, from the equation (IV -3)

$$M_{charge} = D_{charge}. V_{charge}. \quad \text{(IV .3)}$$

For weighing the different proportions of powder, an electronic balance with a sensitivity of 1 mg is used. (Figure IV.4).

Figure IV.4 The electronic balance used for weighing the different proportions of powder

IV.1.1.4.3 Preparation process

The technique used is hand lay-up, which is the most traditional and simplest molding method for the fabrication of composite samples. The infrastructure required for this method is minimal, and the processing steps are also quite simple. All composite samples based on epoxy and different fillers are prepared using this technique, which involves the following steps:

Firstly, the resin, consisting of equal volumes of pure epoxy resin and hardener, is poured into a container, and the two components are manually mixed until they form a single viscous liquid. Air bubbles appear and are removed from the resin using a vibrator.

Secondly, the desired fillers are added, and the entire mixture is stirred thoroughly until no isolated grains remain. Mixing continues to achieve the most homogeneous mixture possible, ensuring that the resin coats all the powder. It is important to note that the mixing phase determines the final product's homogeneity quality.

Thirdly, the mixture is gently poured into parallelepiped and hollow cylindrical molds. Before pouring the epoxy/filler mixture into the molds, the mold walls are wiped with silicone or wax. Applying a layer of wax or spraying silicone facilitates easy removal of the samples from the mold after curing.

It is observed that, as the volumetric fraction of the filler increases, it becomes more difficult for the resin to bind the grains, and it becomes saturated. The viscosity of the mixture decreases, and another difficulty arises with the flow of the mixture into the mold. It is essentially this constraint that determines the maximum filler fraction that cannot be exceeded. The mixture is poured while trying to achieve a uniform spatial distribution in the mold.
Once the mixture is poured, it is left for several hours (>48 hours) at room temperature, while continuously keeping the vibrator under the mold container until the resin is fully polymerized. During this time, the phenomenon of air bubble degassing can be observed. The use of a vibrator helps to eliminate these bubbles from within the mixture. Once the resin is fully polymerized and the mixture has become firm, it is carefully demolded. The result is a relatively hard composite material, with a color that varies from cream to yellowish-white, depending on the filler concentration.[7]

IV.1.1.4.4 Machining of the Samples

Tubular samples are required for characterization on a TDS bench. This shape is obtained from the parallelepiped samples using a hollow cylindrical drill of appropriate dimensions (7 mm in diameter). A 3 mm diameter hole is then drilled. Polishing is necessary to adjust the samples to the dimensions of the coaxial guide used in TDS (a = 3.04 mm and b = 7 mm) and to obtain flat and perpendicular surfaces. This was the former method used in our laboratory, and due to its major drawback, we decided to develop new molds, specifically for the two techniques (TDS and fixed-frequency bench). Through these, we aim to improve the quality of the samples, eliminate previous defects, and resolve dimensional uncertainties while utilizing new features of these molds[8].

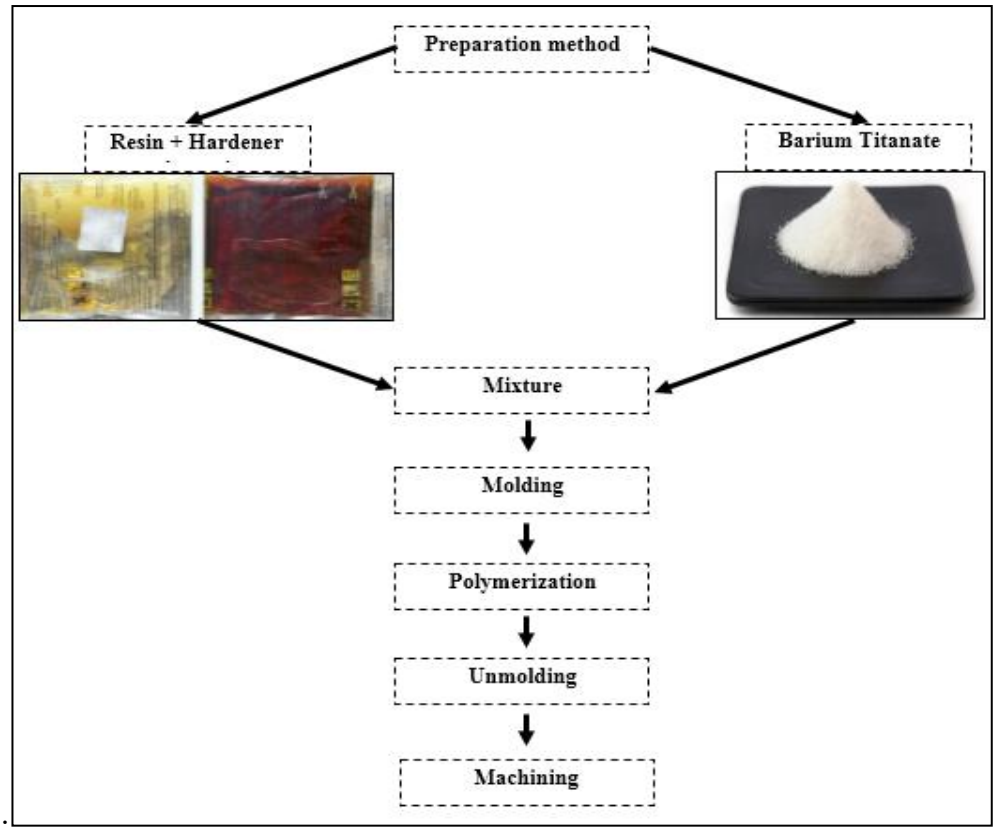

Figure IV.5: Main Steps in the Sample Manufacturing Process by Molding.

Figure IV.6: The Parallelepiped Mold..

For characterization at a fixed frequency, parallelepiped samples are needed, with dimensions identical to those of the rectangular guide used in this measuring bench. Delicate machining must be performed through polishing to obtain flat surfaces that are perpendicular

to the direction of propagation, ensuring that the dimensions are such that when the sample is introduced into the guide, there is complete and perfect contact between its four faces and those of the guide. The guide section has a length L=22.86 mm and a width l=10.16 mm. For this, we developed this mold:

Figure IV.7 Sample Produced by the Parallelepiped Mold.

For characterization on a TDS bench, tubular samples are required. This shape is obtained by extracting with a hollow cylindrical drill of appropriate dimensions for the coaxial guide, with an outer diameter ϕ_{ext} =7 mm and an inner diameter ϕint=3.

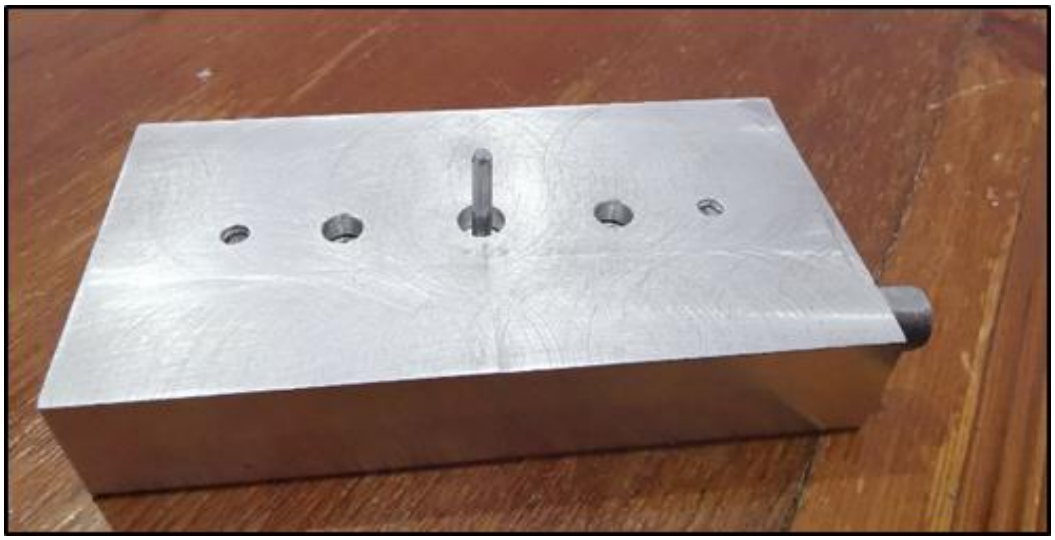

Figure IV.8 The Hollow Cylindrical Mold.

Figure IV.9 Sample Produced by the Hollow Cylindrical Mold.

IV.1.2. Presentation of Results

IV.1.2.1. Binary Mixture of Barium Titanate and Epoxy Resin (RE/TBA)

The authors 'REDDAF A/MALEK' used the TDS technique in modeling the binary mixture RE/TBA and obtained the following results:

The numerical values of permittivity ε and conductivity σ are presented in Table IV.2, along with their graphical representation.

Tableau IV.2: The variation of the real permittivity and conductivity of the (RE/TBA) as a function of the volumetric fraction BT.

BT(%)	permittivity (ε)	Conductivity (S/m).10 $^{-3}$
0	2.567	2.661
5	3.095	6.127
10	3.356	6.051
20	4.436	5.231
25	6.031	7.532
30	7.815	9.323

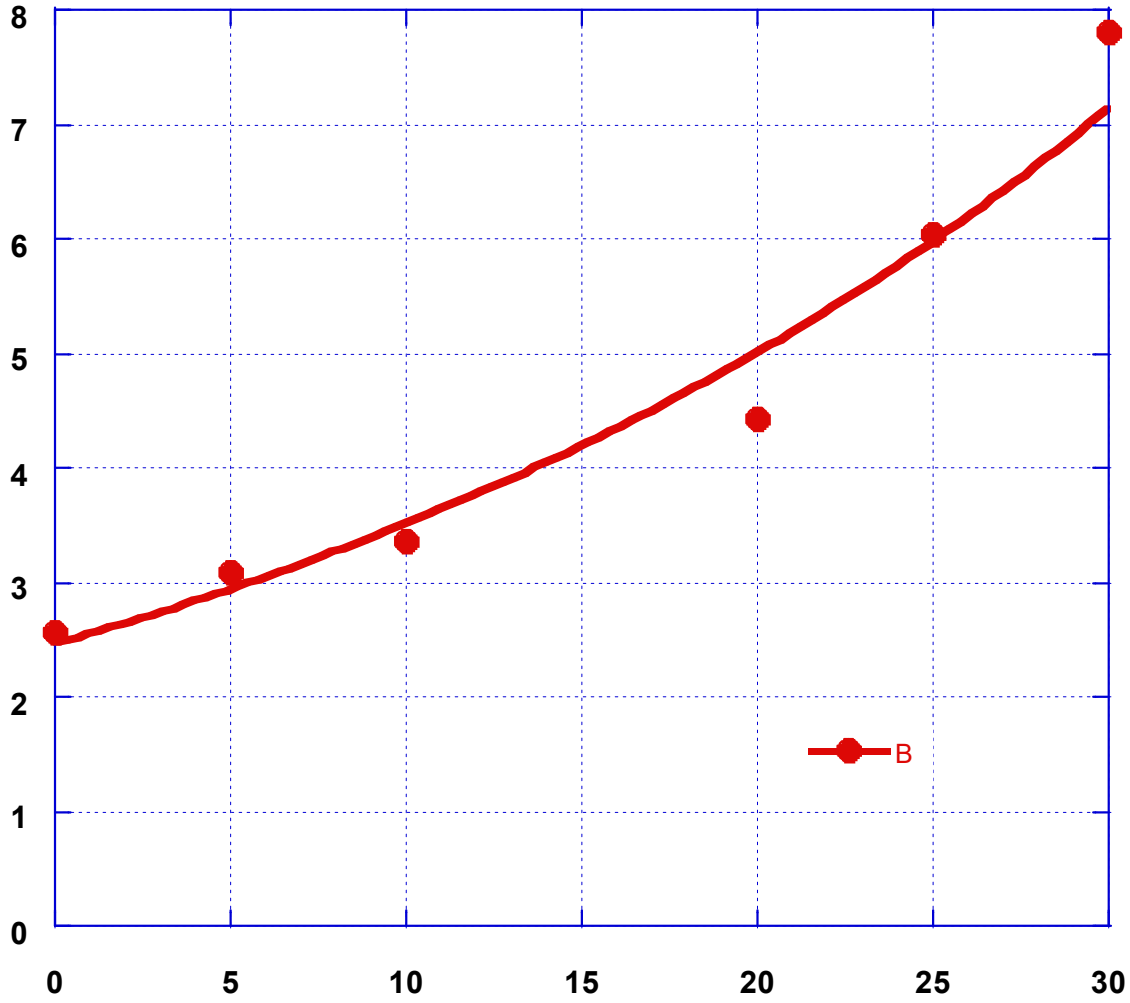

Figure IV.10: The variation of the real permittivity of (RE/TBA) as a function of the volumetric fraction of BT

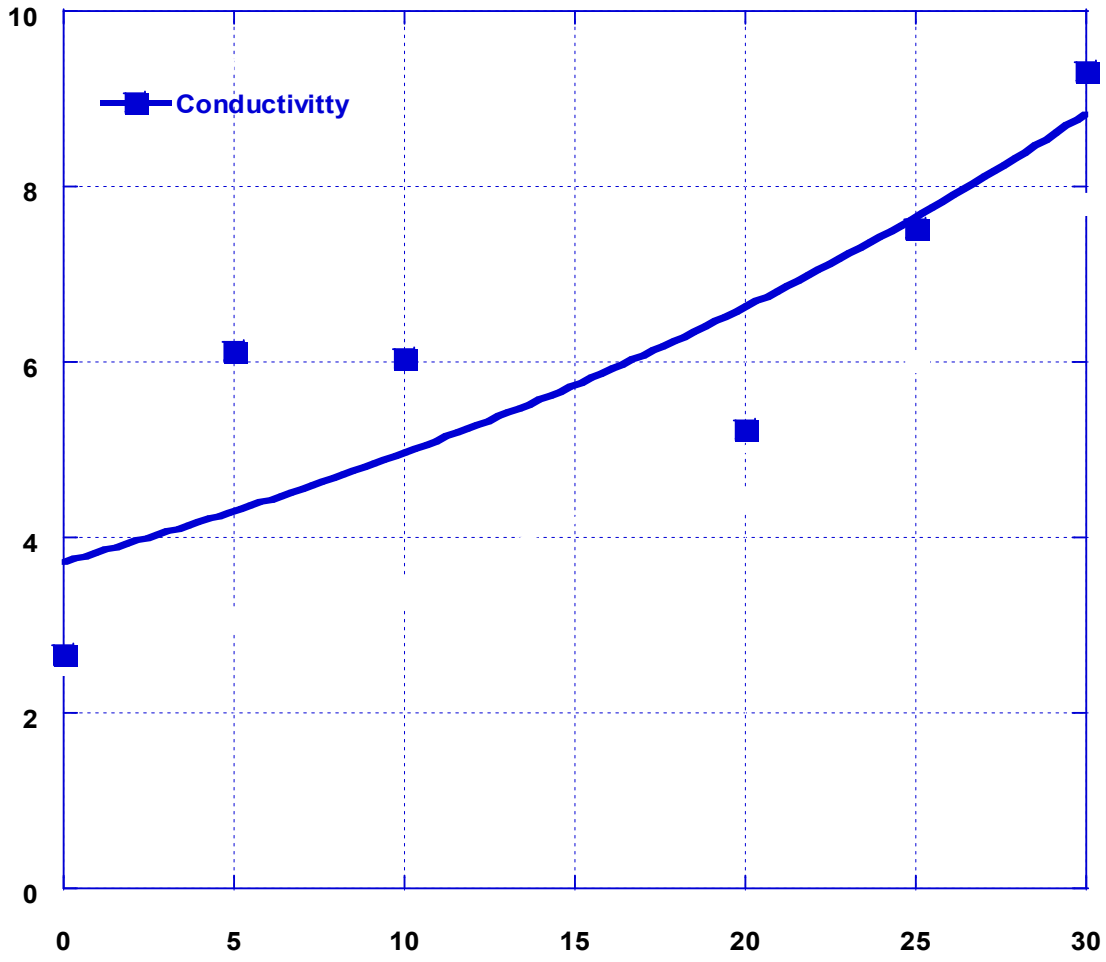

FigureIV.11: The variation of the conductivity of (RE/TBA) as a function of the volumetric fraction of BT.

For the graphical representation of the dielectric constant, we can observe that its variation with charge concentration is composed of two linear segments: from 0% to 17% with a slope of 0.079, and from 17% to 30% with a slope of 0.4072. This is also reflected in the conductivity, where a static minimum is observed at a concentration of 17%. It can be noted in the figure that at this point, there is a significant change compared to the previous behavior, indicating a quasi-percolation change.[9]

The experimental parameters we measured from the rectangular measurement bench MTB include the standing wave ratio, the wavelength in the guide, and the difference between two minima in the presence of the sample and in short-circuit, which is used as a reference.

The bench is adjusted with the klystron power supply set to (Voltage = 110 V; Current = 20 mA), and the operating frequency is 9490 MHz, with the signal attenuated to -32 dB.

Table IV.3: Parameters Measured Experimentally Using the TOS Method.

TOS	Min1 (mm)	Min2 (mm)	Min3 (mm)	Min (mm)	Min (mm)	Min (mm)	Min (mm)	Min (mm)
Short-Circuit	42.9	54	65.3	76.2	87.2	98.4	109.3	120.3

λg with TOS mètre = 44,1 mm; TOS with TOS metre= 20.66db; $\lambda_c = 2a = 45.72$ mm

$$\lambda_{0gmoy} = \frac{\sum \lambda_{0gi}}{i} = \frac{44{,}4 + 44{,}4 + 43{,}8 + 43{,}8}{4} = 44{,}1\text{mm}$$

$$\Delta\lambda_{0g} = sup\left|\lambda_{0gmoy} - \lambda_{0gi}\right| = 0{,}3\text{mm}$$

The obtained values are grouped in the following tables.

Table IV.4: the variation of the real permittivity and the conductivity of (RE/TBA) as a function of the BT volume fraction.

BT	La permittivity(ε)	La conductivity (S/m).10 $^{-3}$
0	2.867	5.81
5	3.245	6.27
10	3.56	6.47
15	3.79	6.4
20	4.32	6.51
25	4.96	7.032
30	615	7.823

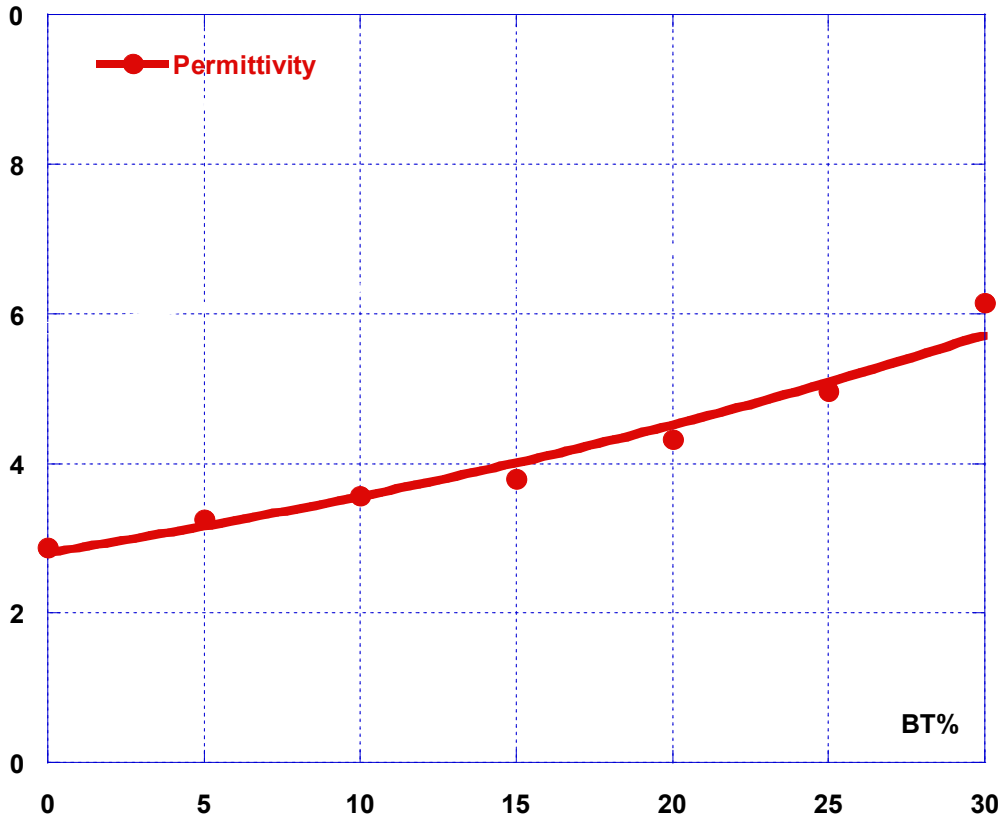

Figure IV.12: The variation of the real permittivity of (RE/TBA) as a function of the volumetric fraction of BT

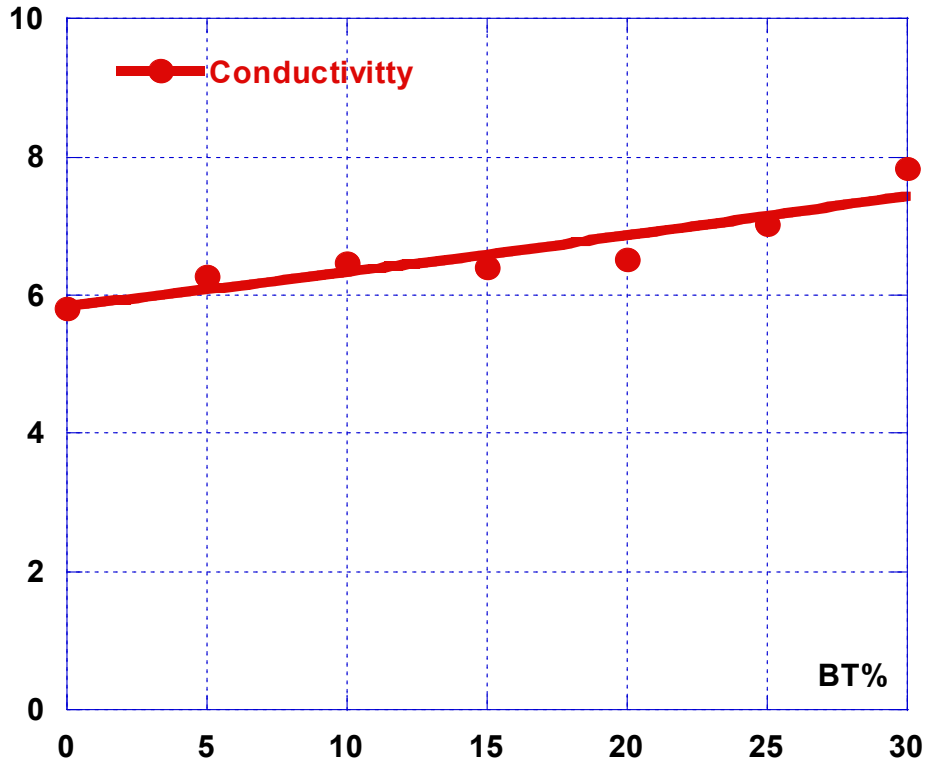

Figure IV.13 The variation of the conductivity of (RE/TBA) as a function of the volumetric fraction of BT.

IV.1.3 Dielectric Analysis

This section discusses the effective dielectric permittivity, dielectric loss, electric modulus, static electric conductivity, dissipation factor, and quality factor for the RE-BT composites. We report that all results were obtained at a fixed frequency of 9.490 GHz for the microwave test bench results in the X-band (MTB) and the data throughput in the range from DC to 9.490 GHz for the time-domain spectroscopy (TDS) results, which is approximately invariant in field length (flat spectrum).

Table IV.5: Prediction of Dielectric Permittivity (ε(TB) = 78.28 et ε(RE) = 26)

RE %	BT %	ε(TDS)	ε(MTB)
100	0	2.567	2.867
95	5	3.095	3.245
90	10	3.356	3.56
85	15	3.956	3.79
80	20	4.436	4.32
75	25	6.031	4.96
70	30	7.815	6.15

IV.1.3.1. Dielectric Permittivity (ε')

An important characteristic in the development of electronic applications is the dielectric constant (permittivity). Figure (IV.5) illustrates how the dielectric permittivity of the RE-BT composites varies as the volumetric percentage of barium titanate increases, based on the results from both characterization methods (TDS and MTB).

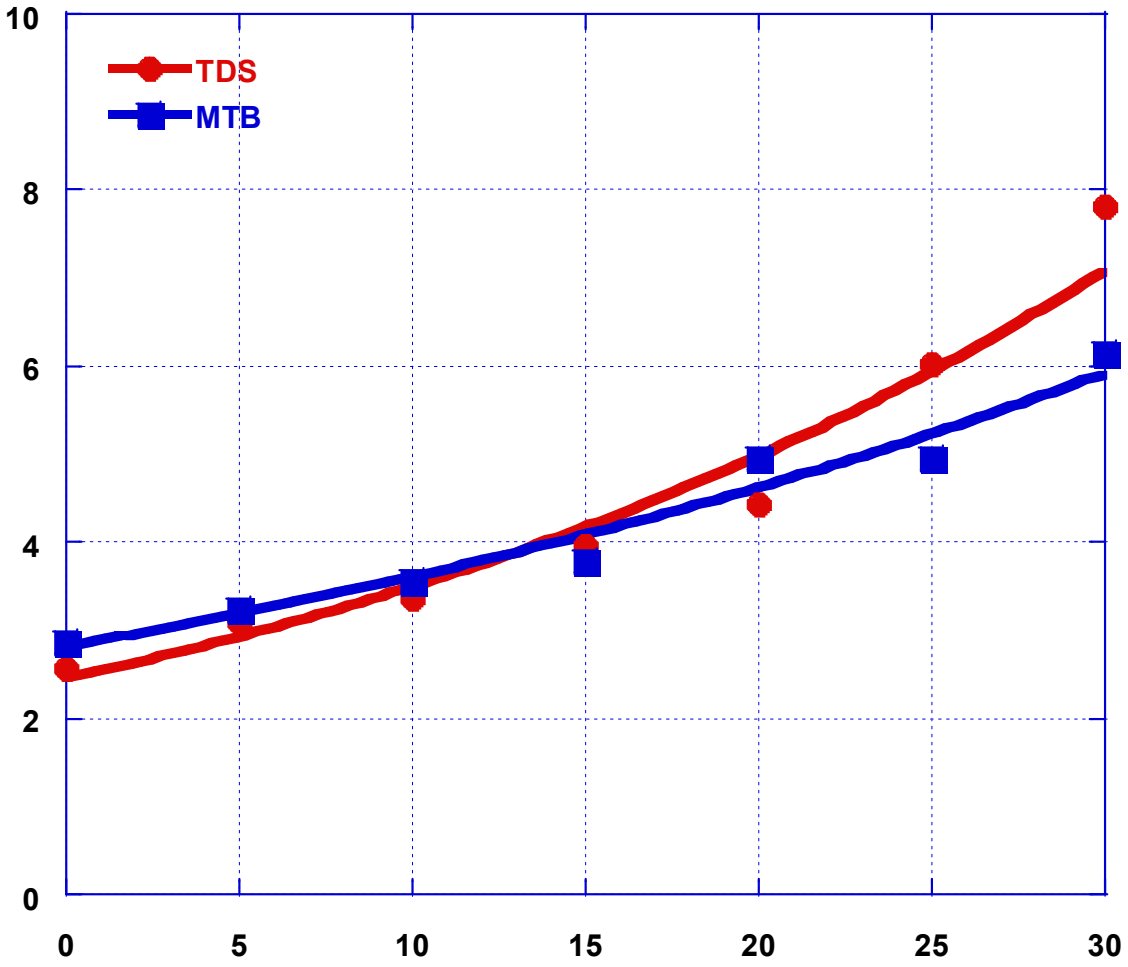

Figure IV.14: Results of Dielectric Permittivity as a Function of the Volumetric Fraction of BT in the Binary Composite for Both Benches.

According to the graph, we can observe that the dielectric permittivity increases as the volumetric fraction of BT rises for both testing benches. However, the permittivity values obtained from the microwave test bench are generally higher than those obtained from the TDS bench for the same volumetric fraction of BT. This increase in dielectric permittivity indicates the same effect of the perovskite titanate BT as observed in previous studies [9-18, 17, 19] on various binary, ternary, and quaternary composites containing perovskite titanates such as calcium and strontium titanate. The curve for the RE-BT composite starts with the first pure RE-BT matrix composite (100% - 0%) and rises until it reaches the second binary composite RE-BT (70% - 30%). At low volumetric fractions of BT, the difference in permittivity between the two testing benches is relatively small. However, as the volumetric fraction of BT increases, the difference in permittivity between the two testing benches

becomes more significant. When the concentration of BT increases, a notable rise in the dielectric permittivity (ε') of the composite is observed in the results from both benches. For example, at a volumetric fraction of 30% of BT, the permittivity value obtained from the TDS bench is 7.815, while that obtained from the microwave test bench is 6.15. This could be due to several factors, including differences in the measurement techniques used by the two benches, or differences in the frequencies of the electromagnetic waves employed by these benches. The main reason remains the larger sample size used in the MTB bench, which implies that the distribution of the filler material is uniform and space to some extent. In comparison, the smaller sample size in the TDS bench, which is three times smaller than the former, indicates that the distribution of the filler material within the matrix is very close. The maximum value, estimated at 7.815, is achieved by the TDS bench with a concentration of 30% BT when the composite is primarily binary. The minimum value of 2.567 is recorded for 100% RE in a composition (100%-0%), corresponding to a pure matrix mixture.

IV.1.3.2 Dielectric Loss (ε'')

The frequency of oscillation of the atoms becomes difficult to control once the electric field is applied. The material undergoes polarization due to dielectric loss.

The dielectric loss of the RE-BT composite is analyzed concerning the volumetric fraction of the filler

Table IV.6: Results of Dielectric Loss and the Volumetric Fraction of BT in the Binary Composite for Both Devices.

BT(%)	ε"(TDS)	ε" (MTB)
0	0.203	0.208
5	0.220	0.225
15	0.217	0.232
10	0.181	0.230
20	0.188	0.234
25	0.270	0.252
30	0.335	0.281

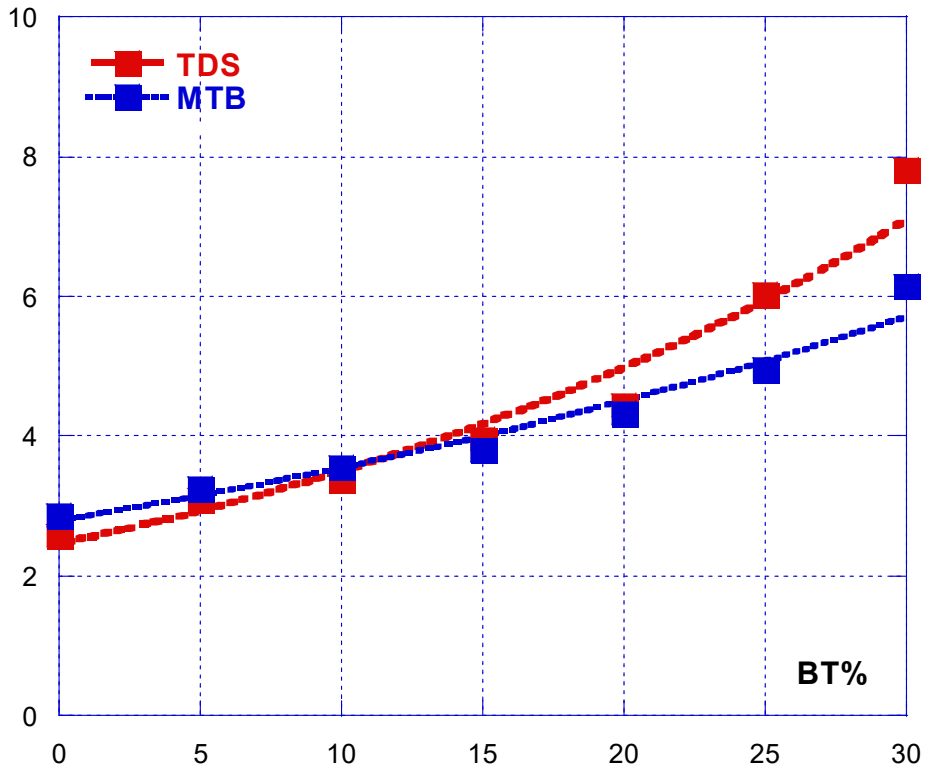

Figure IV.15: Results of Dielectric Loss as a Function of the Volumetric Fraction of BT in the Binary Composite for Both Devices.

Figure (IV.15) shows the results of dielectric loss for a binary composite composed of a BT filler and a polymer matrix, measured using two different methods. Overall, both methods exhibit similar trends regarding the variation of dielectric loss as a function of the volumetric fraction of BT. Losses generally increase with the increasing filler content, with some fluctuations between the two. At the lowest filler content (0%), the TDS measurements yield a slightly lower loss value compared to the MTB method, but the difference is relatively small. As the filler content increases, the losses measured by both methods converge to a similar range (from 0.21 to 0.28 for MTB results and from 0.20 to 0.33 for TDS results).

However, there are notable differences between the two methods. Generally, TDS measurements exhibit larger fluctuations in loss values as the filler content increases, with dips and peaks not present in the microwave results. This could be attributed to the fact that

TDS covers a broader frequency range, which may reveal a more complex behavior of the dielectric properties of the composite. On the other hand, the microwave method operates at a fixed frequency and may not capture some of the nuances of the composite's behavior at different frequencies.

IV.1.3.3 Electric Module (M)

The effects of relaxation phenomena in polymer and composite systems can be presented and studied using different formalisms: dielectric permittivity, electric module, conductivity, and complex impedance. All four of these formalisms can describe the electrical phenomena present in polymers and complex systems, including the one in our case study (binary composite). In this study, we focus on the effects of inclusion concentrations on the behavior of the composite using two measurement techniques, leveraging the electric module. The electric module is the inverse of the permittivity, although it was originally introduced by Macedo [20] and is given by equation (1). To this end, the values of M' and M" are calculated for all samples prepared according to the volumetric fraction of BT.

$$M^* = \frac{1}{\varepsilon^*} = \frac{1}{\varepsilon^{'} - j\varepsilon^{''}} = \frac{\varepsilon^{'}}{\varepsilon^{'2} + \varepsilon^{''2}} + j\frac{\varepsilon^{''}}{\varepsilon^{'2} + \varepsilon^{''2}} = M^{'} + jM^{''} \qquad (\text{IV.4})$$

Where M' and M" represent the real and imaginary parts of the electrical modulus, respectively.

Figure (IV.7) illustrates the variation of the electric module (real and imaginary parts) as a function of the BT concentration in the RE-BT composite, using two characterization methods (TDS and MTB). Examination of the results in the MTB graph shows a noticeable decrease in both the real and imaginary parts of the electric module of the composite as the volumetric fraction of BT increases. The highest value achieved so far is approximately 0.34 and 0.025 for the real and imaginary parts of the electric module, respectively, at a concentration of 0% BT, corresponding to the pure matrix composite (100% epoxy resin). According to the TDS results, it is noted that BT, considered as the second component of this composite, similarly influences the electric module of the resulting mixture, where the highest values are between 0.38 and 0.03 for the real and imaginary parts of the electric module, also obtained at a concentration of 0% BT. We observe a decrease in this parameter with increasing concentrations of BT.

Table IV.7: Results of the electric modulus (real part and imaginary part) and the volumetric fraction of BT in the binary composite for both setups.

	M'		M''	
BT %	TDS	MTB	TDS	MTB
0	0.387	0.346	0.030	0.025
5	0.321	0.306	0.022	0.021
10	0.296	0.279	0.019	0.013
15	0.252	0.262	0.011	0.015
20	0.230	0.230	0.009	0.012
25	0.165	2.201	0.007	0.010
30	0.127	O.162	0.005	0.007

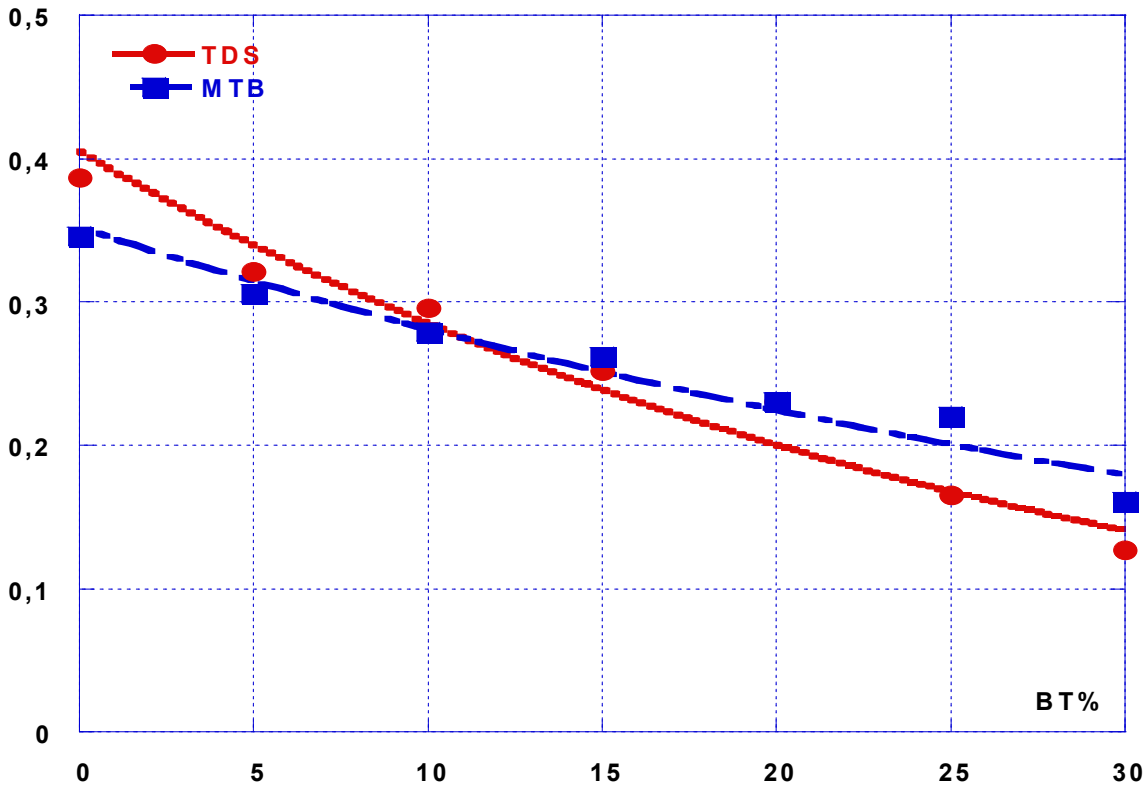

-a-

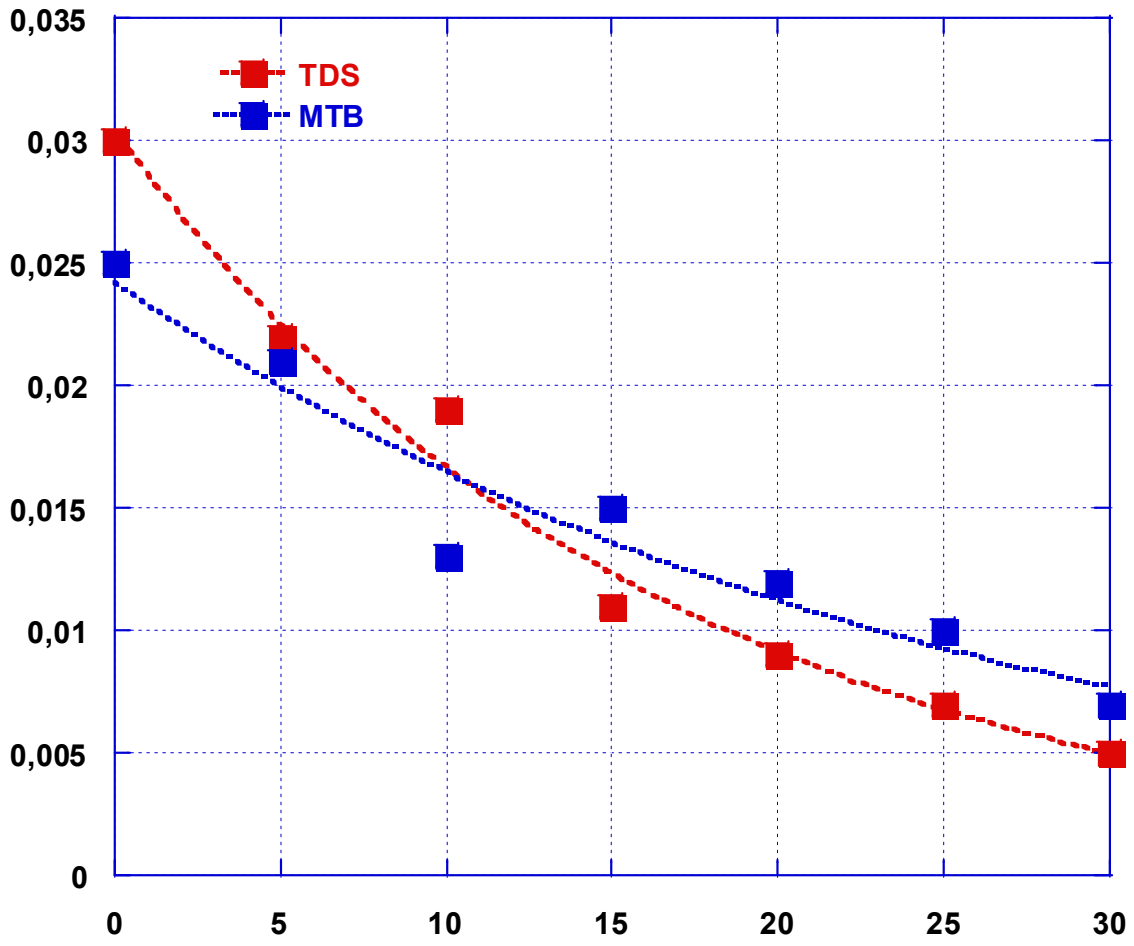

-b-

Figure IV.16: Electric modulus: (a) Real part (b) Imaginary part of the results as a function of the volumetric fraction of BT in the binary composite for both setups

IV.1.3.4 Electrical conductivity (σs)

Figure (IV.17) shows the variation of electrical conductivity as a function of BT concentration in the RE-BT composite using two characterization methods (TDS and MTB). The static conductivity of the dielectric mixture at a fixed frequency f is given by: [21]

$$\sigma_s = 2\pi f \varepsilon_0 \cdot \varepsilon'' \qquad (\text{IV.5})$$

Where ε_0 and ε'' denote respectively the permittivity of free space and the imaginary permittivity (dielectric loss).

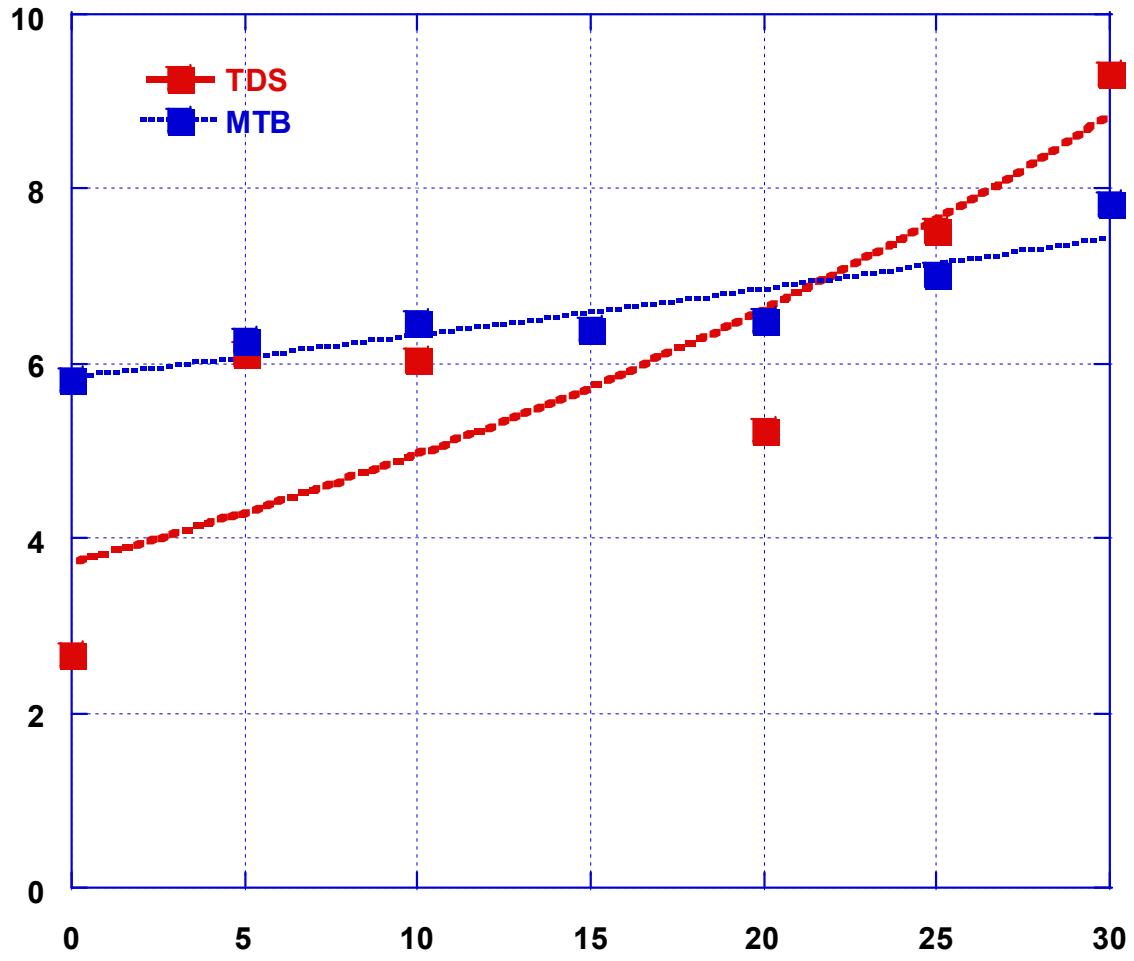

Figure IV.17: Results of Electrical Conductivity as a Function of the Volumetric Fraction of BT in the Binary Composite for Both Devices.

Figure (IV.17) illustrates the conductivity results vs BaTiO3 volume fraction of the binary composite for the TDS bench, we note an evolution of the conductivity which appears at a practically constant value between 0 and 20% concentration of BaTiO3. This behavior is indicative of the onset of the quasi-percolation process at a concentration close to 20% of BaTiO3, where the conductive pathways start to form in the composite material. The behavior of the conductivity vs BaTiO3 volume fraction in the TDS bench is consistent with the quasi-percolation process, which is a well-known phenomenon in composite materials. This process occurs when the filler concentration reaches a critical value, at which point the filler particles start to touch and form a continuous

conductive pathway. This process is highly dependent on the shape and size distribution of the filler particles, as well as their interparticle spacing. Overall, the conductivity results for the TDS bench show a clear trend towards the quasi-percolation process, which is an important consideration for the design and optimization of composite materials

IV.1.3.5 Dissipation Factor (tan δ)

The dissipation factor is the ratio between the energy stored by the dielectric constant and the energy lost due to dielectric loss during the polarization of the composite material, commonly referred to as the loss tangent, which is given by: [22]

$$\tan\delta = \frac{\varepsilon''}{\varepsilon'} \qquad (IV.6)$$

Table IV.8: Results of the loss tangent and the volume fraction of BT in the binary composite for the two test setups.

BT %	TDS	MTB
0	0.079	0.072
5	0.071	0.069
10	0.065	0.065
15	0.045	0.060
20	0.042	0.054
25	0.044	0.050
30	0.042	0.045

This section discusses the impacts of BT filling and how they affect the dissipation factor.

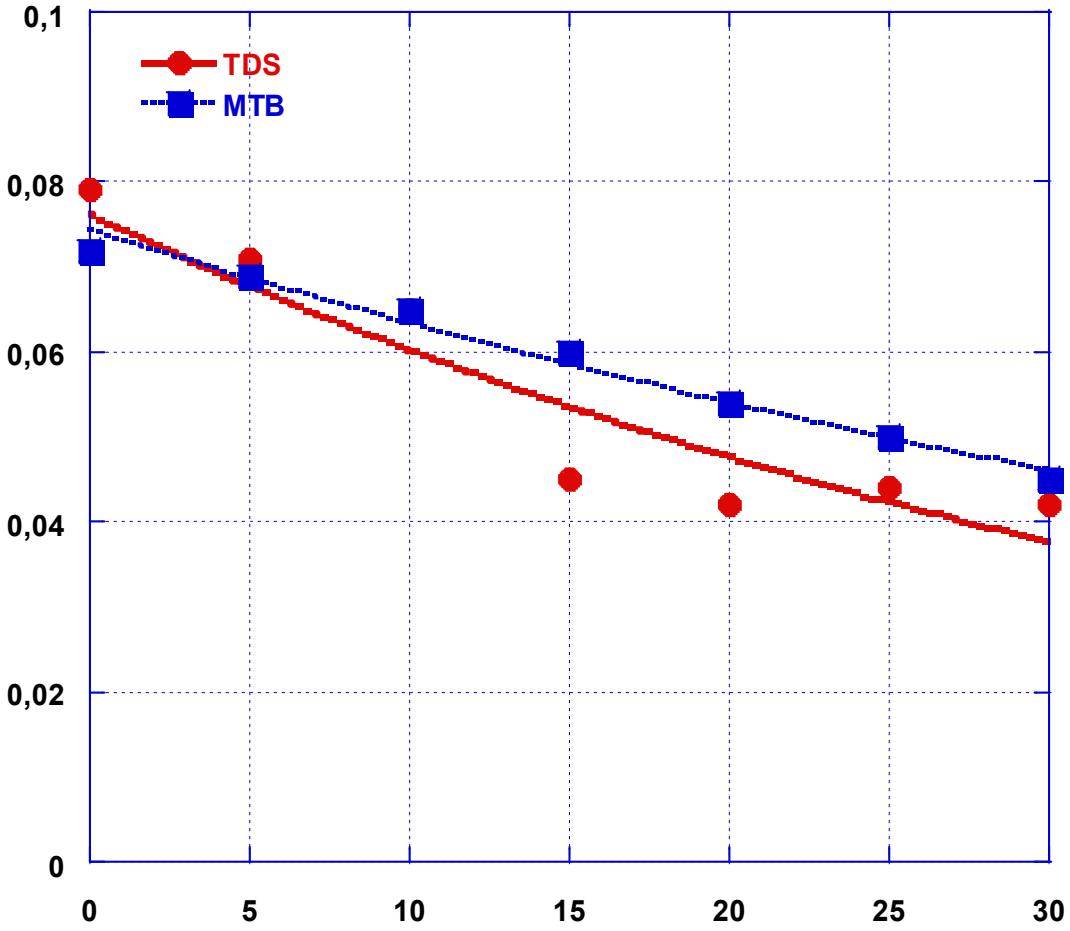

Figure IV.18: Results of the loss tangent as a function of the volume fraction of BT in the binary composite for the two test setups.

Figure (IV.18) illustrates the effect of the volume fraction of barium titanate on the dissipation factor of RE-BT composites using both methods (TDS and MTB). The graph shows that the loss tangent decreases as the volume fraction of BT increases for both TDS techniques and the microwave test bench. This behavior is attributed to the increase in the real part of permittivity, reflecting the material's ability to store electric charge. The decrease in the loss tangent with increasing BT volume fraction indicates reduced energy losses, a desirable property for many electronic applications. The variation in the dissipation factor is significant at medium BT filler concentrations, specifically between 10% and 20%, and to a lesser extent at high concentrations between 20% and 30%, as well as low concentrations between 0% and 10%. In the results from the MTB test bench, a clear decrease in the loss factor value is recorded across the entire range of BT concentrations (from 0.072 to 0.045). Conversely, in the results from the second test bench (TDS), the variation in the dissipation

factor is less pronounced. With increasing filler content, where the average concentration varies between 15% and 30% of BT, an almost constant loss tangent is observed (0.04 The loss tangent measured for the RE-BT composite using both test benches decreases as the volume fraction of BT increases. The initial decrease in dielectric losses can be linked to a reduction in the conductivity of the composite. Comparing the results of the two measurement techniques, we observe that the loss tangent values obtained from the TDS bench are higher than those from the microwave test bench. This difference can be attributed to the frequency range utilized by each technique. The TDS bench covers a broader frequency range from DC to 9.490 GHz, while the microwave test bench operates at a single frequency of 9.490 GHz. This indicates that the loss tangent values obtained with the TDS technique are more sensitive to frequency variations, whereas those obtained from the microwave test bench are more specific to the operating frequency. Overall, the results suggest that incorporating BT into the composite material can enhance its dielectric properties by reducing the loss tangent, an important parameter for electronic applications. The comparison of the two measurement techniques highlights the importance of considering the frequency range of the measurement method when characterizing the dielectric properties of materials.

IV.1.3.6 Quality factor (Q)

The quality factor Q can also represent these losses in the equation presented below : [22]

$$Q=1/\tan\delta. \qquad \text{(IV.6)}$$

TableIV.9: Results of the quality factor and volume fraction of BT in the binary composite for the two test setups.

BT%	TDS	MTB
0	12.606	13.781
5	14.387	14.387
10	15.296	15.296
15	21.747	16.462
20	23.485	18.447
25	22.259	19.608
30	23.303	21.847

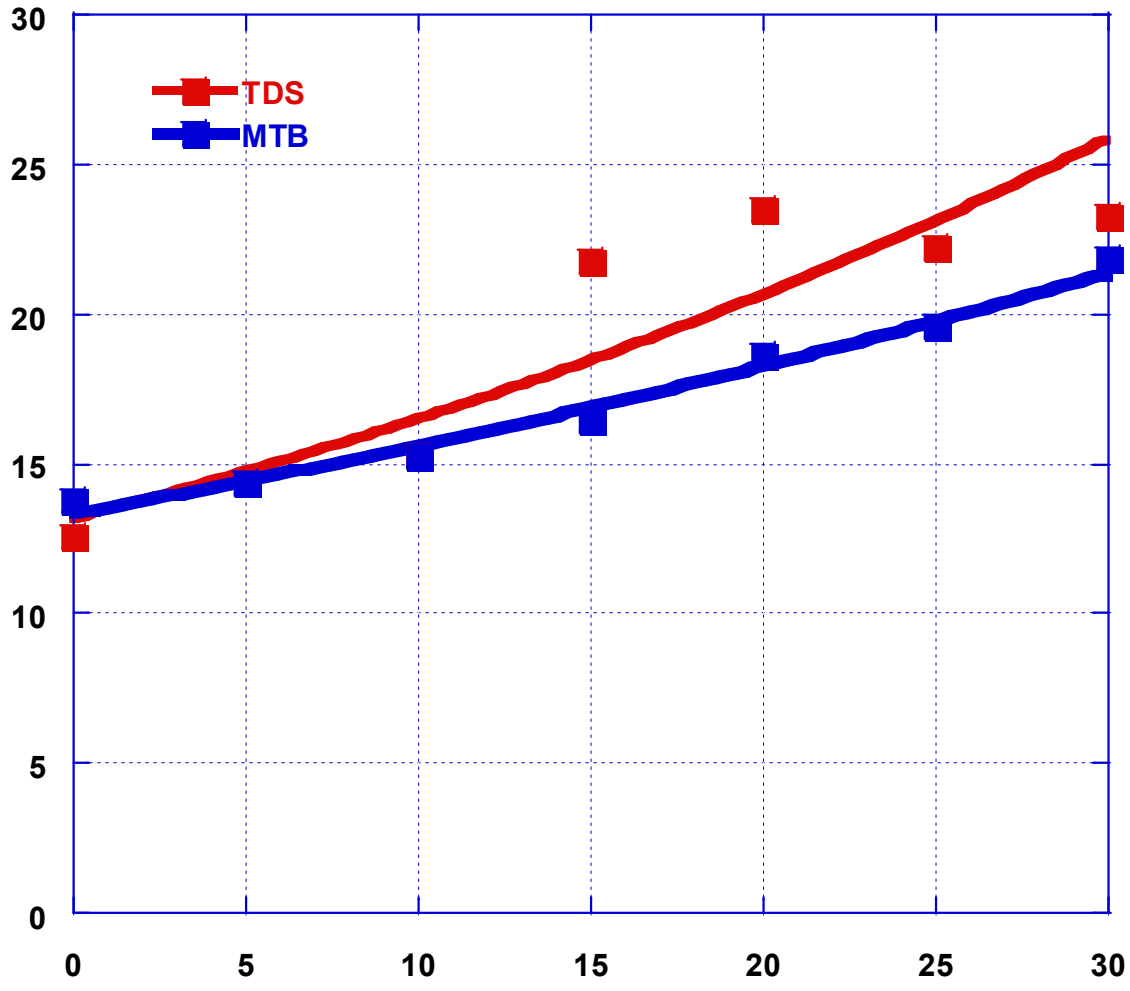

Figure IV.19: Quality factor results based on the volumetric fraction of BT in the binary composite for the two test setups

Figure (IV.19) shows the quality factor (Q) of RE-BT composites using both methods (TDS and MTB). From the graphical examination of the results, it can be seen that the values of Q vary between 12.60 and 23.48, indicating a reduction in dielectric tangent loss (tanδ) that ranges from 0.079 to 0.042 for the TDS test bench results. A similar effect was observed with the MTB test bench results, where Q increased from 13.72 to 21.85, corresponding to a decrease in the loss factor from 0.072 to 0.046. These values for the quality factor are considered relatively high, allowing for maximum energy storage and minimal dissipation.

IV.1.4 Prediction of Dielectric Permittivity

The use of predictive research models supports the interpretation of dielectric permittivity. Figure (IV.20) illustrates the variation of experimental and theoretical results for the effective dielectric permittivity of RE-BT composites as a function of BT concentration. It has been observed that the dielectric permittivity increases with the volume fraction of barium titanate. The same behavior has been noted in references [23,24,25], which discuss binary and ternary composites based on barium titanate and other materials. The graph indicates that the experimental results follow a similar pattern and align with those of the empirical models. As the volume fraction increases, surpassing 20%, the effective dielectric permittivity rises even further in both methods, but more significantly in the TDS method. The effective dielectric constant of the composite using the TDS approach is reported to be substantially higher than that obtained with the MTB method.

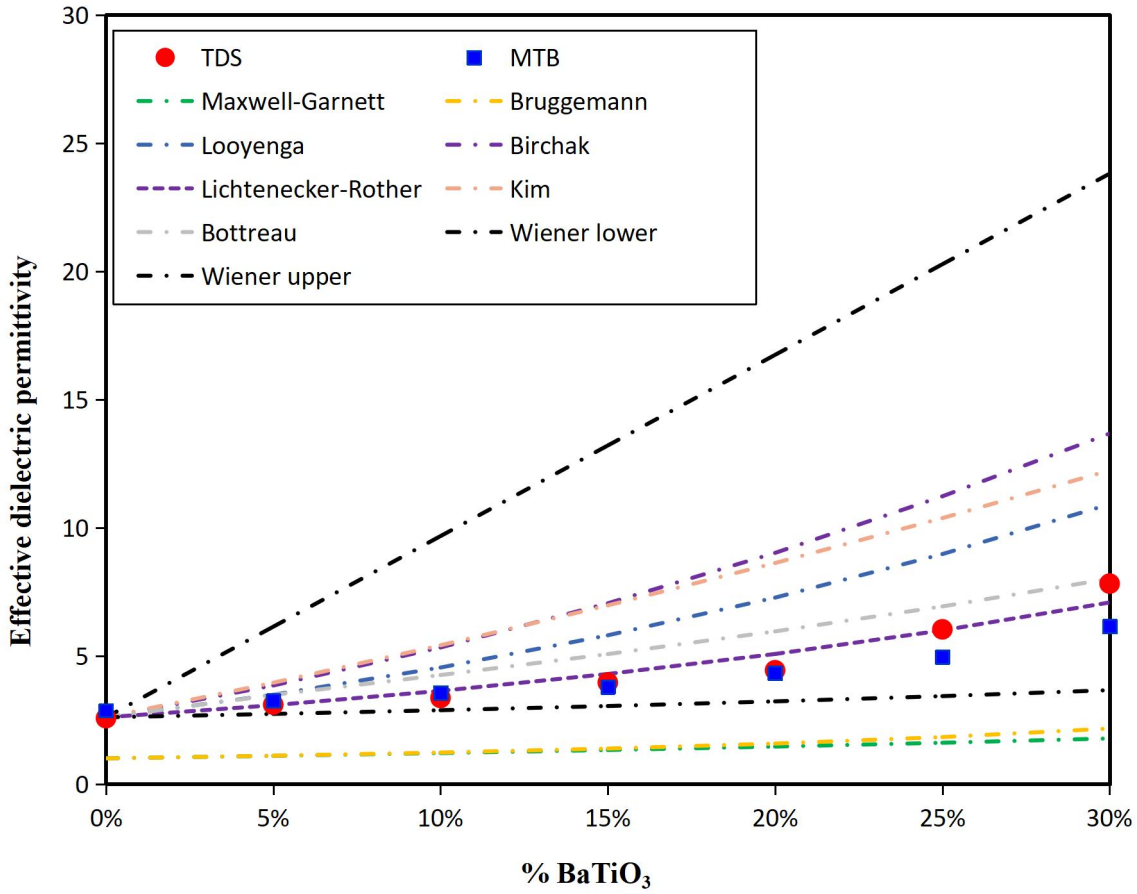

Figure IV.20: Modeling of the effective dielectric permittivity using various mixing laws for the binary composite with different volume fractions of BT (Barium Titanate).

The dielectric permittivity of composites has been illustrated and compared using several empirical models. This article presents the relationship between theoretical models and experimental results. To verify consistency, the practical implications (TDS and MTB, which need clarification) of dielectric permittivity as a function of barium titanate concentration are shown in Figure (IV.20) alongside theoretical predictions.

These models suggest that the permittivity of a composite primarily depends on the permittivity of the charge material. The Maxwell–Garnett model and the Bruggeman model exhibit a significant difference from other models as the charge concentration increases. Furthermore, these models do not adequately describe the experimental results. While they fall outside the Wiener bounds, the Looyenga model, the Kim model, and the Birchak model yield much better results than those of Maxwell-Garnett and Bruggeman, as interactions within the nanocomposite appear to be significant in these models. These models do not demonstrate superiority over earlier models, even within the Wiener bounds. However, due to the significance of surface effects for the current investigation, these models fail to predict the

dielectric permittivity of charge inclusions for the current nanocomposite. Depending on the charge concentration, the Bottreau and Lichtenecker-Rother models behave essentially linearly. These models overlap and provide good matches with experimental results. The following equation was used to generate a mean square error Δε to qualitatively assess the deviations between the theoretical data (empirical models) and the experimental data:

$$\Delta\varepsilon = \frac{1}{N}\sqrt{\sum_{i=1}^{N}\left\{\left(\frac{\left|\varepsilon'_{exp}(i)-\varepsilon'_{model}(i)\right|}{max\left|\varepsilon'_{model}(i)\right|}\right)^2\right\}} \qquad \text{(IV.7)}$$

Where: Δε represents the square root of the mean square error, and N denotes the number of samples, while ε'exp and ε'model represent the experimental and theoretical permittivity, respectively.

Table (IV.10) displays the root mean square error Δε calculated for the two methods, TDS and MTB, applied to the binary composite RE-BT.

Tableau IV.10 : Les valeurs de la racine de l'erreur quadratique moyenne (Δε) du composite binaire (RE-BT) pour diverses lois de mélange.

	Δε	
Mixing Models	TDS	MTB
Maxwell-Garnett	2,193366432	2,02149363
Bruggeman	1,957789913	1,822432897
Looyenga	0,243292091	0,288811149
Birchak	0,344782895	0,382832879
Lichtenecker-Rother	0,058463247	0,106580612
Bottreau	0,136814756	0,19592027
Kim	0,32925981	0,370835847
Wiener lower	0,412390599	0,320605982
Wiener upper	0,567207808	0,593884029

In this context, Δε represents the square root of the mean square error, and N denotes the number of samples, while ε'exp and ε'model refer to experimental and theoretical permittivity, respectively.

Table IV.10 displays the values of the root mean square error (Δε) for the binary composite (RE-BT) across various mixing laws. According to Table IV.10, the Lichtenecker-Rother model emerges as the most efficient and closest to the experimental data for the two test bench results, evidenced by the low error ratios of 0.058 and 0.11 for the TDS and MTB results, respectively.[26]

IV.2 .PART 2 :

IV.2.1. Sample Preparation Procedure

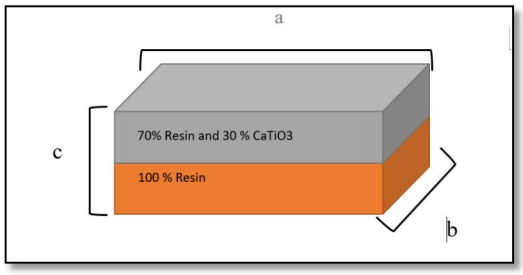

Figure IV. 21: Sample of Dielectric Material with Two Layers

The test material consists of a rectangular sample (a × b × C) with effective permittivity $\varepsilon_{eff} = \varepsilon'_{eff} - j\varepsilon''_{eff}$, comprising two homogeneous layers with flat and parallel faces. Figure IV.23 presents the 3D structure of the sample. Layer (1), characterized by thickness (1/2C) and permittivity $\varepsilon_1 = \varepsilon'_1 - j\varepsilon''_1$, was considered as a substrate (pure resin), upon which we deposited the second layer with the thickness (1/2C), and permittivity $\varepsilon_2 = \varepsilon'_2 - j\varepsilon''_2$. For a dielectric medium, permeability is often assumed to be equal to unity ($\mu=1$).[2]

In the second layer, We employed a matrix medium of epoxy resin, which serves to bind the filler particles and eliminate air pores, using Calcium Titanate (CaTiO3) as the component. The included fillers are present in volume fractions ranging from 0% to 30%, with increments of 5%. This necessitates prior calculations.

Figure IV. 22: The resin and the liquid hardener.

***a*. Determination of the volume fractions of the two constituents**

Our calculations were carried out considering that the total volume, which is the sum of the volume of the matrix and that of the fillers, is equal to one, in percentage terms 100%. If we denote by V1 the volumetric fraction of the matrix and V2 the volumetric fraction of Calcium Titanate, then:

$$V1\% + V2\% = 100\% \qquad \text{(IV.8)}$$

To do this, we set the volume of epoxy resin and determine that of calcium titanate for the different volumetric fractions. To measure the volume of powder, we used their masses, which are derived from their known densities. For this:

- We set the total volume Vtot of a sample; in our case, we chose Vtot = 7.2 ml.

- Next, we established the percentage of each constituent, starting with the epoxy resin (V1).

- We then determine V2 to find the mass corresponding to each component.

- Finally, we calculate the mass mi of powder corresponding to the different volumetric fractions used: $m_i = d_i.v_i$.

In the following table (IV.11), we present the various prepared samples, with increments of 5% in volumetric fraction.

To establish the laws governing the electrical properties of such systems, it is essential to know the volumetric concentrations of each constituent; knowing the volumetric fraction of each constituent in the sample is sufficient to determine its volumetric concentration:

$$\begin{cases} m_{tot} = m_1 + m_2 = d_1.v_1 + d_2.v_2 \\ v_1 + v_2 = 1 \end{cases} \quad \text{(IV.9)}$$

That is to say:

$$\begin{cases} m_{tot} = d_1.v_1 - d_2.v_1 + d_2 \\ v_2 = 1 - v_1 \end{cases} \quad \text{(IV.10)}$$

We deduce from equation (IV.10) the rate of the constituents:

$$v_1 = \left(\frac{m_{tot} - d_2}{d_1 - d_2}\right) \quad \text{(IV.11)}$$

$$v_2 = \left(\frac{m_{tot} - d_1}{d_2 - d_1}\right) \quad \text{(IV.12)}$$

b. Presentation of the Various Prepared Samples

- The density of CaTiO3 = 4,1.

- The total volume of epoxy =7,2 (ml).

Table IV.11: Samples prepared with a 5% increment in volumetric fraction.

Samples	Volume (ml)	CaTiO3 %	Masse of CaTiO3(g)
1	**5.04**	**0**	**0**
2		**5**	**0.29**
3		**10**	**0.58**
4		**15**	**0.87**
5		**20**	**1.16**
6		**25**	**1.45**
7		**30**	**1.76**

Note : Poly epoxyde 100% = 3,6 ml (Resin) + 3,6 ml (Durcisseur) = 7,2 ml

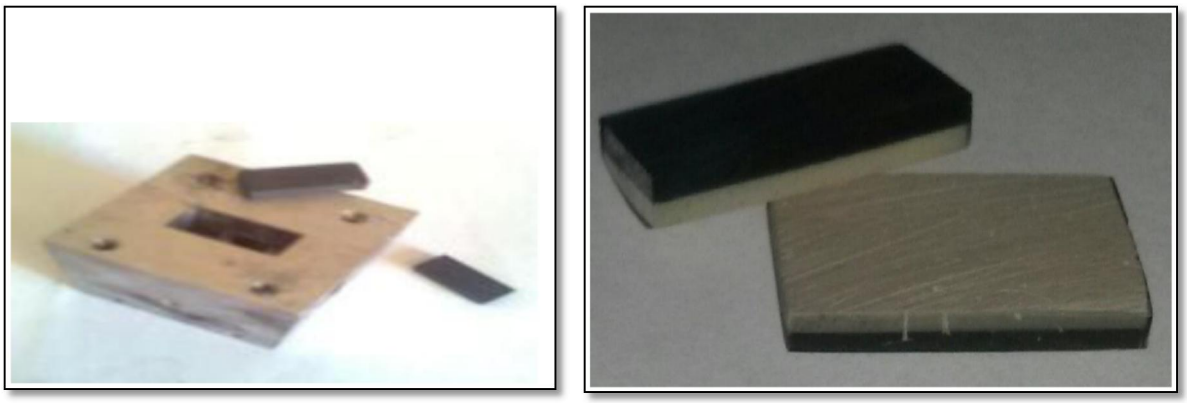

Figure IV.23: The bilayer sample after grooming.

e. Measurement of samples

According to the measurements of the dismantling and the mass of each sample, one can calculate the density with $d = m / v$

d: The density.

m: The mass of the sample.

v: The volume of the sample.

The measurements are taken after the finishing. The caliper was used to measure the dimensions of each sample and the digital scale for the masses.

f. Machining of the samples

For fixed frequency characterization, we need samples in the shape of a rectangular parallelepiped, with dimensions identical to those of the rectangular guide used in this MTB measurement bench. Delicate machining must be done by polishing, to obtain flat surfaces perpendicular to the direction of propagation, and we must have the appropriate dimensions so that when the sample is introduced into the guide, there must be complete and perfect contact between its four faces and those of the guide. The guide's section (R100) has a length a = 22.86 mm and a width b = 10.16 mm.

Figure IV 24: measuring the dimensions and mass of samples.

Table IV.12: Overview table of the different samples.

COMPOSITION OF SAMPLES	1	2	3	4	5	6
Resin (%)	95	90	85	80	75	70
CaTiO3 (%)	5	10	15	20	25	30

IV .2.2. Results and analyses

IV.2.2.1. Presentation of Results

a. Modeling of the Lichtenecker Model

$$\ln \varepsilon_{eff} = \sum_{i=1}^{n} f_i . \ln \varepsilon_i \qquad \text{(IV.13)}$$

$$\ln \varepsilon_{eff} = V_1 \ln \varepsilon_1 + V_2 \ln \varepsilon_2 \qquad \text{(IV.14)}$$

ε_1: Permittivity of pure la resin

ε_2: Permittivity of calcium titanate.

$$\ln \varepsilon_{\text{eff}}(1) = (100\%)\ln \varepsilon_1 + (0\%)\ln \varepsilon_2$$
$$\Rightarrow \varepsilon_{\text{eff}} = \varepsilon_1$$

$$\ln \varepsilon_{eff}(2) = (70\%)\ln \varepsilon_1 + (30\%)\ln \varepsilon_2$$
$$\Rightarrow \ln \varepsilon_2 = \frac{\ln \varepsilon_{eff}(2) - 0{,}7\ln \varepsilon_1}{0{,}3}$$

And so on:

$$\Rightarrow \ln \varepsilon_2 = \frac{\ln \varepsilon_{eff}(3) - 0{,}75 \ln \varepsilon_1}{0{,}25}$$

$$\Rightarrow \ln \varepsilon_2 = \frac{\ln \varepsilon_{eff}(4) - 0{,}8 \ln \varepsilon_1}{0{,}2}$$

$$\Rightarrow \ln \varepsilon_2 = \frac{\ln \varepsilon_{eff}(5) - 0{,}85 \ln \varepsilon_1}{0{,}15}$$

$$\Rightarrow \ln \varepsilon_2 = \frac{\ln \varepsilon_{eff}(6) - 0{,}9 \ln \varepsilon_1}{0{,}1}$$

$$\Rightarrow \ln \varepsilon_2 = \frac{\ln \varepsilon_{eff}(7) - 0{,}95 \ln \varepsilon_1}{0{,}05}$$

Table IV .13 Representation of the permittivity ε' measured and the one simulated by the Lichtenecker model as a function of the volume fraction of CaTiO3.

CaTiO3 (%)	ὲ of Lichtenecker	ὲ Measured
0	4.3807	4.72701
5	4.6327	4.68869
10	4.8847	4.35478
15	5.1367	4.87547
20	5.3887	5.75921
25	5.6407	5.59249
30	5.8927	6.00765

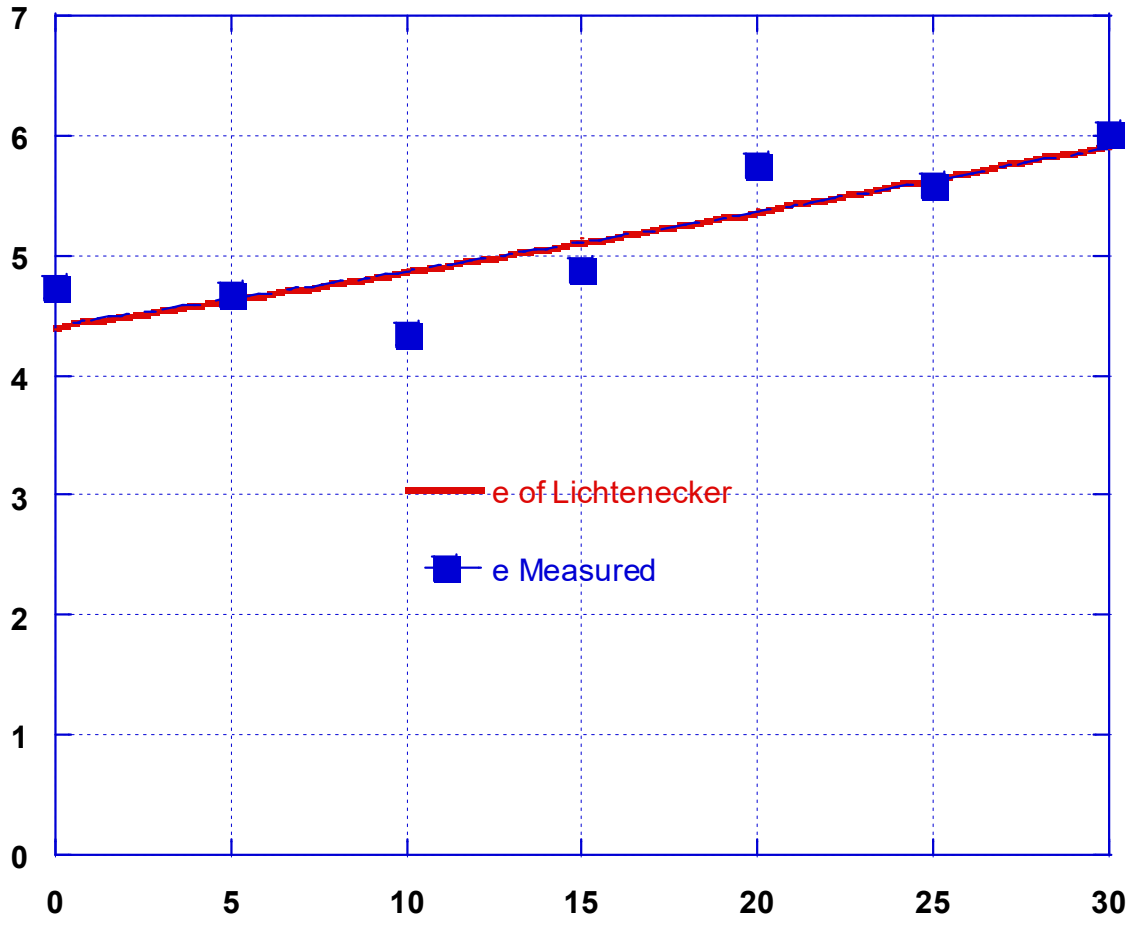

Figure IV.25: the measured permittivity ε' and the Lichtenecker permittivity ε' as a function of the volume fraction of CT

Lichtenecker Permittivity (ἐ): The Lichtenecker permittivity (ἐ) increases consistently as the volume fraction of $CaTiO_3$ increases. This is expected because the Lichtenecker model assumes that the effective permittivity is a logarithmic function of the volume fractions of the constituent materials. In general:

- At 0% $CaTiO_3$, the permittivity starts at 4.3807.

- At 30% $CaTiO_3$, it rises to 5.8927.

This increase suggests that $CaTiO_3$ has a higher permittivity than the surrounding matrix, and as its volume fraction increases, the overall permittivity of the mixture rises.

Measured Permittivity ἐ: The measured permittivity ἐ exhibits a more complex behavior compared to the Lichtenecker permittivity:

- At 0% $CaTiO_3$, the permittivity starts at 4.72701, higher than Lichtenecker's prediction.

- It decreases slightly for 5% and 10% $CaTiO_3$ to 4.68869 and 4.35478, respectively.

- Then it rises again at 15% to 4.87547 and shows a more substantial increase for higher $CaTiO_3$ fractions, reaching 6.00765 at 30%.

b.Comparison of ἐLichtenecker and ἐMeasured Permittivity

- At low volume fractions (0-10%), the measured permittivity is lower than the Lichtenecker permittivity after starting slightly higher at 0%. This could be due to measurement inaccuracies, experimental conditions, or some nonlinear interactions within the material that Lichtenecker's model doesn't account for.

- At medium volume fractions (15-25%), the measured permittivity begins to align more closely with the Lichtenecker model but shows greater fluctuations. The Lichtenecker model provides a smoother progression, whereas the measured values show some deviations.

- At higher volume fractions (30%), the measured permittivity surpasses the Lichtenecker value, indicating that the real material behavior becomes more prominent and deviates from the idealized model. This could be attributed to the higher dielectric contribution of $CaTiO_3$ at these concentrations or enhanced interfacial effects that the Lichtenecker model does not capture.

c.Possible Explanations for Deviations

- Interfacial effects: At higher $CaTiO_3$ content, the interfaces between $CaTiO_3$ and the matrix could create polarization effects that increase the measured permittivity above the predicted values.

- **Inhomogeneities:** The mixture might not be perfectly homogeneous, especially at intermediate volume fractions, leading to fluctuations in the measured values.

- Nonlinear effects: As the volume fraction increases, nonlinear interactions between the CT particles and the matrix could contribute to the deviation from the Lichtenecker model, which assumes a more straightforward relationship.

Table IV.14 Represents the calculated real and imaginary permittivities.

Volume fraction(CaTiO3)	0	5	10	15	20	25	30
έ Measured	4.72701	4.68869	4.35478	4.87547	5.75921	5.59249	6.00765
ε̋ Measured	0.00150	0.00077	0.00524	0.00086	0.00360	0.00088	0.00192

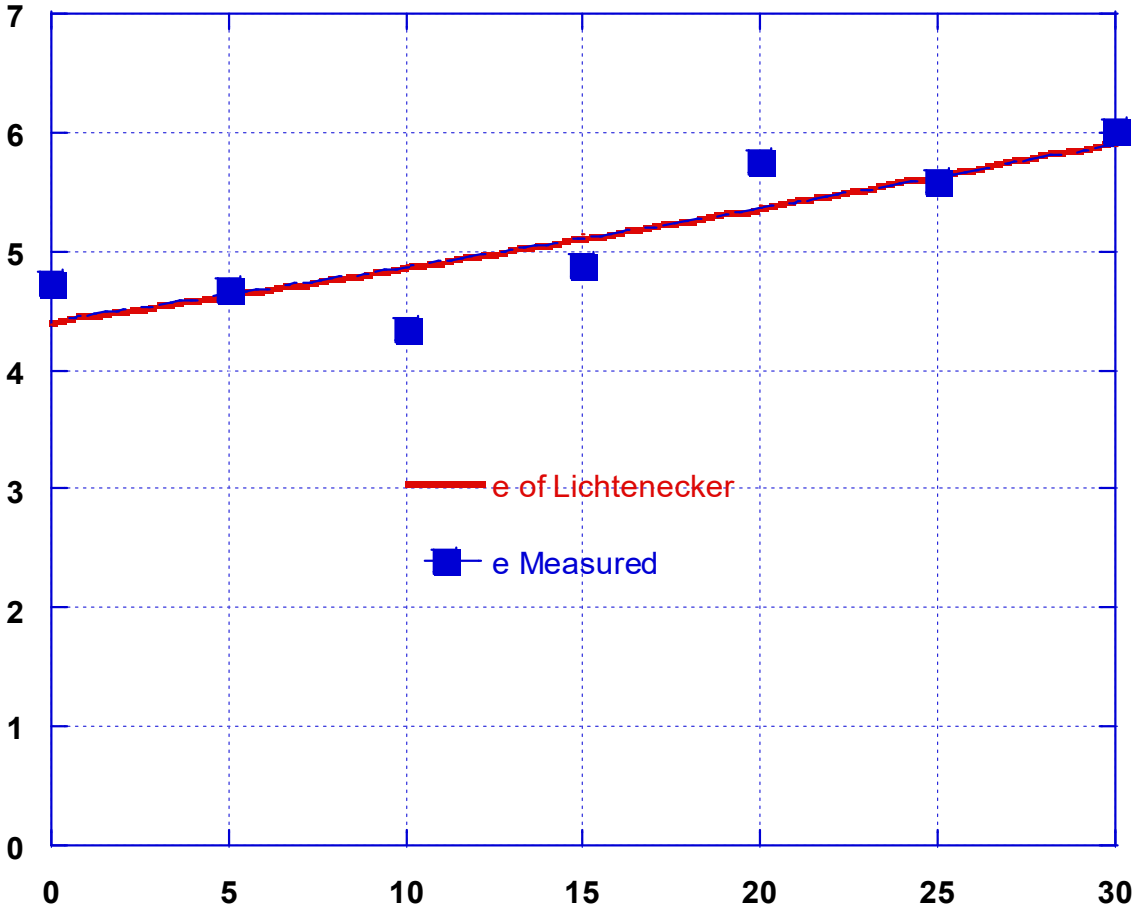

Figure IV.26: Variation of ε' measured as a function of the volumetric fraction of CT

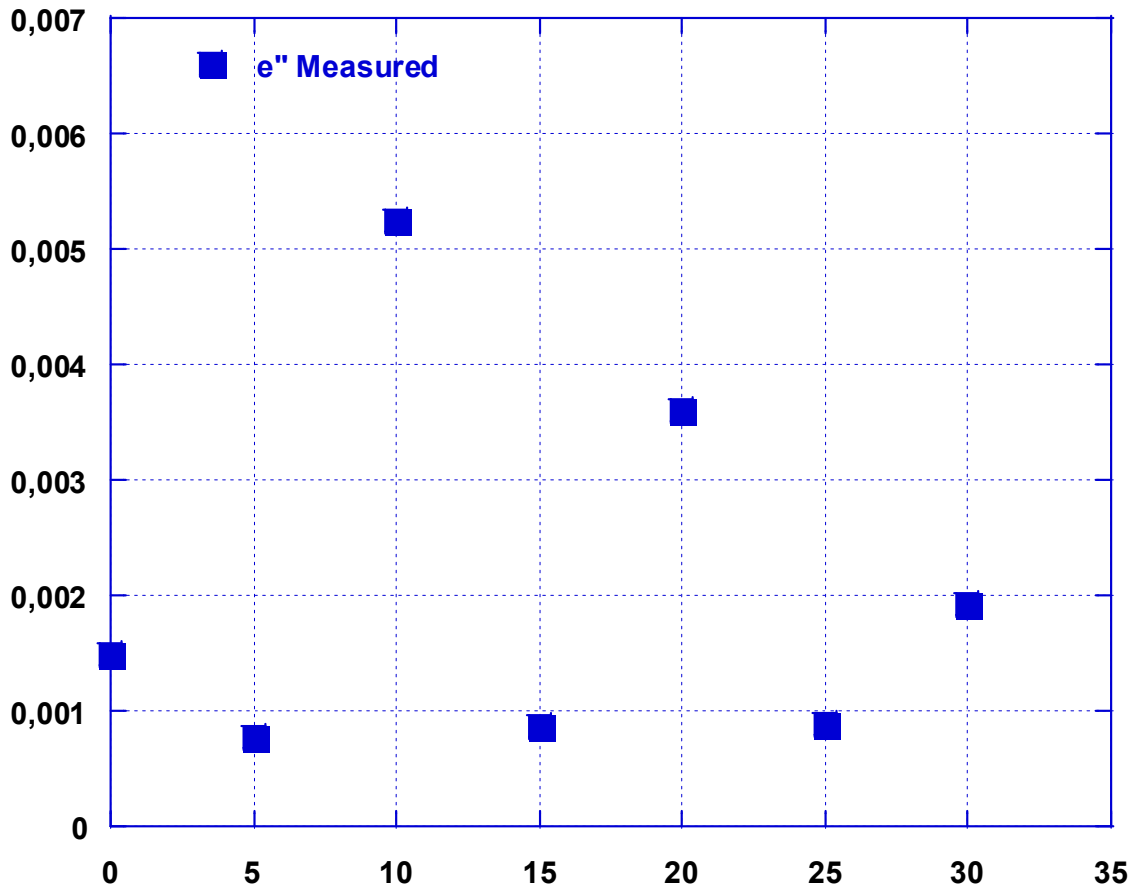

Figure IV.27: Variation of ε" measured as a function of the volumetric fraction of CT

According to the two graphical representations of real permittivity (first curve) and imaginary permittivity (second curve), the following observations can be made:

Inverse relationship: As mentioned, there is indeed an inverse relationship between the two quantities. When real permittivity increases, imaginary permittivity decreases, and vice versa. This is typical in many dielectric materials, where losses (associated with imaginary permittivity) decrease as the field storage capacity (associated with real permittivity) increases. At 10% CT: The first curve (real permittivity) shows a slight decrease. At this same point, the second curve (imaginary permittivity) indicates an increase. This confirms the inverse behavior between these two quantities.

General trend: After 10% CT, real permittivity tends to gradually increase, which may indicate an improvement in dielectric properties with a higher proportion of CT in the

material. Simultaneously, imaginary permittivity tends to decrease again after 10%, suggesting that losses in the material are reduced at higher concentrations of CT.

In summary, these two curves demonstrate typical dielectric behavior, where the field storage efficiency (real permittivity) and energy losses (imaginary permittivity) are balanced and vary with the concentration of CT, showing a clear inversion at around 10% concentration.

IV.3 Conclusions

Part 1: The main objective of the current work is to evaluate the dielectric behavior of RE-BT composites using a new preparation method with newly developed molds. The microwave dielectric characterization of various binary composite samples was studied at room temperature using two experimental setups: one utilizing a fixed frequency MTB technique and the other employing a wideband TDS approach

Adding varying amounts of BT to the composite results in different conductivity characteristics. The highest values of dielectric permittivity observed in this study were approximately 7.25 and 6.15 from the TDS and MTB benches, respectively, and the dielectric loss measured from both benches ranged from 0.2 to 0.33. The low dielectric excess observed in these studies, varying from 0.042 to 0.079, confirms this. The Q coefficient values obtained were reasonably high (reaching up to 23.48), allowing for greater energy storage and minimal dissipation, indicating the wise choice of materials used in this research. To confirm the effective dielectric permittivity of the composite material, several empirical models have been discussed.It has been found that the models of Lichtenecker and Bottreau are extremely similar to the composite material present. Current research can serve as a starting point for the dielectric characterization of the composite made of polymer and ceramic. The results of this study will surely contribute to the development of new materials to be used in many applications, such as sensors, wave absorbers, electronic components, and resonators, as well as energy harvesting and storage.

Part 2: We sought this work to determine the variation of the dielectric permittivity of the composite Epoxide-CaTiO3 according to the volume fraction. By the characterization at a fixed frequency, and by the use of several samples at different volume fractions, we were able to observe that the permittivity of such a composite follows Lichtenecker's logarithmic law.

To conclude, We can say that :

-the dielectric permittivity of the composite follows Lichtenecker's logarithmic law for two constituents.

-dielectric losses are quite minimal in the same frequency band.

Références

[1] Cheng, Kuo-Chung, et al. "Dielectric properties of epoxy resin–barium titanate composites at high frequency." *Materials Letters* 61.3 .2007.

[2] Dib, Radwan. Caractérisation de couches diélectriques et magnétiques de structures multicouches par cavité résonante microonde. Diss. Université Jean Monnet-Saint-Etienne; Université Libanaise, 2014.

[3] Bakhti, Haddi. *Caractérisation diélectrique d'un mélange de Titanate et d'oxyde (Résine époxyde, BT, Cu2O) fritté en fonction de la fréquence*. These de doctorat , Diss. 2018.

[4] J. Yu, J. Chu, Nanocrystalline Barium Titanate, Encyclopedia of Nanoscience and Nanotechnology, Edited by H. S. Nalwa, Volume 6: Pages (389–416), American Scientific Publishers, 2004.

[5] J. Akimoto, Y. Gotoh, Y Oosawa, Refinement of hexagonal BT, Acta Crystallographica C 50, pp. 160-161, 1994.

[6] N. Bourouba, K. Lalla, J.P. Martínez Jiménez, N. Bouzit, Eur.Phys. J. Appl. Phys.65, 10202 (2014).

[7] .M. Robinovitch. Contribution à l'étude de la permittivité des poudres diélectriques et des mélanges de poudres à 10 GHz. Thèse de doctorat, Bordeaux. 1964.

[6] Delfouf, Rabah. Modélisation et Caractérisation des Matériaux Composites à Base de (Polymère/Titanates/Magnétite) en Hyperfréquences . These de doctorat, Diss. 2023.

[9] Reddaf, Abdelmalek. Etude et simulation du comportement des matériaux diélectriques à fréquence fixe. Diss. 2018.

[10] R. Delfouf, N. Bouzit, N. Bourouba, J. P. Martinez Jimenez, A. Brahimi, H. Khouni, and T. Arab, "Dielectric characterization and modeling of composite materials based on epoxy resin/black iron oxide/titanates in several frequency, ranges." ECS J. Solid State Sci. Technol., 11, 073006 (2022).

[11] H. Bakhti, N. Bouzit, N. Bourouba, and J. P. Martinez Jimenez, "Dielectric the behavior of a sintered heterogeneous ternary composite resin/BT/Cu2O." Eur. Phys. J. Appl. Phys., 80, 20202 (2017).

[12] A. Brahimi, N. Bourouba, J. P. Martinez Jimenez, N. Bouzit, and R. Delfouf, "A ternary composite's dielectric modeling as a binary one." 19th International Multi-Conference on Systems, Signals & Devices (SSD), 629 (2022).

[13] R. Delfouf, N. Bouzit, N. Bourouba, A. Brahimi, and J. P. Martinez Jimenez, "Dielectric behavior investigation of composite materials based on epoxy Resin/Fe3O4/CaTiO3, SrTiO3 using mixture laws." ECS J. Solid State Sci. Technol., 11, 093003 (2022).

[14] N. Bouzit, “Caractérisation diélectrique de matériaux hétérogènes par spectroscopie temporelle: Application à l'étude de composites polyesters chargés par des titanates.” Thèse de Doctorat, (Université Ferhat Abbas Sétif-1: Setif) (2002).

[15]T.Hengcharoen, K. Eaiprasertsak, and M. Fuangfoong, “Microwave dielectric measurement of liquids by using waveguide plunger technique.” Procedia Engineering., 8, 270 (2011).

[16] S. B. Kumar, U. Raveendranath, P. Mohanan, K. T. Mathew, M. Hajian, and L. P. Ligthart, “A simple free-space method for measuring the complex permittivity of single and compound dielectric materials.” Microwave Opt. Technol. Lett., 26, 117 (2000).

[17] H. Bakhti, “Caractérisation diélectrique d’un mélange de Titanate et d’oxyde (Résine époxyde, BT, Cu2O) fritté en fonction de la fréquence.” Thèse de Doctorat, (Université Ferhat Abbas Sétif-1: Setif) (2018).

[18] S. Roberts and A. Von Hippel, “A new method for measuring dielectric constant and loss in the range of centimeter waves.” J. Appl. Phys., 17, 610 (1946).

[19] S. Gunasekaran, R. K. Natarajan, A. Kala, and R. Jagannathan, “Dielectric studies of some rubber materials at microwave frequencies..” Indian J. Pure Appl. Phys.,46, 733 (2008).

[18] S. Birajdar, N. D. Vagshette, S. S. Birajdar, D. B. Suryawanshi, and A. R. Lathi, “Structural characterization of acetonitrile-xylene binary mixtures at 301 K using high-frequency X-band technique.” VIIRJ., 12, 125 (2021).

[21] A. Bounar, “Caractérisation électromagnétique d’un composite Titanate-Noir deCarbone par spectroscopie temporelle.” Thèse de Doctorat, (Université Ferhat Abbas Sétif-1: Setif) (2017).

[22] H. Khouni, “Modélisation et Simulation Numérique de Mélanges de Matériaux Diélectriques Binaire et Ternaire.” Thèse de Doctorat, (Université Mohamed Boudiaf de M’Sila: M’sila) (2017).

[23] S. B. Basturk, C. E. Dancer, and T. McNally, “Dielectric performance of composites of BaTiO3 and polymers for capacitor applications under microwave frequency.” J. Appl. Polym. Sci., 138, 50521 (2021).

[24] A. Brahimi, N. Bourouba, R. Delfouf, J. P. Martinez Jimenez, and N. Bouzit, “Characterization, modeling, experimental validation and dielectric properties studies of a ternary composite (RE-BaTiO3-SiO2) using time-domain spectroscopy.” Asian J. Research Chem., 16, 148 (2023).

[25] N. Bourouba, “Investigation on Dielectric, Electric, and Magnetic Properties of (Epoxy Resin-Titanate- Oxide/Ferrite) Ternary Composites at Microwave Frequency.” ECS J. Solid State Sci. Technol., 12, 043005 (2023).

[26] D . Djouada, et al. "Dielectric characterization of heterogeneous composites using time-domain spectroscopy and microwave test benches in microwave frequency." ECS Journal of Solid State Science and Technology 12.6 (2023)

General Conclusion

General Conclusion

The rapid growth of electronics over the past four decades, primarily driven by the telecommunications boom, has necessitated significant advancements in electronic systems and components. This evolution has propelled the exploration and development of composite materials, which offer a unique combination of mechanical, thermal, and dielectric properties, essential for modern applications. Composite materials, particularly those enhanced with inorganic nanofillers like barium titanate (BT), have shown immense potential in improving electronic performance and facilitating miniaturization.

The integration of BT into polymer matrices, such as epoxy resin, has emerged as a critical area of research due to its high dielectric constant and ability to enhance the performance of capacitors and other electronic components. This study employs advanced measurement techniques, including Time Domain Spectroscopy (TDS) and the X-Band Microwave Test Bench (MTB), to investigate how varying BT volume fractions influence the dielectric properties of composites. The findings demonstrate the limitations of traditional empirical mixing laws in accurately predicting the behavior of complex composites, highlighting the need for advanced numerical modeling techniques.

Through the use of modern methods that account for factors like phase morphology and constituent interactions, this research provides deeper insights into the optimization of composite materials for high-frequency applications. These include microwave communications, where high dielectric constants and minimal losses are crucial. By improving the accuracy of material modeling, the study contributes to more efficient, cost-effective, and reliable electronic systems.

Additionally, the research explores the characterization of heterogeneous multilayer dielectric materials, such as CT, which offer unique properties distinct from homogeneous counterparts. These findings underscore the versatility and superior performance of composite materials, making them indispensable for future advancements in electronics, telecommunications, and other high-frequency domains.

Overall, this work emphasizes the critical role of BT-based composites in addressing the evolving demands of modern electronics. The continuous refinement of measurement techniques and modeling approaches is essential for unlocking the full potential of composite materials, paving the way for innovative solutions in next-generation electronic devices. The insights gained from this research will guide future developments, ensuring that electronic systems continue to advance in efficiency and performance, meeting the challenges of an ever-evolving technological landscape.

ANNEXE A

PROGRAMME MATLAB

```
% lois_melange
A=1/2; f=0:.02:1;%size(f);
ei=5000;
em=2.0,
emaxwell=1+(ei/em-1).*f./(1+A*(1-f)*(ei/em-1));%_imp-FDTD-these-Mejdoubi-Etude par simulation numerique des proprietes dielectriques-2013.pdf
ebrugemann1=(1-A*(1+ei/em)+f*(ei/em-1)+sqrt((1-A*(1+ei/em)+f*(ei/em-1)).^2+4*A*(1-A)*(ei/em)))/(2*(1-A));
elooyenga=(f*(ei^(1/3)) + (1-f)*(em^(1/3))).^3;
ewiener1=(1-f)*em+f*ei; ewiener2=1./((1-f)/em+f/ei);
ebirchak=(f*(ei^(1/2)) + (1-f)*(em^(1/2))).^2;
%maxwell, brugemann, looyenga, wiener1, wiener2, birchak
%plot(f,em*emaxwell)%plot(f,em*ebrugemann1)%plot(f,em*[emaxwell;ebrugemann1])plot(f,[em*emaxwell;em*ebrugemann1;elooyenga])
plot(f,em*emaxwell,'g-.'), hold on, plot(f,[ewiener1;ewiener2],'k-.'),
plot(f,[em*ebrugemann1;elooyenga;ebirchak])
elicht=10.^(f*log10(ei) + (1-f)*log10(em)) ; %Lichtenecker
vi=.5; alpha=.8; vn=(1-f).*(1-vi)./(f.*vi); p1=1./(1+vn.^alpha);
p2=(vn.^alpha)./(1+vn.^alpha);
ebottreau=exp( p1*log(ei) + p2*log(em) );
A=0.49; B=0.074;
ekim=( f.*(ei.^(A*(1-f)+B)) + (1-f).*(em.^(A*(1-f)+B)) ).^(1./(A*(1-f)+B));
ehashin2=ei+3*ei*(em-ei)*(1-f)./(em+2*ei-(1-f)*(em-ei));
ehashin1=em+3*em*(ei-em)*f./(ei+2*em-f*(ei-em));
plot(f,[ehashin1;ehashin2],'b--')
plot(f,[elicht; ebottreau;ekim],'r')
```

Scientific work accomplished.

I hereby list the works in which we have participated.

International publications:

1. **D. Djouada**, N. Bouzit, R. Delfouf, L. Chioukh, J. P. Martinez Jimenez, "Dielectric Characterization of Heterogeneous Composites Using Time Domain Spectroscopy and Microwave Test Benches in Microwave Frequency." ECS J. Solid State Sci. Technol., 12, 063003; 2023.
2. T. Arab, R. Delfouf, H. Khouni, N. Bouzit, **D. Djouada,** J. P. Martinez Jimenez, N. Bourouba,"Investigation on Dielectric, Electric, and Magnetic Properties of (Epoxy Resin-Titanate-Oxide/Ferrite) Ternary Composites at Microwave Frequency." ECS J. Solid State Sci. Technol.,12, 043005; 2023.

International communications:

1- Djouada Djahida, Bouzit Nacerdine International Conference on Ferhat Abbas University Sétif-1, Materials and Mechanics ICMM 2019 Institute of Optics and Precision Mechanics, Entitled (Characterization of heterogeneous multilayer dielectric materials at microwave frequencies) 1 November 11-12, 2019 Oral Conference presented by Djouada Djahida.

2- Djouada Djahida, Bouzit Nacerdine International Conference on Gedik University, Istanbul, Turkey,3rd International Modern Scientific Research Congress Conference Entitled (Determination of The Dielectric Properties Of A Composite Material In The X-Band) May 2022'Conference Oral' Presented by **Djouada Djahida.**

3- Djouada Djahida, Bouzit Nacerdine and Delfouf Rabah Conference on Konya University, Turkey - 1st International Conference On Engineering and Applied Natural Sciences Modern Scientific Research Congress Conference Entitled (Characterization Of The Permittivity Of Hyper frequency Multilayer Dielectric Materials) May 2022 - "Conference Oral Presented by **Djouada Djahida**.

4- Delfouf Rabah, Bouzit Nacerdine, Tlili Salah and **Djouada Djahida**, Conference University, Khenchela, 1st International Conference on Engineering Applied Natural Sciences Modern Scientific Research Conference Entitled (Investigation of two-layer binary composite materials based on epoxy resin and calcium titanate using microwave test bench) June 2022, conference Oral Presented by Delfouf Rabah

Co-Encadrement de PFE

- Mr. Laidani Redha Master Instrumentation Intitulé « Simulation de Guide d'Ondes par le Logiciel COMSOL 2019/2020
- Mme. Halim Hadjira Master Instrumentation Intitulé Intitulé «la balance du watt. 2020/2021
- Mme. Abbas Houria Master Instrumentation Intitulé Intitulé Mesure De La Permittivité Diélectrique ε*=έ-jε̋ De La Résine Epoxy En Bande X. 2021/2022

الملخص

تركز هذه الأطروحة على تمييز ودراسة المواد المركبة العازلة، التي تتألف من البوليمرات والسيراميك الحديدية، والتي ظهرت مؤخرًا كمكونات أساسية لتطبيقات توليد وتحويل وتخزين الطاقة المستدامة. يعد توازن السماحية العازلة، والفقدان العازل، وعامل التبديد أمرًا بالغ الأهمية، حيث يكون الهدف النهائي هو سعة تخزين الطاقة. يتم إعداد عينات المركب من راتنج الإيبوكسي (RE) / تيتانات الباريوم (BaTiO3) باستخدام طريقة الصب المختلط مع قوالب جديدة. يتم تحليل الخصائص العازلة، بما في ذلك السماحية والفقدان والمعاوقة الكهربائية والتوصيلية الساكنة وعوامل التبديد المؤثرة بتركيز تيتانات الباريوم وتأثير التردد على المركبات من خلال طريقتين للتوصيف. تهدف الدراسة إلى تحديد السماحية العازلة للمادة باستخدام طريقتين للموجات الدقيقة: التحليل الطيفي في المجال الزمني (TDS) ومنصة اختبار الميكروويف في نطاق X بارتفاع السماحية (BaTiO3) يتم استخدام قوانين الخليط التجريبية المختلفة لتقدير السماحية العازلة. يرتبط زيادة تركيز المادة المالئة (MTB). العازلة الفعالة، ويتم تأكيده من خلال نماذج خليط تجريبية متنوعة. تعد نتائج البحث واعدة لتطبيقات كهربائية متنوعة، بما في ذلك الأجهزة الاستشعارية وممتصات الأمواج والرنانات والهوائيات.

كلمات مفتاحية :

السلوك العازل، طريقة الميكروويف، المركب الثنائي.، المركب الثنائيTB، منصة اختبار، SDTا السماحية،؛

Résumé

Cette thèse se concentre sur la caractérisation et l'étude des matériaux composites diélectriques, comprenant des polymères et des céramiques ferroélectriques, qui ont récemment émergé en tant que composants essentiels pour la génération, la transformation et le stockage d'énergie durable. Équilibrer la permittivité diélectrique, la perte diélectrique et le facteur de dissipation est crucial, avec pour objectif ultime la capacité de stockage d'énergie. Des échantillons composites de résine époxy (RE)/titanate de baryum (BaTiO3) sont préparés en utilisant une méthode de coulée en mélange avec de nouveaux moules. Les propriétés diélectriques, comprenant la permittivité, la perte, le module électrique, la conductivité statique et les facteurs de dissipation influencés par la concentration de titanate de baryum et les effets de fréquence, sont analysées via deux méthodes de caractérisation. L'étude vise à déterminer la permittivité diélectrique du matériau en utilisant deux méthodes micro-ondes : la spectroscopie dans le domaine temporel (TDS) et le banc d'essai micro-ondes en bande X (MTB). Diverses lois empiriques de mélange sont utilisées pour estimer la permittivité diélectrique. Une augmentation de la concentration de charge (BaTiO3) est corrélée à une permittivité diélectrique effective accrue, confirmée par divers modèles empiriques de mélange. Les résultats de la recherche promettent des applications électriques diverses, incluant des capteurs, des absorbeurs d'ondes, des résonateurs et des antennes.

Mots-clés : permittivité, SDT, banc d'essai, TB ; comportement diélectrique, méthode micro-ondes, composite binaire.

Abstract

This thesis focuses on characterizing and studying dielectric composite materials, comprising polymers and ferroelectric ceramics, which have recently emerged as vital components for sustainable energy generation, transformation, and storage applications. Balancing dielectric permittivity, dielectric loss, and dissipation factor is crucial, with the ultimate goal being energy storage capacity. Epoxy resin (RE)/barium titanate (BaTiO3) composite samples are prepared using a mixture cast method with new molds. Dielectric properties, including permittivity, loss, electrical modulus, static conductivity, and dissipation factors influenced by barium titanate concentration and frequency effects, are analyzed via two characterization methods. The study aims to determine material dielectric permittivity using two microwave methods: time-domain spectroscopy (TDS) and X-band microwave test bench (MTB). Various empirical mixture laws are employed to estimate dielectric permittivity. Increasing filler concentration (BaTiO3) correlates with heightened effective dielectric permittivity, confirmed through diverse empirical mixture models. The research findings hold promise for diverse electrical applications, encompassing sensors, wave absorbers, resonators, and antennas.

Keywords: permittivity, SDT, test bench, TB; dielectric behavior, microwave method, binary composite.